Enhancement of Starting Performance of an Induction Motor by Improving Rotor Design

A Thesis Submitted to the Department of Electrical and Electronic Engineering in Partial Fulfillment of the Requirement for the Degree of

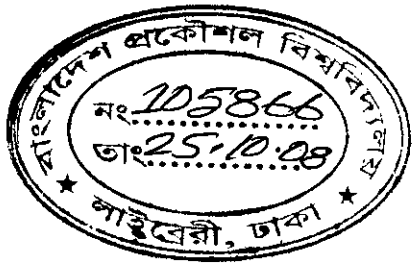

DOCTOR OF PHILOSOPHY

by

Md. Fayyaz Khan

Department of Electrical and Electronic Engineering
BANGLADESH UNIVERSITY OF ENGINEERING AND TECHNOLOGY

2008

The thesis titled **"Enhancement of starting performance of an Induction Motor by Improving Rotor Design"** Submitted by **Md. Fayyaz Khan**, Roll no. 001/06/00P Session April, 2000 has been accepted as satisfactory in partial fulfillment of the requirement for the degree of DOCTOR OF PHILOSOPHY on 21 May 2008.

BOARD OF EXAMINERS

1. May 21, 2008
Dr. M. A. Choudhury
Professor, Department of EEE, BUET — Chairman

2.
Dr. Satya Prasad Majumder
Professor and Head, Department of EEE, BUET — Member (Ex-officio)

3.
Dr. S. M. Lutful Kabir
Professor and Director, IICT, BUET — Member

4.
Dr. S. Shahnawaz Ahmed
Professor, Department of EEE, BUET — Member

5.
Dr. Md. Quamrul Huda
Professor, Department of EEE, BUET — Member

6.
Dr. Md. Shah Alam
Associate Professor, Department of EEE, BUET — Member

7.
Dr. M. H. Haque
Associate Professor, Department of EEE
Nanyang Technological University, Singapore — Member (External)

Declaration

It is hereby declared that this thesis or any part of it has not been submitted elsewhere for the award of any degree or diploma.

Signature of the candidate

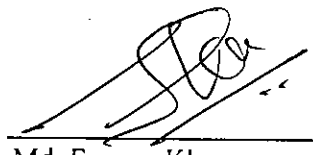

Md. Fayyaz Khan

Acknowledgements

The author expresses his heartfelt gratitude to his supervisor, Professor Dr. M.A.Choudhury for his guidance throughout the research period. Professor Choudhury has taken care of the author in every respect that he needed. The author wishes to acknowledge the valuable discussions that he had from time to time with the members of his Examination Committee and for their valuable suggestions which greatly helped to expedite the work. The author also expresses his heartfelt gratitude to Professor Dr. M. Rezwan Khan (Former Professor of EEE Department, BUET and presently Vice-Chancellor, United International University (UIU), Bangladesh) for his valuable suggestions, encouragement and necessary support and help throughout the research work.

The author thanks the Head of the Department of Electrical & Electronic Engineering Department, BUET who has provided unfailing support in various circumstances.

The author remembers with deep gratitude Dr.Alessandra Sitzia, Technology Consultant, Slim Electromagnetic Engineering, Areva T&D, UK for providing the "SLIM" Electromagnetic software free of cost and providing important suggestions and help in modeling the rotor of the induction motor with the help of the "Slim" software.

The author wishes to thank Professor Dr. Quamrul Ahsan of EEE Department, BUET for giving permission to use the machine laboratory, where the author performed his experimental work. The author also thanks Professor Quamrul Islam of Mechanical Engineering Department, BUET for providing valuable suggestions during the fabrication work and rendering logistic support in this regard. The author also thanks Dr. Md. Feroz Alam Khan, Professor, Physics Department, BUET for helping to setup experimental work for the study of magnetic properties of the materials which was used in the research work.

The author is grateful to the Head of the Department of Materials and Metallurgical Department for granting permission to use the Foundry shop for the fabrication work

and for providing necessary help in this regard. The author also expresses his profound gratitude to Professor Dr. Mohar Ali, Professor Dr. A K M Bazlur Rashid and Professor Dr. Md. Fakhrul Islam of the Department of MME for constant help and valuable suggestions during fabrication work done in the Foundry shop of the Department of MME of BUET. The author appreciates the valuable support provided by his employing institution The University of Asia Pacific in pursuit of the Degree and constant encouragement he has received from the Vice-Chancellor Professor Dr. A. M. Patwari and Dr. Sultan Mahmud of Physics Department. The author is also deeply indebted to Mr. Faruk Hossain and Mr.Abdul Matin of Computer Science & Engineering Department of the University of Asia Pacific for constant help in various phases of the research work. The author is also extremely grateful to his student Mr. Arif Reza Anwary who is presently a Ph.D student at the Memphis University, USA for his valuable help and suggestions.

The author expresses his deep sense of gratitude to his parents for their continuous encouragement for the completion of the Degree. The author greatly owes to his wife for providing constant support and encouragement which helped to complete the thesis work. The author owes to the lab technicians of the Advanced Machine and the Power Electronic Lab, Foundry and Machine shop of BUET for providing the logistic support. The author conveys his special thanks to Mr. Debasis Das of Advanced Machine lab and Mr. Rafiqul Islam of Power Electronics lab, BUET for constant help during the experimental work in the lab.

The author is indebted to Mr. Monir Hossain, proprietor of M/S Shawon Metal Work, Dhaka, Bangladesh for casting successfully Ferro-magnetic material in the rotors of the squirrel cage induction motors. Many of the foundry shops failed to do the proper casting job earlier. It was Mr. Monir Hossain of M/S Shawon Metal Works who showed great interest in the work and made fruitful casting for a number of induction motor rotors.

Abstract

The goal of the thesis is to develop a novel technique to enhance the starting torque and starting performance of a three phase squirrel cage induction motor by changing the material composition of the end connections of the rotor. Magnetic materials show significant skin effect properties at power frequency. This property has been exploited in this research work to change the resistance of the end connections of the rotor to enhance the starting performance of the squirrel cage induction motor. Commercially available iron strips having relative permeability of the order of 5000-6000 have been introduced in the rotor end connections for the purpose. At start, the rotor induced current has a frequency of 50 Hz which shows skin effect large enough to increase the rotor resistance. As the starting torque of the motor is a function of rotor resistance, the starting torque increases appreciably together with the decrease in the starting current. As the motor acquires its rated speed, the frequency of the rotor current decreases, diminishing the skin effect and thereby reducing overall resistance of the rotor. Thus the overall performance of the motor remains virtually unaffected.

At first, experimentally determined motor parameters were used in MATLAB and the performance of the motor was evaluated to ascertain the impact of skin effect on the modified rotor end connections. The simulation results show appreciable enhancement in the starting performance of the motor. Using the simulation software, the optimum size of the magnetic materials placed at the end connections has been determined to achieve high starting torque without affecting the overall running performance of the motor. The dimension thus obtained is used to modify the end connection of the rotor for experimental verification of the simulated results. The experimental results are in good agreement with the simulated ones. It is worth mentioning that, the starting current is also reduced significantly, as expected.

For further validation of the experimental results analytical study has also been carried out with the help of software package SLIM.

Further, single phase motor was studied to observe its performance with ferromagnetic insertion in the rotor. It was found that the running performance of the 1-phase motor improved significantly.

Another point worth mentioning here is the significant improvement of current wave shape and reduction of harmonics for both 3-phase and 1-phase motors with the introduction of ferromagnetic materials in end rings of rotor.

Contents

Title i

Certification ii

Abstract vi

List of Tables xi

List of Figures xii

List of Symbols xv

1 Introduction 1

1.1. Historical Development of Induction Motor 1

1.2 Literature Review 3

1.2.1 Summary on End Ring work..... 13

1.3 Problem Identification 15

1.4 Thesis Objective 17

1.5 Thesis Outline..... 18

2 Basics of Induction Motor 20

2.1 Equivalent circuit of induction motor..... 20

2.2 NEMA Design..... 23

2.2.1 Deep bar rotor..... 24

2.2.2 Double cage rotor..... 25

2.3 Single Phase induction motor..... 26

2.3.1 Torque Speed characteristic of single phase motor..... 28

3 Effect of Ferromagnetic Insertion in the Rotor Circuit 30
3.1 Skin effect due to magnetic property of a conductor 30
3.2 Application of skin effect in the rotor circuit of induction motor 33
3.3 Different methods of ferromagnetic insertion in the rotor Circuit of an induction motor 34
3.4 Proposed method of Ferromagnetic insertion in the squirrel Cage rotor ... 37
3.5 Effect of ferromagnetic insertion on induction motor performance 38
3.5.1 Improvement of Starting performance 38
3.5.2 Improvement of running performance 40
3.5.3 Effect of harmonics on motor performance 40
3.5.4 Performance of single phase Induction motor 41
3.6 Impact on motor performance for variation of rotor resistance due to Variation of speed 42
4 Experimental Set up and Results 43
4.1 Experimental Design Process 43
4.2 Experimental Set up 50
4.3 Experimental Measurements 53
4.3.1 Performance of the Standard Motor 54
4.3.2 Performance of Motor with Ten Rotor Strips 55
4.3.3 Performance of Motor with Five Rotor Strips 55
4.3.4 Performance of Motor with Three Rotor Strips 56
4.3.5 Performance of Motor with Two Rotor Strips 57
4.3.6 Performance of Copper Motor 57
4.3.7 Comparative study of 3-phase motor with different Rotor Configurations 58
4.3.8 Performance of Single Phase Motor 61
4.4 MATLAB based simulation Results 63
4.5 Current wave shape for different rotor configurations 65
4.5.1 Current wave shape and FFT for 3-phase motor 66
4.5.2 Current wave shape and FFT for 1-phase motor 68

4.6 Discussion on the Results..... 69
4.6.1 Comments on power factor and efficiency..... 70
4.6.2 Comments on current wave shape and harmonics..... 70
5. Validation of Proposed Scheme..... 72
5.1 By theoretical calculations 72
5.2 Torque and current characteristics by SLIM software..... 75
5.2.1 Mesh generation of 3-phase ¼ HP Motor..... 76
5.2.2 Mesh generation for 90kW, 415V, 3-Phase Motor..... 79
5.2.3 Discussion on the simulation results..... 83
6. Conclusions 84
6.1 Conclusions..... 84
6.2 Limitation of the work..... 86
6.3 Suggestions for further research..... 87
References..... 89
Appendix A: Motor data and Experimental results..... 94

List of Tables

4.1 Comparative table showing starting torque for different rotor configurations 60

4.2 Comparative table showing starting Current for different rotor configurations 60

A.1 Table for experimental data for torque speed curve of motors 98

A.2 Table for blocked rotor current for different rotor geometry 99

A.3 Table for efficiency and power factor of aluminum rotor 99

A.4 Table for efficiency and power factor for rotor with two iron strips 100

A.5 Table for Torque speed data for single phase motor 100

List of Figures

2.1 Equivalent circuit of an induction motor 20

2.2 Modified equivalent circuit of induction motor 20

2.3 Thevenin's theorem applied at A-B 20

2.4 Thevenin's equivalent circuit 21

2.5 Torque/Current Vs. Slip curve of induction machine showing motor and generator modes of operation 22

2.6 Torque slip curve for different NEMA design induction motors 23

2.7 Deep bar rotor 24

2.8 Double cage rotor 25

2.9 Effect of voltage on Torque-slip curve 26

2.10 Single phase induction motor with main winding..... 26

2.11 Equivalent circuit of single phase induction motor with rotor stationary..... 27

2.12 Equivalent circuit in the light of double revolving theory..... 27

2.13 Equivalent circuit of 1-phase induction motor under running condition..... 28

2.14 Torque-Slip curve for 1-phase Induction motor..... 29

3.1 Flux density distribution in an iron slab at different frequencies..... 30

3.2 Variation of resistance of strip due to skin effect..... 32

3.3 Skin depth as a function of frequency..... 33

3.4 Skin effect in a conductor cross section..... 34

3.5 Ferromagnetic material inserted in alternate slot of rotor..... 35

3.6 Ferromagnetic material inserted at the end of slot..... 36

3.7 Embedded iron cylinder over rotor..... 36

3.8 Side view of rotor..... 37

3.9 Top view of rotor with iron insertion..... 37

3.10 Simulated Torque-Slip curve for modified rotor..... 39

4.1 Aluminum rotor (locally casted)..... 44
4.2 Aluminum rotor after machining..... 44
4.3 Iron strip for insertion in rotor..... 45
4.4 Iron strip in rotor after rotor casting..... 46
4.5 Rotor with copper casting..... 46
4.6 Skin effect in an iron strip. 47
4.7 Rotor slot section with iron Strip 48
4.8 Iron strip (0.2mm+0.2mm) for insertion 49
4.9 Experimental set up..... 51
4.10 Experimental set up..... 52
4.11 Motor coupled to dynamometer 52
4.12 Performance of standard motor 54
4.13 Performance curve for motor with ten rotor strips 55
4.14 Performance curve for motor with five rotor strips 56
4.15 Performance curve for motor with three rotor strips 56
4.16 Performance curve for motor with two rotor strips 57
4.17 Performance of motor with copper rotor..... 58
4.18 Torque Speed curve of 3-phase motor with different rotor configurations..... 58
4.19 Starting current for motor with different rotor configurations..... 59
4.20 Single phase motor and stator winding..... 61
4.21 Torque Speed curve for single phase motor..... 62
4.22 Locked rotor current -voltage curve for single phase motor..... 62
4.23 Simulated curves for standard motor..... 63
4.24 Torque-slip curve for different rotor configurations..... 64
4.25 Stator current wave shape for different rotor configurations..... 66
4.26 Stator current wave shape for different rotor configurations..... 67
4.27 Stator current and FFT for single phase Motor..... 68

5.1 Outline of rotor section and dimension of rotor slot for ¼ HP motor..... 76
5.2 Outline of stator section and dimension of stator slots for ¼ HP motor 77
5.3 Stator mesh, rotor mesh and combined mesh for ¼ Hp motor..... 78
5.4 Rotor slot dimension and 90^0 rotor section for 90 kW motor..... 79
5.5 Stator slot dimension and 90^0 stator section for 90 kW motor..... 80
5.6 Mesh for 90 kW motor..... 81
5.7 Torque Speed curve for 90 kW motor..... 82
5.8 Current Slip curve for 90 kW motor..... 82

List of Symbols

R_1 Stator resistance of induction motor

X_1 Stator reactance of induction motor

R_m Core resistance of induction motor

X_m Core reactance of induction motor

R_2 Rotor resistance of induction motor

X_2 Rotor reactance of induction motor

R_2' Rotor resistance referred to stator

X_2' Rotor reactance referred to stator

s Rotor slip

s_f Forward slip

s_b Backward slip

N_S Synchronous speed of rotating magnetic field

N_R Rotor speed

ω_s Agular synchronous speed

V_{TH} Thevenin's voltage at certain terminals

Z_{TH} Thevenin's equivalent impedance between two terminals

R_{TH} Thevenin's equivalent resistance

X_{TH} Thevenin's equivalent reactance

f Supply frequency

T Torque

ρ Resistivity

σ Conductivity

μ Permeability

μ_r Relative permeability

δ Skin depth

F Magneto motive force

E Electric field intensity

B	Magnetic flux density
H	Magnetzing force
J	Current density
J_s	Surface current density
S_{NL}	Input Volt ampere at no load
Q_{NL}	Reactive Power at no load
P_{NL}	Real power at no load
P_{BR}	Input power under blocked rotor condition
I_{BR}	Blocked rotor current

Abbreviations:

VVVF	Variable voltage variable frequency
HTS	High temperature superconductor
PCIM	Pole changing induction motor
PWM	Pulse width modulation
FEM	Finite element method
NEMA	National Electric Manufacturer's Association
MMF	Magneto motive force
FOC	Field oriented control
HTS	High temperature superconductor
VSI	Voltage source inverter

Chapter 1

Introduction

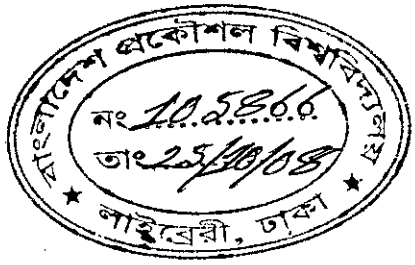

1.1 Historical developement of Induction Motor

Michael Faraday in 1831 discovered electromagnetic induction which was extensively used to model the performance of electric motors and generators. Later series of work were done by different scientists to develop commercial version of electric motors. In 1887, Nicolas Tesla introduced alternating current motors.

Electric motors are classified as dc and ac motors according to the type of supply used. Earlier types of motor were basically dc motors as dc supply was first commercially used in transmission and distribution networks. DC motors are again subdivided into i) Series motor ii) Shunt motor and iii) Compound motor. Series motors have high starting torques ($T_a \propto I_a^2$) while shunt motors have constant torque-speed characteristics. Compound motors integrate the advantages of high starting torque of series motor and constant torque characteristic of shunt motors. However, disadvantages of dc motors are: i)extremely low armature resistance, which requires starter to limit high starting current ii) sudden decrease of flux tends to raise the speed to an abnormally high value and causes unacceptably high inrush of current iii) DC motors have relatively complex construction and are expensive and also require frequent maintenance.

AC motors are mainly divided into two groups: i) Synchronous motors ii) Induction motors. Synchronous motors are not self starting and need to be started by auxiliary means. Besides, a dc source or sets of permanent magnets are required for the field circuit of synchronous motor. These motors are expensive and may need dual supply for operation. Induction motors are single source motors, simple to construct, rugged and inexpensive. Induction motors are classified as i) Squirrel Cage and ii) Wound rotor motors. In squirrel cage motors, solid aluminum bars are placed at the slots of the iron core of the rotor. Ends of these bars are short circuited at both sides by

shorting rings. Due to simple construction, ruggedness, low cost and easy operation, induction motors (specially squirrel cage induction motors) have beeome the most popular motors among all types of ac and dc motors. Disadvantages of squirrel cage motors are its low starting torque, high starting current and limitation of operation within a certain region called stable region. To improve starting performance, wound rotor induction motors are used where windings are placed in the rotor slots and their connections are brought outside so that additional resistance can be connected to improve starting performance. These motors are more expensive due to their relatively complicated construction.

Another commonly used induction motors are single phase induction motors which have the same type of rotors to that of squirrel cage rotors. Stator houses two sets of windings namely main and auxiliary windings placed at 90^0 apart. Such single phase motors are not self starting. So starting is achieved with the help of auxiliary winding in series with a capacitor.

As already mentioned, squirrel cage induction motors have the limitations of low starting torque and high starting current. Researchers have been trying to improve the starting performance of induction motors by various methods. Hadfield and his colleagues [1] were the first to demonstrate in 1900 that addition of small amount of silicon or aluminum to iron would reduce the iron loss by a factor of 4. Modern commercial electrical steel can be grouped under non-oriented, grain oriented and rapidly quenched alloy types of which first two dominate the applications in machine research. Silicon control is critical to the performance of electrical steel because it increases the resistivity, reduces the anisotropy and magneto-restriction but decreases the saturation and permeability. This makes the material more brittle. The continuing development of high permeability silicon steel, metallic glass, ferrites, aluminum ceramics, permanent magnetic materials like Neomax(Nd-Fe-B) and rare cobalts have been influencing the construction and design of machines.

1.2 Literature Review

Various conventional methods are adopted to improve starting performance of squirrel cage induction motors. High starting current and low starting torque are the two major factors that need to be improved for such type of motors. In conventional method, low starting current is achieved by starters. In this method, less voltage is applied during starting and then full voltage is gradually applied once the motor attains speed. As the starting torque is directly proportional to the square of the applied voltage, starting torque is significantly reduced in this case.

As the squirrel cage motors are inexpensive and easy to manufacture, substantial research work is being done to improve its overall performance.

Deep bar rotors [2], [3] are employed to enhance the starting torque with a decrease in starting current. This requires a complicated molding and casting process for the rotor which increases the manufacturing cost.

Research on the development of performance of Squirrel cage induction motors got further impetus due to availability of i) Solid state devices ii) Cheap micro-processor based systems iii) Artificial Intelligence(AI) tools and iv) CAD/CAM tools. Semiconductors and solid state switches like Thyristers, GTO's, MOSFETs, IGBTs etc. These devices have opened new dimensions for electrical switching and control of motors.

Better starting performance may be achieved by changing the stator voltage. The stator voltage may be changed by i) Ac voltage controller ii) Voltage fed variable dc link inverters and iii) PWM inverters [4].

Volts/Hertz [5] method is a popular technique to improve starting performance of a simple squirrel cage induction motor. In order to keep the air-gap flux constant, voltage to frequency (V/f) ratio should be kept constant. However, such a method needs complicated solid state switching devices and digitally controlled circuits. Switching circuits generate lot of harmonics which eventually heats up the rotor core. At low frequency, the air-gap flux is reduced due to drop in the stator impedance [6] and the voltage has to be increased to maintain the desired torque level.

Enhanced starting performance may be achieved in other ways [7] by changing the stator voltage. These are: i) scalar control ii) vector control and iii) adaptive control etc. This control system is generally characterized by two control loops: outer loop and inner loop. The outer loop controls the inner loop. The above three controls are suitable for improving steady state performance of the motor but the dynamic performance remains poor. For improvement of dynamic performance as well as steady state performance, Field oriented control (FOC) [8] has been adopted which decouples two components of stator current: one providing the air-gap flux and the other producing the torque.

Due to harmonic generation by solid state switching devices, attempts are being made to develop the properties of the materials used for the motor to enhance their performance.

The effect of rotor skew, rotor end rings and the distribution of electromagnetic field towards the axial direction affect the overall performance of induction motor. This was studied in [9] and it was shown that rotor bar currents and the rotor axial force developed greatly depend on rotor skew and size of end ring. The relationship between rotor bar current and rotor end ring current in cases of motors was studied without rotor skew and with rotor skew. It has been found that harmonics of rotor bar current and rotor end ring current become sufficiently small in case of rotor with large skew. Also there was slight increase of rotor torque with the increase of rotor skew. In [10], study was made to forecast the effect of end ring shape on the performance of squirrel cage induction motor. An algorithm was developed to determine the best size of end ring to meet user's specifications. Rotor resistance change can be predicted by change of end ring shape.

End ring inductance [11] has a significant influence on locked rotor current. The ring inductance can be splitted into leakage component and the component that couples between the end ring and the end winding. Simulation results show that by varying this coupled inductance i.e. by changing the size of the end ring, the locked rotor current may be contained within some acceptable limit.

Double cage rotors are used for high starting torque. The action of double cage rotor relies largely on the difference between the inductance of inner and outer cages which is emphasized by lengthening or reducing the width of that part of the slot that

lies between them. This produces low reluctance path for the flux driven by inner cage current. Rotor equivalent circuit parameters can be changed by changing the width of the slot [12].

In [13], theoretical, numerical and experimental studies have been carried out to develop a solid rotor design for high speed application such as drive for diesel engine turbo-charger. For high speed application, the mechanical strength of solid rotor is recognized as significant benefit and makes it possible to construct motors having higher ratings than that of squirrel cage design.

Due to high frequency current during starting, rotor current distribution becomes highly uneven and causes thermal stress between upper and lower portions of the rotor bar. In [14] with visual aided finite element method electromagnetic field and the thermal stress during starting has been analyzed.

The concept of introducing paramagnetic rotor bars to improve starting performance has been highlighted in [15]. In this paper new paramagnetic rotor material was made by mixing small fraction of iron with aluminum and the mixed material was casted in rotor slot to make new paramagnetic rotor.

Theoretical study was made in [16] to predict motor performance. For design and analysis, the equivalent circuit was obtained by splitting the rotor bar into equal units such that current density was uniform along the depth of each unit. The bar was splitted into unequal depths having greater number of smaller sections at the top of the bar and fewer larger sections at the bottom.

Dependence of the rotor resistance on the shape and size of end ring has been analyzed by 2-D and 3-D finite element method in reference [17]. End leakage flux and size of end rings have been considered for such analysis. The resistance of the bar was found to have influenced by shape of the end ring. Simulation results show that for a particular model, end leakage inductance is 14% of primary leakage inductance. Increase of axial length of rotor conductor has been proposed in [18] resulting increase of efficiency.

High conductivity materials have been proposed as cage materials to improve the motor performance. In [19] test results were obtained for similar motors having aluminum and copper as cage materials. Experimental results show an improvement of efficiency of maximum 3% for motors ranging from 1kW~3kW with copper as

the cage material. For bigger size motors, improvement has been in the range of 1.2~1.6%. In [20], two bars of copper rotors have been suggested namely starting bar and the running bar. Rotor resistance increased during starting for such arrangement.

The incorporation of copper as conductor bars and end rings of induction motor in place of aluminum results in the improvement of motor performance. Six different sizes and types of rotor were die-casted using pure and high conductivity copper for different motor companies [21]. Compared with identical aluminum rotor, die cast copper rotor reduced total energy losses by 15-23% [1.2-1.7% improvement in efficiency over aluminum] depending on the rotor design. The shape of torque-speed curve is quite sensitive to the rotor circuit resistance which in turn is inversely proportional to the conductivity of the conductor bar material and its cross-sectional area.

Three design strategies have been investigated in [22] to improve efficiency of induction motors. The strategies are: a) substituting the copper cage with aluminum cage with standard electrical steel without changing any motor dimension. b) Substituting copper cage with aluminum cage with high performance electrical steel without changing any motor dimension and c) Design optimization of copper cage motor by changing stator winding and the stack length.

Eight high efficiency designs have been proposed in [23] with trapezoidal slots and rectangular teeth. Such designs resulted in higher efficiency motors.

Induction motor analysis was done by considering both harmonics and end effects using 2D and 3D finite element method in [24]. The characteristic of induction motor is influenced by electro magnetic fields at the ends of the motor. The secondary resistance was determined by finite element method as a function of inner radius difference of the end ring. End ring resistance decreases exponentially with the increase in difference of inner radius.

A model has been developed in [25] based on coupled magnetic circuit theory and complex space vector analysis taking into account the actual non sinusoidal rotor bar current distribution. Both stator and rotor circuits were modeled by four coupled differential equations. The rotor bar currents were changed by modifying the bar and end ring resistance to obtain better starting performance. In [26[, resistance and

leakage reactance of end rings of a cage induction motor has been determined from the impedance of an identical ring that carries a circulating current of certain frequency. Such resistance and reactance thus determined have been used for consideration of impedance of end rings in machines to improve starting performance. A method using AC PWM chopper has been suggested in [27] to improve the efficiency of induction motor by controlling the input power. The source voltage was controlled by a power controller unit. The current for various loading was detected and stored in micro computer memory and the source voltage was adjusted till minimum starting current was obtained.

An algorithm for improving efficiency of a lightly loaded, field oriented induction motor drive has been developed [28]. This has been accomplished through determining optimal torque per flux ratio necessary for obtaining the desired flux position. A relation in terms of motor speed and optimal torque per flux ratio has been derived. The results show that an efficiency improvement is achieved specially at light loads along with high dynamic performance obtained through applying the field oriented concept.

A new material termed as HTS (High temperature superconducting) tape has been used in [29] as rotor bars and rotor end ring to enhance efficiency and starting torque. Starting torque obtained with HTS (High temperature superconducting) tape has been found to be appreciably higher for the same size aluminum rotor motor.

Winding harmonic has significant impact on starting performance. The variation in the starting performance can be predicted based on the type of harmonic generated. In [30] it has been shown that excessive winding harmonic generation deteriorates the starting performance.

A six phase pole changing induction motor (PCIM) has been proposed in [31] for application in electrical vehicles. A new prototype PCIM has been designed which gave better steady state characteristic.

A new control strategy has been proposed in [32] to improve starting torque without changing main circuit of the soft starter. The strategy defines triggering instants of Thyristers to include or exclude half cycles of ac power. The strategy is similar to that of VVVF inverters to make the motor to have low starting current and high starting torque. To obtain high efficiency motors [33], the following design strategies

have been investigated: i) substituting aluminum cage by copper cage and standard steel without changing of dimension, ii) Substituting aluminum cage with copper cage and high performance electrical steel without change of motor dimension, iii) Design optimization of copper cage motor by changing stator winding and stack length and iv) design optimization of copper cage by changing the stator winding, stack length and stator and rotor dimensions. Standard design copper cage with premium steel showed increase in efficiency of 2.5% when compared to the aluminum motor of same rating. Higher stack length with premium steel showed an overall increase of efficiency by 4.8%.

One major point in the design of high efficiency motor is to reduce the rotor resistance. Better conducting material like copper is used as cage material. However there are alternative designs to increase the cross-sectional area which helps to improve efficiency and at the same time influences the torque performance. In view of this, two design concepts [34] have been analyzed. First one consists of 48 slot stator and 36 slot rotor. The second one has the same stator layout but with 40 slot rotor. It has been found that efficiency for 48/36 combination was 91.5% and for 48/40 combination was 91.7%. 48/40 combination produced smaller slip for the same load leading to lower copper loss. Power factor was almost identical in both the cases and starting current was slightly less in the 36 rotor slot.

In [35] the performance of 3-phase 6-pole, 400W inverter driven induction motor was investigated using a variety of non-oriented electrical steel for stator core at PWM inverter fundamental wave frequencies of 30-300Hz. There existed an optimum silicon (si) content of the material depending on the tooth flux density. Both reduction of material thickness and stress relief annealing of the stator core improved motor efficiency. The influence of si.content on the efficiency was small at lower PWM frequencies while at higher frequencies, motor efficiency increased with the increase of si content. Newly developed materials RMA having lower iron losses after stress-relief annealing and higher flux densities with lower si contents showed motor efficiencies superior to the conventional JIS grade materials with comparable iron loss.

The variation of slot dimension on the performance of induction motor has been highlighted in [36]. In deep bar squirrel cage rotor model, starting bar diameter was

varied from 2mm to 10mm and then slot height was varied from 1mm to 5mm holding starting bar diameter constant. Starting torque was the highest for rotor bar diameter of 5mm or above or below which starting torque showed gradual decay. However, efficiency showed marked improvement with the increase of bar diameter. In case of change of bar height, starting torque increased with the increase of height but the efficiency consistently reduced.

In order to limit starting current, a novel method has been proposed in [37]. DC supply is momentarily connected to one of the stator winding and then another coil is momentarily connected. Once the motor starts up, normal supply may be applied to the motor. Starting current may be derived from a charged capacitor.

A high starting torque induction motor has been designed in [38] having two end rings. The first end ring is fixed on the rotor while a second moveable end ring having lower resistance than the first ring and a centrifugal device associated with the second ring and operable upon the rotation of the rotor such that first ring connected at starting produces high torque and the second ring engages at running thereby reducing the overall resistance.

In [39] starting characteristic of induction motor has been studied with the help of Fuzzy controller. By measuring input current and processing Fuzzy inference the Fuzzy controller can change the control angle of Thyrister to apply increased voltage to obtain better starting and running performance.

The rotor of an induction motor has been replaced by a permanent magnet (U-shaped permanent magnets buried in the rotor below squirrel cage) rotor [40] to achieve an efficiency that meets the highest requirements of the motor class.

A method has been presented in [41] for predicting the performance of saturister induction motor with idle bars of permanent magnet material in rotor slots. It has been shown how the analysis may be used to synthesize the physical design of a motor in order to achieve a specified starting performance. This procedure has been applied to design a 400Hz aircraft motor to obtain reduced starting current compared with the original cage motor without significant detriment to its normal running performance. Test results demonstrate validity of the treatment and the success of an experimental design incorporating bars of Hycomax III.

Normal aluminum cage rotor can be used to provide [42] multiple resistance characteristic. By segmenting the end rings in such a way that a particular rotor bar is not electrically connected to the adjacent rotor bars rather to some specific rotor bars by segmented shorting rings. Thus the current tends to flow through the steel core of the rotor. However when the motor attains its full operational speed, the segmented shorting rings are shunted and all the rotor conductors are connected to the end ring so that running performance of the motor does not degrade. The first method of shunting the segmented shorting ring is a mechanical arrangement which delays shunting action. The second method of shunting is a solid state switching device and the circuit is confined entirely within the rotor with no connection to the motor winding or frame.

In [43], two sets of end rings, resistance of the first end ring is higher than the other are installed on the rotor. The first end ring is permanently connected to the rotor bars and the second end ring operable at a pre-determined speed by solid state device can lock in parallel with the first ring. At start, high resistance of the first ring produces high starting torque with low starting current and the second ring engages at a pre-determined speed reducing the effective resistance of the rotor. The overall efficiency of the motor remains unaffected.

Rotor is made by a solid Ferro-magnetic cylinder in [44] over which iron coating alloys of high electrical conductivity (termed as screen) is rigidly mounted on the rotor surface. The screen exhibits a multi-layer structure, conductivity of each succeeding layer decreases towards the outer periphery. At the start of the motor, due to high frequency and the skin effect, the rotor resistance increase which in turn increases the starting torque and decreases the starting current. At normal speed, with the decrease of the rotor frequency, rotor resistance swings back to the normal value and thus the motor running performance remains unchanged.

In a double cage rotor of [45], resistance of rotor circuit is increased by reducing the thickness of the end rings near the outer periphery of the conductors while the end rings connecting the inner cage are kept thicker.

In [46], it has been proposed to start the induction motor and then fill-up the rotor space with liquid nitrogen to achieve superconductivity once the motor is running.

Although desired result may be achieved by this method, but the method is not practical.

Two cages similar to the double cage rotor having two sets of cage materials have been proposed in [47]. The outer cage is made of high resistance material like brass and inner cage of low resistance material such as copper. Upon start, skin effect limits the rotor current by means of high resistance brass material in the outer cage while skin effect is lessened afterwards and rotor current can penetrate deep into the rotor reducing the rotor resistance. High resistance at the start of the motor limits the high inrush current and increases the starting torque. As the rotor resistance is reduced with the increase of rotor speed, the overall efficiency of the motor is unaffected.

Fractional windings of induction motors are analyzed in [48] to reduce the end winding length and to clean the air gap mmf from the point of view of spatial harmonics. Amount of copper can be reduced by proper arrangement of the windings. The example presented in the paper for a 1.5 slot/pole/phase shows the possibility of improved performance (efficiency, pf, starting torque, noise level).

A poly phase (12 phase) induction machine operated by an inverter drive system can be constructed with concentrated full span winding. Twelve or more phases have been used to sufficiently cover the air gap region in contrast to the conventional three phase using distributed and chorded windings. Improved efficiency and starting torque has been achieved by such arrangement in [49].

In an induction motor having short circuited rotor windings, extra magnetizable pipes/tubes are inserted in [50] with projections at both ends of the rotor. The tubes are made of cast magnetizable materials. By utilizing skin effect in the tube, the starting performance has been improved at high rotor frequency. And at running condition, with reduction of skin effect, the overall performance of the motor remains unchanged. Hollow tubes also perform self ventilation and reduce heating of the conductor.

Rotor windings are wound on the poles of each of two salient pole type rotor cores and the rotor windings on the salient poles axially aligned on the two cores are series connected in [51]. Two stators and two dc magnetic excitation windings surround the face of two rotor cores. A voltage phase shifter is provided to one of the two stators

to selectively produce a phase difference of $0\text{-}180^0$. With such arrangement, motor produces a large starting torque as well as large running torque.

V/f operation at low frequency is challenging due to non linear behavior of modern pulse width modulated voltage source inverter (PWM-VSI). In [52] a new stator resistance and frequency compensation technique has been proposed. The stator resistance voltage drop is fully compensated by vectorially adding this drop to the supply voltage using both in phase and quadrature components of the stator current. Frequency compensation is based on estimation of air-gap power and a non-linear relationship between slip frequency and air-gap power. It has been shown that large torque is obtainable even in the low speed range with almost no steady state error in speed.

Enhanced motor starting performance was obtained in [53] by employing two types of Bi-2223/Ag multi filamentary tapes over the conductors of squirrel cage rotor. Tests have been performed after the fabricated motor was immersed in liquid nitrogen. The motor starting performance was enhanced at temperatures ranging from 65 to 77K.

Starting of large motors especially for reversible pumped storage purpose has been designed in [54]. One method of starting such large motors (having high inertia load) is by means of a starting motor which is mounted directly on the main machine shaft. In such an arrangement, a large wound rotor is often used which is expensive and requires a rheostat (usually water rheostat) to dissipate the energy involved during starting. In the investigation of [54], a hollow ferromagnetic rotor has been designed which comprises of a relatively thin ferromagnetic rim serving as rotor winding. In order to reduce the starting current, a poly phase saturable reactor is connected with the stator windings.

The shape of torque-speed curve of a solid rotor machine is dictated by a dimensionless parameter called Gamma factor (.GAMMA.). In [55] generalized torque-speed curves for solid rotor, eddy current couplings has been given. It has been shown that a homogeneous ferromagnetic rotor has a .GAMMA. factor which provides good starting characteristics is in the range of 0.1 to 0.3 depending on specific requirements.

In [56], a .GAMMA. factor of 0.1 to 0.3 is achieved by placing conducting materials in axial grooves. Number of grooves is so chosen to keep .GAMMA. factor within 0.1 to 0.3 which gave minimum high frequency loss and reduced parasitic reluctance torque with overall increase of starting torque.

In [57], a methodology has been defined to identify the electric conductivity and permittivity of lossy dielectric materials employed in a class of small di-electric motors. The stators and rotors are hollow cylinders made of dielectric materials. For a given set of material properties, the time averaged value of the starting torque produced is evaluated by finite element method. A family of curves of starting torque of induction motor Vs conductivity for different values of rotor permittivity is obtained. This method can be applied to estimate the conductivity of rotor conductor that gives rise to prescribed value of starting torque.

1.2.1 Summary on end ring work

Researchers have tried to improve the performance of squirrel cage induction motor by modifying the design of the end ring. End ring had been a focal point for performance enhancement (specially starting performance enhancement) for its unique location in the rotor of the squirrel cage motor. For squirrel cage induction motor, end ring is easily accessible and any design modification can be easily implemented in that region of the rotor. Some research work done on the end ring portion of squirrel cage motors to improve performance of induction motors are described below:

A high starting torque induction motor was designed having two end rings. The first end ring having higher resistance than the second ring was fixed to the rotor bars like normal squirrel cage rotors. The second end ring was moveable and can be fixed or detached from the first ring by a mechanical device. The motor is started with the first end ring in the rotor circuit. As the motor speeds up, the second end ring is engaged by centrifugal action with the first end ring. Thus at start, the rotor resistance becomes high that enhances the starting torque and at the same time reduces the starting current. At the normal speed of the motor the overall resistance of the rotor becomes less due to engagement of the second ring in parallel with the

first so that running performance is not hampered. Such an arrangement of employing two end rings not only makes the manufacturing process extremely complicated, but also enhances the motor size for the same rating of the motor. Also frequent maintenance will be needed for the whole assembly. Also there may be possibility of improper engagement of the second ring with the first one which may affect the running performance of the motor.

Another research work suggests to make segments in the end ring in such a way that particular rotor bar currents are forced to pass through the core of the rotor. The purpose is to increase the rotor resistance so as to improve the starting performance of the motor. As the motor speeds up, the segmented end rings are either shunted by mechanical device or by solid state switches.

End ring segmentation and then subsequent short circuiting these end ring segments for normal running of the motor also involves special techniques which make manufacturing process complicated. Forcing rotor current to pass through selected section of the core makes the rotor resistance extremely high which may give rise to sluggish response of the motor. In this case also, frequent maintenance of the rotor will be necessary. Special circuit has to be designed and embedded in the rotor for shorting the end ring sections by solid state devices.

A new material termed as HTS (High temperature superconducting) tape is used in rotor bars and in end rings to utilize its high skin effect to improve motor performance.

Employment of HTS tape over the end ring produces high skin effect at the start of the motor. However, whole motor assembly has to be kept at extremely low temperature to utilize the superconducting property of the HTS tape. Such motor construction and operation is expensive and may be used for special applications where high torque and high efficiency are required.

Modifications in the design of end rings have also been made in the double cage squirrel cage induction motors to improve its starting performance. For such motors, rotor resistance is increased by reducing the thickness of the end ring near the outer peripheri of the conductors. The end ring of the inner cage is kept thicker to keep its resistance low. At start, due to skin effect, the overall rotor resistance becomes high to improve the starting performance of the motor. At the rotor normal speed, skin

effect is lessened and the current is distributed among the inner and outer peripheri and the overall rotor resistance falls. Thus the running performance is not adversely affected.

Double cage rotors are not commonly used for its comparatively high cost and complicated manufacturing process. Although under normal running condition of the motor, the overall rotor resistance falls, but due to employment of thin end ring in the outer peripheri of the rotor conductors, higher rotor resistance is always present in the rotor circuit to affect the running performance of the motor.

Rotor inductance can be changed by changing the dimension of the end ring. The ring inductance can be splitted into leakage component and mutual component (that couples between end ring and end winding) of the motor. By proper design of the end ring shape, the rotor inductance can be varied to limit the locked rotor current.

Such change of inductance by modification of the end ring design remains as a constant parameter in the rotor and may affect the running performance of the motor. Also there is limited scope for variation of the end ring dimension due to space constraint in the rotor. Moreover change of rotor inductance is not significant due to small flux linkage in the end ring region of the motor.

Similar study on the effect of size of end ring on the motor starting performance was analyzed by simulation program. End ring flux linkage and end ring size produced change in rotor impedance. By the simulation program, optimum size of the end ring that may produce better starting performance can be determined.

In this case also the change of impedance due to end ring flux linkage is small and significant starting performance cannot be achieved by such modification in the end ring design.

1.3 Problem Identification

It is evident from the literature review that improving starting performance of squirrel cage Induction motor is a complex task and various methods are being adopted for the improvement which may fall into two broad categories:

1) The cage portion of the rotor may be designed to reduce starting current and enhance the starting torque with a relatively simple change in design of cage bars

with a view to increase the resistance of the rotor at the start of the motor. Also rotor reactance is altered to reduce the starting current.

2) Most frequently used method of reducing high current on start-up is done with reduced voltage controllers. Reduced voltage controllers (starters) can be subdivided into five categories: a) auto-transformer starters b) wye-delta starters c) part winding starters d) primary resistor starters and e) solid state starters.

Modifying the squirrel cage is a novel and economical method which eliminates the need for any reduced voltage starting equipments. The motor is directly started at full voltage. However rotor has an internal regulating means which limits starting current during rotor acceleration period. After the rotor has reached the operating speed, the regulating means readjusts for normal operation.

In most cases, reduction in inrush current and enhancement of starting torque is achieved by designing a rotor which has two or more resistance values for rotor cage. At start-up, resistance of this cage becomes high and afterwards drops down to a low value when the motor attains its rated speed.

Change of rotor resistance can be achieved by changing the shape, dimension of rotor end rings. However, this change is accompanied by insignificant change of rotor resistance. If the user's specification requires high resistance for improving starting performance, end ring shape may be altered accordingly, however, this high resistance will always be present in the rotor circuit to affect its running performance. In case of double cage rotors, length/width of a cage is modified to attain a low reluctance path for the flux driven inner cage current.

High conducting materials are being used for cage materials to improve the efficiency of motors. However, major problem of high starting current and low starting torque remains in this case. For the same size motors, use of copper gives an overall efficiency improvement of 1.5~2% for 1~3kW motors. Copper casting is a difficult process as the melting point of copper is high. Research is going on to improve the copper casting techniques. Higher efficiency motor design is being adopted by using bigger rotor slots or slots of special shape like trapezoidal slots.

Two end rings were simultaneously used to improve the starting performance without affecting the overall efficiency. At start, only one ring having higher resistance was coupled with the rotor bars to increase the rotor resistance and then at

rated speed both the end rings were engaged to reduce the overall rotor resistance. To achieve this, manufacturing of rotor becomes complicated.

The concept of introducing Ferromagnetic rotor bars i.e. mixing iron with the Aluminum utilizing skin effect property yielded better starting performance. Introduction of iron in aluminum makes the liquid aluminum more viscous and there is high possibility of void space formation during casting. Voids in rotor bars cause excess heat generation due to non uniform resistance. Also due to non uniform distribution of current between upper and lower ends of a rotor bar (which will be prominent for big size motors) uneven axial force as well as thermal stress may be produced for such rotors.

1.4 Thesis objective

The aim of the thesis is to achieve enhanced starting performance of a squirrel cage induction motor i,e increasing of starting torque and decreasing of starting current by insertion of ferromagnetic materials in the rotor. Particular attention is given so that running performance is not degraded while improving the starting performance of the motor.

As a first step in achieving the goal of enhanced starting performance, the dimension of the material to be inserted in the rotor end ring is continuously modified through simulation software MATLAB till an optimum torque-slip curve is obtained that produces enhanced starting torque without degrading the running performance of the motor. Improved rotor design thus obtained is fabricated and its performance is determined experimentally to compare with the results obtained through MATLAB simulation. Experimental results and concept of ferromagnetic insertion in the rotor are further validated by SLIM software popularly used to evaluate motor performance.

In this research work, an improved method has been proposed to enhance the starting performance of a squirrel cage induction motor by insertion of ferromagnetic materials (in the form of iron strips) at the end rings. The iron strips inserted at the end ring between the rotor conductors will increase the overall resistance of the rotor due to flow of current through the surface of the strip at the power frequency during starting of the motor. This increases the starting torque and reduces the starting

current. As soon as the motor attains its rated speed, current distribution through the ferromagnetic strip becomes normal, rotor resistance decreases appreciably and the motor runs at normal efficiency.

Introduction of ferromagnetic strip at the end ring is not only an easy process from the fabrication point of view but also avoids formation of void space (in case of mixing magnetic material with aluminum during casting) and prevents brittleness and generation of excessive thermal stress.

1.5 Thesis outline

This dissertation is divided into six chapters and an appendix. Chapter-1 focuses on the chronological history of induction motor and the literature review on the starting and running performance of squirrel cage induction motors.

Chapter-2 highlights the basic principles related to three phase and single phase induction motors. Basic formulae for torque, current of both three phase and single phase motors are presented in this chapter. NEMA design classes for squirrel cage motors and two commonly used squirrel cage rotors for starting performance enhancement are also described in this chapter. Harmonic generation in induction motors and total harmonic distortion (THD) are also included here.

In chapter-3 effect of ferromagnetic insertion in the rotor circuit has been described. Theory of skin effect with relevant formulae is presented here. Variation of resistance of ferromagnetic strip as a function of frequency is highlighted with necessary simulation curves. Different possible methods of ferromagnetic insertion in the rotor are also discussed in this chapter. Subsequently the optimum location of ferromagnetic insertion has been suggested.

In chapter-4 experimental design process has been discussed first. Then a mathematical model has been developed taking into consideration the skin effect in the ferromagnetic strip after insertion in the rotor end ring. Through a simulation program different performance curves are plotted with insertion of different number and size of iron strips in the rotor. Experimental verification of the proposed scheme is also presented in this chapter. To study the effect of ferromagnetic insertion in the squirrel cage rotor of single phase induction motor, experimental work was done on a single phase motor ¼ hp motor.

Harmonic generation with and without ferromagnetic insertion in the rotor was also studied here.

Validation of the proposed scheme is presented in chapter-5. The validation results were achieved through theoretical calculations made on the mathematical model of the machine and also through simulation software SLIM.

Conclusions, limitations of the work, scope for further research are given in chapter-6. Relevant mathematical formulae and experimental results, motor data etc. are presented in Appendix of the thesis.

Chapter 2

Basics of induction motor

2.1 Equivalent circuit of induction motor

Following is the standard equivalent circuit of a squirrel cage induction motor.

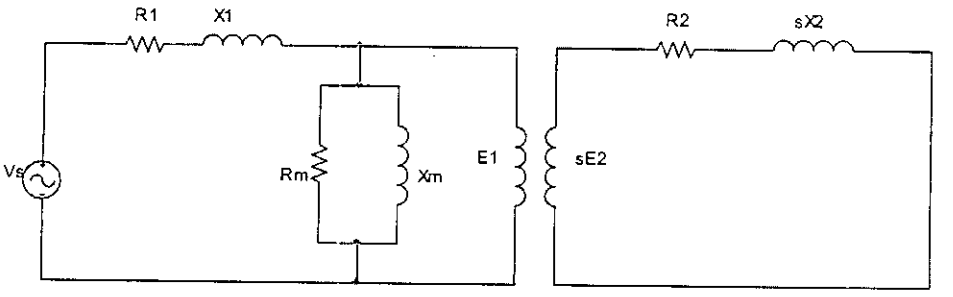

Figure 2.1: Equivalent circuit of an induction motor

The above circuit of Fig.2.1 may be modified as:

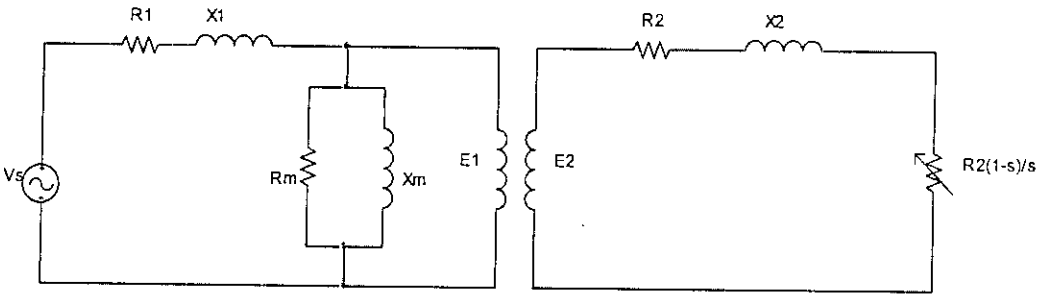

Figure 2.2 Modified equivalent circuit of induction motor

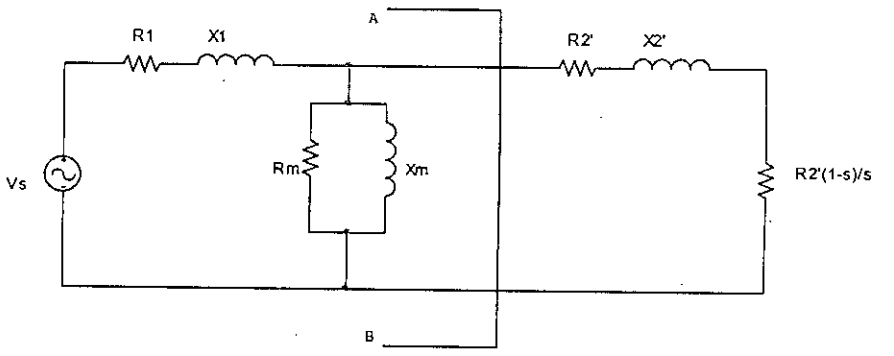

Figure 2.3: Applying Thevenin's Theorem at A-B

In practical case, $R_m \rangle\rangle X_m$, so in the mathematical formulae and in the Thevnin's equivalent circuit R_m has been neglected.

Thevnin's Voltage $V_{TH} = \dfrac{V_s \times jX_m}{R_1 + j(X_1 + X_m)}$ (2.1)

And Thevenin's equivalent Impedance $Z_{TH} = (R_1 + jX_1)//jX_m$

$= R_{TH} + jX_{TH}$ (2.2)

The circuit of Fig.2.3 reduces to:

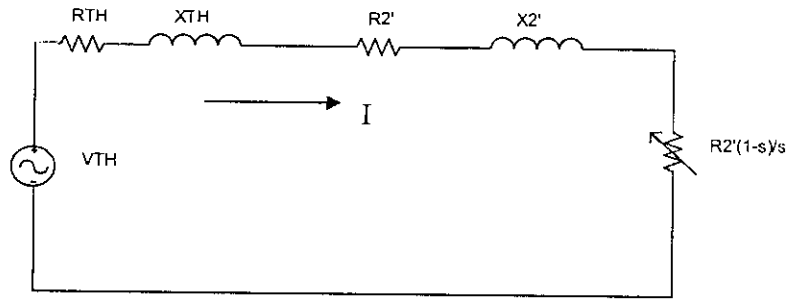

Figure 2.4: Thevenin's Equivalent circuit

$$I^2 = \frac{V_{TH}^2}{\left\{\left(R_{TH} + \dfrac{R_2'}{s}\right)^2 + \left(X_{TH} + X_2'\right)^2\right\}} \quad (2.3)$$

and the developed torque $T = \dfrac{3 \times I^2 \times \dfrac{R_2'}{s}}{\omega_s}$

$$= \left(\frac{3}{\omega_s}\right) \frac{\left(V_{TH}^2 \times \dfrac{R_2'}{s}\right)}{\left(R_{TH} + \dfrac{R_2'}{s}\right)^2 + \left(X_{TH} + X_2'\right)^2} \quad (2.4)$$

The standard torque equation for an Induction motor is given by the following formula

$$T = \frac{(3/\omega_s) \times V_{TH}^2 \times R_2' / s}{(R_{TH} + R_2/s)^2 + (X_{TH} + X_2)^2} \quad (2.5)$$

Where ω_s is the angular synchronous speed, R_2' is the rotor resistance referred to the stator, X_{TH} and R_{TH} are the Thevenin's equivalent reactance and resistance respectively and V_{TH} is the Thevenin's voltage applied at the core reactance point. It is seen that the developed torque is a function of the square of the applied voltage and the slip. During starting(s=1), $(X_{TH}+X_2)^2 >> (R_{TH}+R_2)^2$ and the torque becomes a function of R_2' i.e.$T \propto R_2'$

The main problem for squirrel cage induction motor is i) its high starting current [load resistance $\frac{R_2'}{s}(1-s)$ =0 during starting] and ii) low starting torque (as the rotor resistance is normally small). In order to enhance starting torque, extra resistance has to be added with the rotor circuit which should be by-passed once the motor reaches the rated speed.

Certain features of torque-slip curve are shown in figure 2.5 when the supply voltage remains constant.

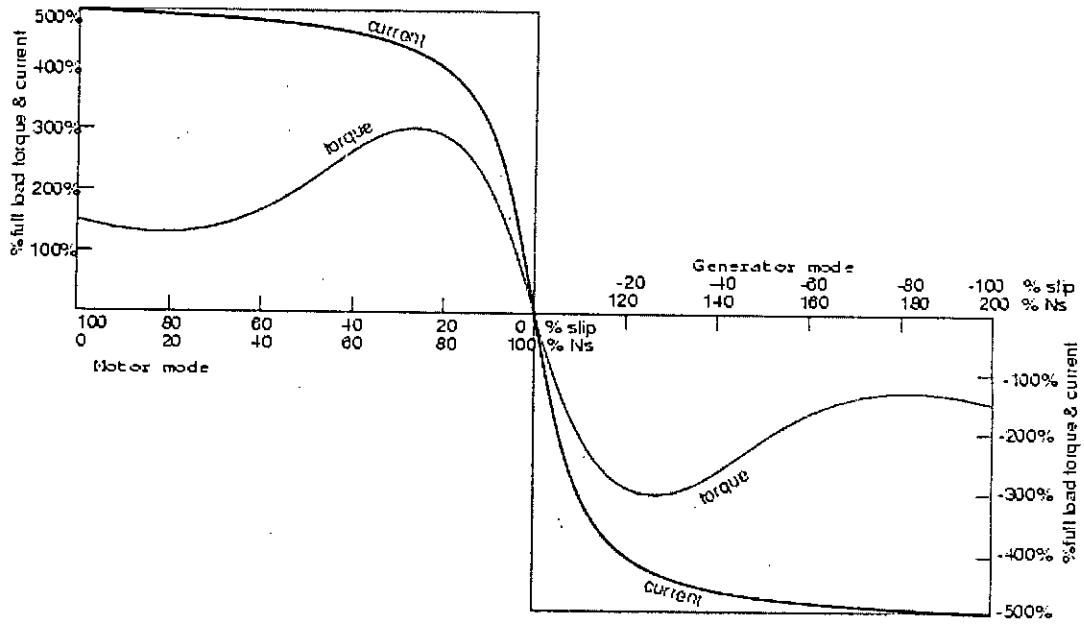

Figure 2.5: Torque/Current vs. Slip Curve for an Induction Machine showing Motor and Generator mode operation.

Motoring Mode ($0 \le s \le 1$)

In the motoring mode, mechanical power or load developed is in the direction in which the rotor rotates.

Generating Mode (s< 0)

Negative slip implies that rotor is running at super synchronous speed i,e $n>n_s$. This means that mechanical power has to be supplied to generate electrical power.

Breaking Mode

The motor runs in opposite direction to the rotating field absorbing mechanical power which is dissipated as heat in the rotor copper.

Condition for Maximum Torque:

Maximum torque occurs when $\frac{R_2'}{s_{max,T}} = \sqrt{R_{TH}^2 + \left(X_{TH} + X_2'\right)^2}$ (2.6)

And to have maximum torque at starting, $s_{max,T} = 1$

$$\text{Then } R_2' = \sqrt{R_{TH}^2 + \left(X_{TH} + X_2'\right)^2} \quad (2.7)$$

2.2 NEMA Design

Design Types of Induction Motor (NEMA Design):

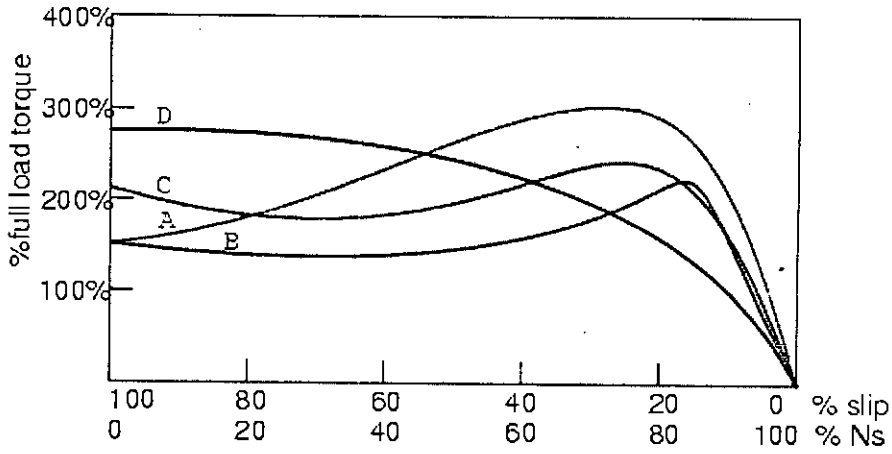

Figure 2.6: Torque slip curve for different NEMA design Induction motors

National Electric Manufacturer's Association (NEMA) standardized five basic design categories of Induction motor to match torque-speed requirement of most common types of mechanical loads by different rotor construction.

Design class C has its maximum torque at starting, so also design class D. Design D has a higher maximum torque than that of C. Class A and B have maximum torque at a slip of 15%. Design class E (Energy efficient motors) has a torque-slip characteristic similar to class B.

Class D has higher rotor resistance and low reactance bar situated close to the surface. Class B & A have low resistance rotor bars that extends deep into iron resulting low rotor resistance and high blocked rotor reactance. Class C combines features of both B and D: high resistance and low reactance at the surface and low resistance, high reactance at deeper bars.

2.2.1 Deep Bar Rotors:

In this type of construction, bars of narrow width are laid down in deep semi-enclosed slots. The rotor bars may be considered as composed of elementary strips in parallel (top most and bottom most strips are shown). Much larger flux links with the bottom element strip. As a consequence, starting reactance for bottom strip becomes much larger than the top strip. The overall resistance at starting increases. At higher speed, reactance falls and the current density over the conductor cross-section becomes uniform.

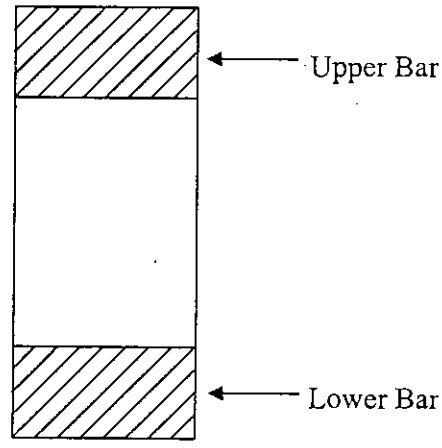

Figure 2.7: Deep Bar Rotor

2.2.2 Double Cage Rotor:

The squirrel cage rotor in this case, consists of layers of bars shorted by end rings. The upper bar has a small cross-sectional area than the lower bar. Outer cage has a higher resistance and lower reactance while the inner cage has high reactance and low resistance. As a result during start, current is mainly confined in the upper cage with consequent decrease in starting current and increase in starting torque.

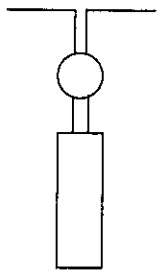

Figure 2.8: Double Cage Rotor

Torque control of Induction motor:

$$T = \left(\frac{3}{\omega_s}\right) \frac{\left(V_{TH}^2 \times \frac{R_2'}{s}\right)}{\left(R_{TH} + \frac{R_2'}{s}\right)^2 + \left(X_{TH} + X_2'\right)^2} \tag{2.8}$$

From the torque equation, it can be seen that developed torque is a function of square of the applied voltage, slip and rotor resistance. During starting (s=1), $(X_{TH}+X_2')^2 >> (R_{TH}+R_2')^2$ and T becomes directly proportional to rotor resistance R_2'. The main problem for squirrel cage induction motors are i) high starting current [load resistance $\frac{R_2'}{s}(1-s) = 0$ during starting] and ii) low starting torque. In order to enhance the starting torque, extra resistance has to be inserted which should be by-passed once the motor attains its rated speed or the supply voltage has to be increased within the rated voltage limit of the motor. As most of the commercially available motors are of squirrel cage type, adding extra resistance in the rotor circuit

and by-passing this extra resistance at the rated speed is not possible. The other option left is to increase the starting torque is to increase the supply voltage which is not also an option as motors have fixed rated voltage. Besides, for optimum motor performance, increase of voltage requires proportional increase of frequency (to keep V/f constant). This requires complicated circuits which generates lot of harmonics and eventually heats up the motor to degrade its performance. Thus improvement of starting performance by solid state devices are complicated as well as expensive. In this research work, squirrel cage rotor geometry has been modified to obtain optimum starting performance without degrading the normal running performance.

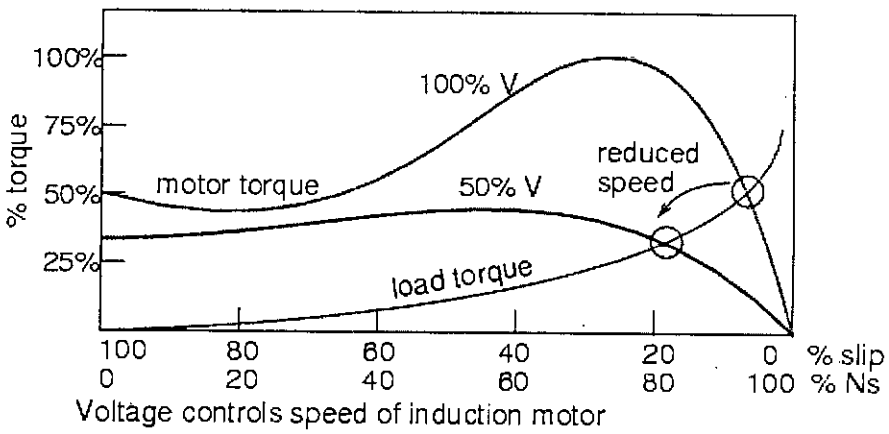

Figure 2.9: Effect of voltage on Torque-slip curve

2.3 Single Phase Induction Motor

A single phase Induction motor has a single phase distributed winding on the stator and a normal squirrel cage rotor.

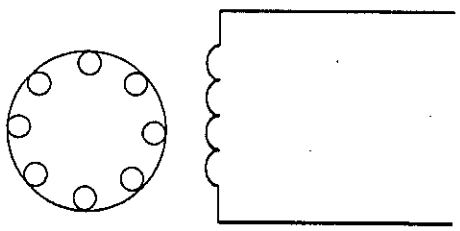

Figure 2.10: Single Phase motor with main winding

When winding carries a sinusoidal current, an MMF is produced which has both space and time distribution expressed as:

$$F = F_{max}\cos\theta\cos\omega t = 1/2F_{max}\cos(\theta-\omega t) + 1/2F_{max}\cos(\theta+\omega t) \quad \text{where} \tag{2.9}$$

$1/2F_{max}\cos(\theta-\omega t)$ is the forward rotating field = F_f and

$1/2F_{max}\cos(\theta+\omega t)$ is the backward rotating field= F_b

Rotor slip with respect to two rotating fields:

If n is the speed of the rotor in the forward direction,

$$\text{then } s_f = \frac{n_s - n}{n_s} \tag{2.10}$$

$$\text{and } s_b = \frac{n_s - (-n)}{n_s} = \frac{2n_s - (n_s - n)}{n_s} = (2\text{-}s) \tag{2.11}$$

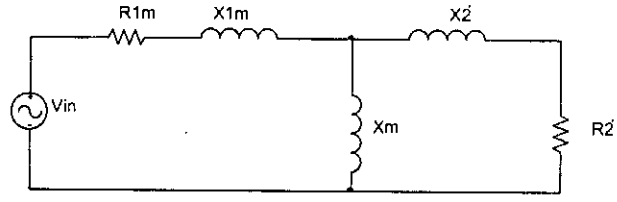

Figure 2.11: Equivalent circuit of 1-phase motor with rotor stationary

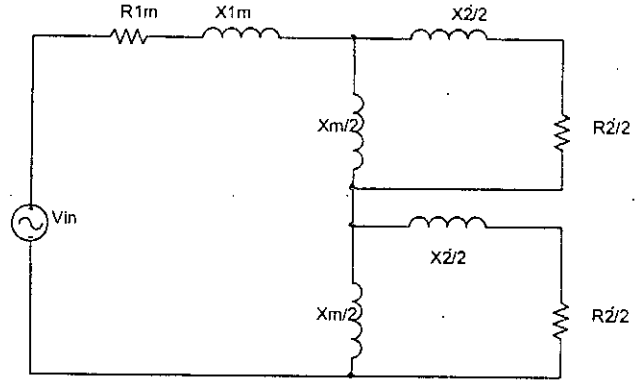

Figure 2.12: Equivalent circuit highlighting two field theory with rotor stationary

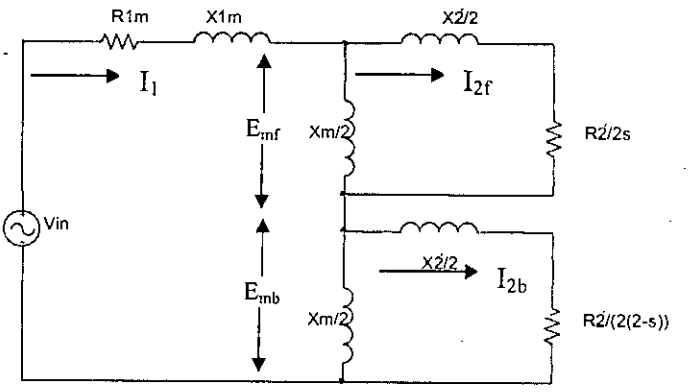

Figure 2.13: Equivalent circuit under running condition

2.3.1 Torque-speed Characteristic

The two rotating fields have the same strength and produce equal and opposite torque resulting a net starting torque of zero. If the rotor is made to run at speed n in the direction of forward field, the two slips are now 's' and (2-s) respectively. For normal operation, (2-s)>>s and as a result, backward field induced rotor currents are much larger than at stand still and have a low power factor. On the other hand, low slip forward rotating field induces smaller current of higher pf in the rotor than at stand still. This leads to great enhancement in the forward flux wave.

The impedance due to forward field

$$Z_f = R_f + jX_f = \frac{R_2'}{2s} + j\frac{X_2'}{2} \text{ in parallel with } \frac{jX_m}{2} \tag{2.12}$$

$$Z_b = R_b + jX_b = \frac{R_2'}{2(2-s)} + j\frac{X_2'}{2} \quad \text{in parallel with } \frac{jX_m}{2} \tag{2.13}$$

$$I_{2f} = \frac{Emf}{\frac{R_2'}{2S} + j\frac{X_2'}{2}} = \frac{I_1 Z_f}{\sqrt{\left(\frac{R_2'}{2S}\right)^2 + \left(\frac{X_2'}{2}\right)^2}} \tag{2.14}$$

$$I_{2b} = \frac{Emb}{\frac{R_2'}{2(2-S)} + j\frac{X_2'}{2}} = \frac{Emb}{\sqrt{\left(\frac{R_2'}{2(2-S)}\right)^2 + \left(\frac{X_2'}{2}\right)^2}} \tag{2.15}$$

$$P_{\text{air gap}}(f) = (I_{2f})^2 . \frac{R_2'}{2s}, \qquad P_{\text{air gap}}(b) = (I_{2b})^2 . \frac{R_2'}{2-s} \tag{2.16}$$

$$\text{Tnet} = \frac{[Pairgap(f) - Pairgap(b)]}{2\pi N_s / 60} \tag{2.17}$$

Under running condition, total stator current is:

$$I_1 = \frac{V_{in}}{R_1 + jX_1 + Z_f + Z_b} \approx \frac{V_{in}}{R_1 + jX_1 + Z_f} \; ; \; Z_f \rangle\rangle Z_b \text{ for running condition ;} \tag{2.18}$$

$$\text{And } Z_f = \frac{(R_2'/2s)(jX_m)}{R_2'/2s + jX_2'} = \frac{(R_2'/2s)(jX_m)}{\sqrt{(R_2'/2s)^2 + (X_2')^2}} \approx \frac{(R_2'/2s)(jX_m)}{(R_2'/2s)} \approx X_m \tag{2.19}$$

The above approximation is true as for a small motor as R_2' is high and in the normal running condition, $(R_2'/2s)^2$ is high enough to neglect $(X_2')^2$.

$$\text{And the air-gap power } P_{AG} = I_1^2 \frac{R_2'}{2s} \approx \frac{V_{in}^2}{(R_1 + jX_1 + jX_m)^2}\left(\frac{R_2'}{2s}\right) \tag{2.20}$$

$$P_{Converted} = (1-s)(P_{AG}) = (1-s)\frac{V_{in}^2}{(R_1 + jX_1 + jX_m)^2}\left(\frac{R_2'}{2s}\right) \tag{2.21}$$

$$T_{induced} = \frac{P_{Converted}}{\omega_s} \text{ where } \omega_s \text{ is the angular synchronous speed of the motor} \tag{2.22}$$

Thus the induced torque is directly proportional to the rotor resistance under normal running condition of the motor. The approximation is reasonably accurate for fractional horse power motors.

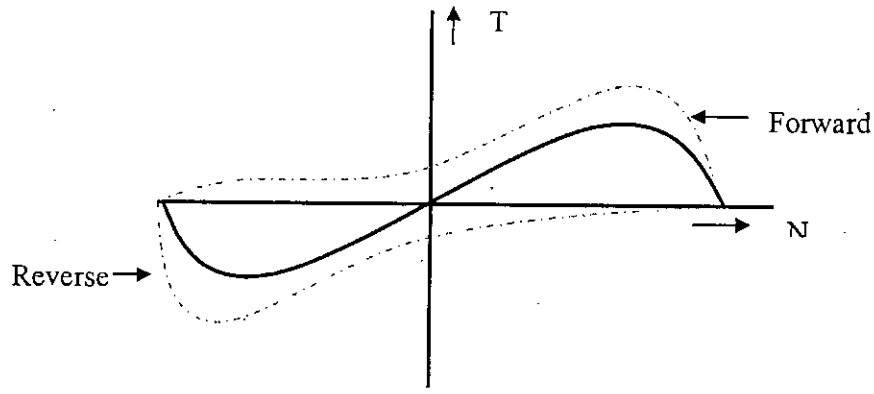

Figure 2.14: Torque Speed Curve for Single phase motor.

Chapter 3

Effect of Ferromagnetic insertion in the rotor circuit

3.1 Skin effect due to magnetic property of a conductor

In a conductor, distribution of current is uniform throughout the cross-section only in case of direct current. However, for alternating current passing through the conductor, current distribution is not uniform. Increase of frequency causes more non-uniform distribution and the current through the conductor and tends to concentrate near the surface or skin of the conductor. Such effect is called the skin effect. Figure 3.1 shows typical distribution of magnetic flux density at different frequencies in an iron slab of finite width (but infinite in other two directions).

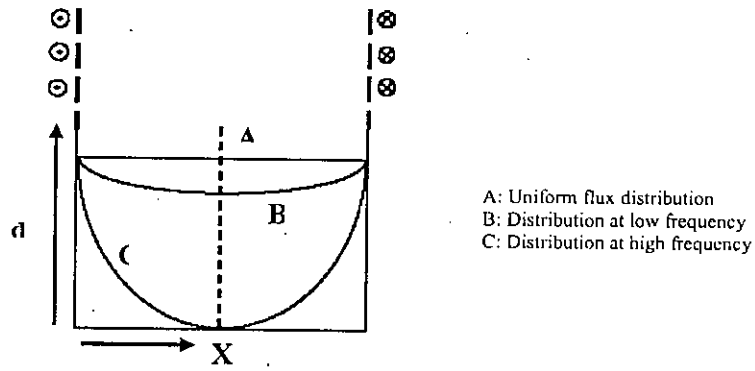

Figure 3.1: Flux density distribution at different frequency in an iron slab

At high frequency, flux density is higher near the surface and lower at the center.

The skin depth in a conductor can be derived using Maxwell Equation. The basic assumptions for the derivation are,

a) the material needs to be a good conductor i.e., there is no charge accumulation

b) net charge density is zero and net movement of electrons is proportional to Electric field

c) there is no variation of electric field along width or length of the conductor.

$$\nabla \times \vec{E} = -\frac{\partial \vec{B}}{\partial t} = -j\omega\vec{B} \tag{3.1}$$

where E is the Electric field intensity

And B is the magnetic flux density

$$\text{or, } \nabla \times \nabla \times \vec{E} = -j\omega\nabla \times \vec{B} \tag{3.2}$$

$$\text{or, } \nabla(\nabla.\vec{E}) - \nabla^2\vec{E} = -j\omega \times \vec{B} \tag{3.3}$$

$$\text{or, } \nabla^2\vec{E} = j\omega\mu\nabla \times \vec{H} = j\omega\mu\sigma\vec{E} \tag{3.4}$$

Assuming Electric field vector along z-direction

$$\frac{d^2E_z}{dx^2} = j\omega\mu\sigma Ez = \tau^2 Ez \; Where \tau^2 = jw\mu\sigma \tag{3.5}$$

$$\because \tau = \sqrt{j}\sqrt{\omega\mu\sigma} = (i+j)\sqrt{\pi f\mu\sigma} = \frac{i+j}{\delta} \; where \; \delta = \frac{1}{\sqrt{\pi f\mu\sigma}}$$

$$\text{or, } \delta = 503\sqrt{\frac{\rho}{\mu_r f}} \tag{3.6}$$

δ is known as skin depth.

μ is the permeability of the conductor

μ_r is the relative permeability of the conductor

μ_0 is the permeability of free space = $4\pi \times 10^{-7}$

σ is the conductivity of the conductor

ρ is the resistivity of the material of the conductor

From equation (3.6), it is evident that skin depth of a conductor is a function of its permeability i,e higher the permeability, lesser will be the skin depth.

Due to skin effect, the current density J in any infinitely thick plane conductor decreases expotentially with skin depth (δ) as,

$$J = J_s e^{-x/\delta} \tag{3.7}$$

Skin depth is defined as the depth at which the current density decreases to 1/e (about 0.37) of the current density at the surface J_s. The skin depth is also a property of a material that varies with the frequency of the applied wave.

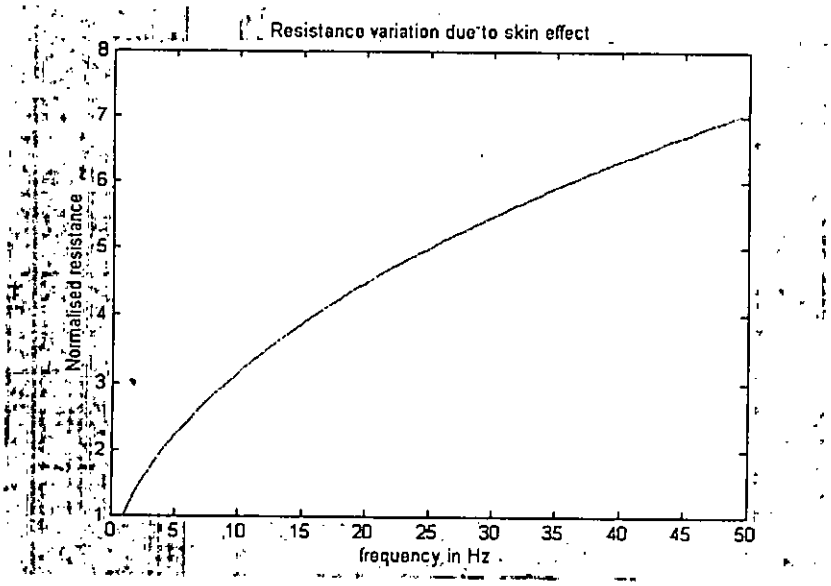

Figure 3.2: Variation of resistance of a strip due to skin effect

Thus the resistance of a material (relative permeability 5000) at 50 Hz is approximately 4 times higher than its resistance at 2.5 Hz (figure 3.2). Materials having high relative permeability(μ_r) will exhibit higher resistance due to skin effect. Due to high conductivity of copper and aluminum, these metals are used as rotor conductors of a squirrel cage induction motor. However, these conductors have low relative permeability (μ_r=1) and are regarded as paramagnetic materials. If small percentage of ferromagnetic material is inserted or mixed with rotor conductors, then skin effect will be quite prominent at starting of the motor. As the motor starts up, the rotor frequency drops and the overall resistance of the ferromagnetic material decreases reducing any possibility of degrading the performance of the motor.

3.2. Application of skin effect in the rotor circuit of induction motor:

For an induction motor, induced current in the rotor at standstill has a frequency of 50Hz. But as the motor speeds up, the rotor frequency decreases with the increase of speed according to the formula $f_R = sf$ where f_R is the rotor frequency

$$s = \frac{N_S - N_R}{N_S} \quad ; \text{ where } f = \text{Supply frequency} \tag{3.8}$$

N_S = Synchronous speed of magnetic field in rpm

N_R = Rotor speed in rpm

At rated speed (s=3~5%) the rotor frequency becomes 1.5Hz~2.5Hz. Thus there is a range of frequency variation form starting to the full rated speed of the motor. A conductor which has a high relative permeability and good conductivity can be inserted in the rotor to utilize the skin effect property to improve the motor's performance. As this insertion will be permanent in the rotor, the resistance should not be high enough to affect the running performance of the motor. A thin strip of a conducting material having large relative permeability can be used with the rotor conductor of squirrel cage induction motor to utilize the skin effect property.

Ferromagnetic materials (commercially available iron) having high relative permeability (μ_r=5000) exhibits a change of skin depth from 3.45 mm to 0.4 mm for a rotor frequency variation of 2.5Hz to 50Hz. Figure-3.3 shows such variation of skin depth as a function of frequency for iron.

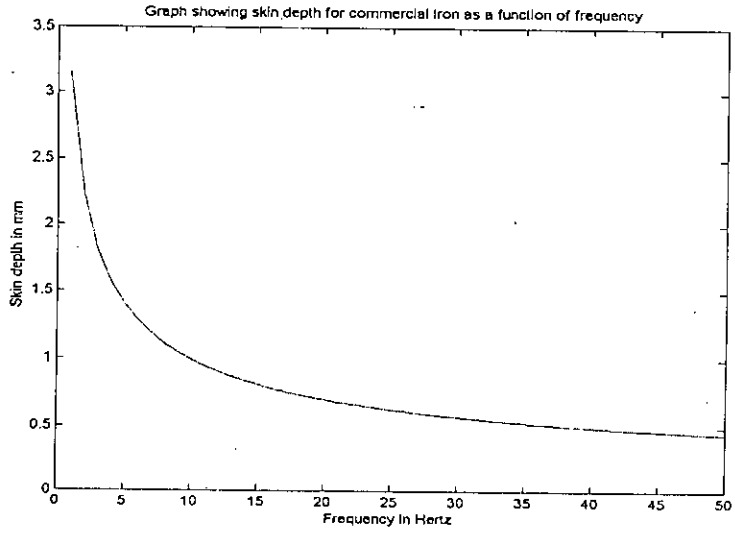

Figure 3.3: Skin depth as a function of frequency for Ferro-magnetic material

Commonly used rotor conductors in squirrel cage induction motor is aluminum which is a paramagnetic material (μ_r=1). Another material used as rotor conductor is copper which is also a nonmagnetic material. However, due to low cost, low melting point and low specific gravity, aluminum is preferred over copper although copper possesses better electrical properties. Aluminum and copper show insignificant skin effect due to their low relative permeability. As the skin depth for magnetic material is low at high frequency and vice versa, so the resistance of magnetic material is high at 50Hz due to concentration of induced current at the surface of the conductor. This resistance is significantly reduced at low frequency.

a) original conductor b) Variation of current

Figure 3.4 : Skin effect in a conductor cross section

Such change of resistance can be better explained by considering cross section of a conductor. The section of the conductor is divided into four lamina of equal area and is subjected to varying magnetic field. Flux linkage is maximum in lamina 1 and minimum at lamina 4. Hence inductance at 4 is minimum while at 1 is maximum. Thus lamina 4 will carry the maximum current while lamina 1 will have minimum current. Due to concentration of current in lamina 4, its resistance will also increase significantly. High concentration of current in lamina 4 will be more prominent if a ferromagnetic conductor is considered.

3.3 Different methods of ferromagnetic insertion in cage rotor

The major shortcomings of squirrel cage induction motor are its low starting torque and high starting current. To start the motor, resistance is inserted in a specially made rotor (wound rotor) to enhance the starting torque and reduce the starting

current. As the motor runs at full speed, the extra resistance inserted in the rotor circuit is gradually by-passed. Thus the overall performance of the motor remains unaffected.

Can this change of resistance from standstill to the rated speed be achieved automatically? A conducting material whose resistance will be high at standstill of the rotor and low at the rated speed can effectively be used for this automatic change of resistance. If ferromagnetic material is inserted in the rotor conductor, due to its skin effect property such automatic change of resistance can be achieved. Now, the question is how to insert ferromagnetic materials in the rotor to achieve better starting performance. One method may be mixing of iron grains with liquid Aluminum and the whole mixture may be casted in rotor slot as suggested in [15]. However, this process may have certain disadvantages like improper and non-uniform mixing of iron grains with liquid aluminum and due to high density of iron, iron particles tend to accumulate at the bottom in spite of rigorous stirring of the mixture. Secondly, there may be possibility of void space formation during casting specially in those motors having very narrow slots for rotor conductors.

Another possibility of introducing Ferro-magnetic material in the rotor is to make extra slots and cast ferromagnetic material in these slots and shorting the

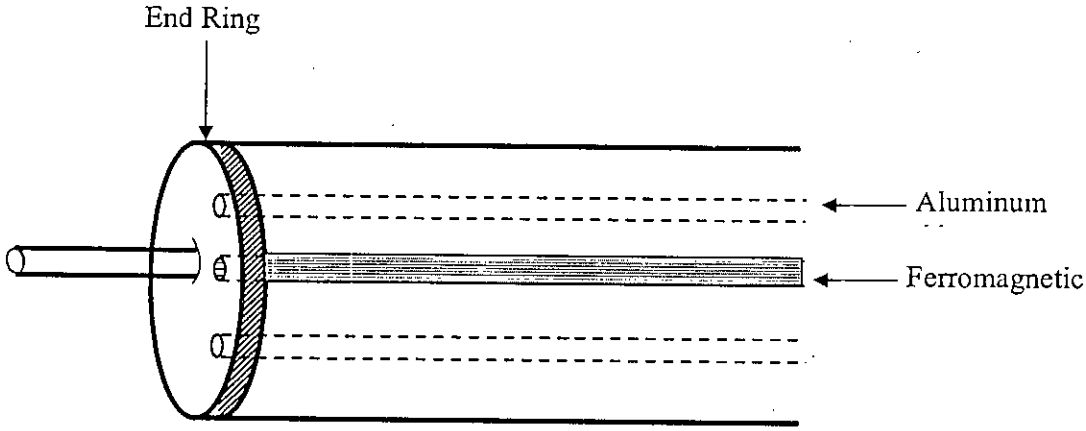

Figure 3.5: Ferro-magnetic material inserted in alternate slots of rotor

whole assembly by Aluminum shorting rings. The size of the slots for ferromagnetic casting may be calculated to give enhanced performance. Extra cost is involved in

arranging extra rotor slots and the overall casting process becomes difficult. Due to high melting point of iron casting of such material in the slot may be difficult.
Another possible method is to introduce Ferro-magnetic strip at one end of the end ring as shown in figure 3.6.

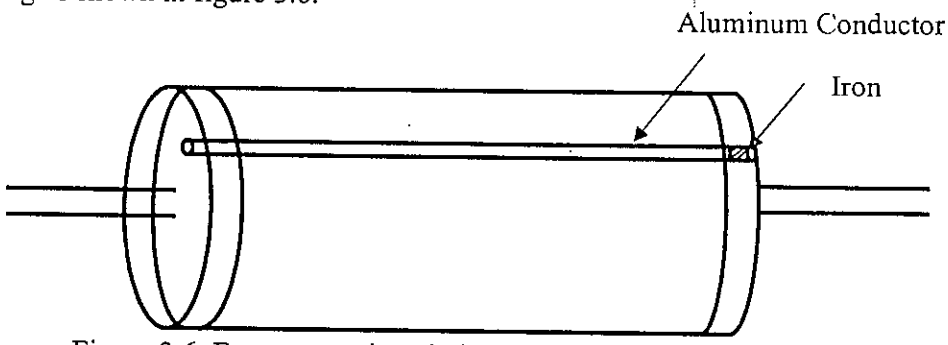

Figure 3.6: Ferromagnetic strip inserted at the end of the slot

The difficulty for such method is to place the iron strip over the rotor slot and then to make aluminum casting over the rotor slots and the end rings. There is possibility of development of high contact resistance at the Al-Fe-Al interface at the point of insertion of the ferromagnetic material.
Another possibility of utilizing the skin effect is to surround the whole rotor assembly by thin iron cylinder as shown in figure- 3.7. Due to skin effect, the rotor resistance will increase significantly but it will have some disadvantages. The surrounding iron cylinder will act as magnetic screen as flux penetration will be less to the rotor conductors. There will be large eddy current losses and possibility of magnetic locking with the stator magnetic field.

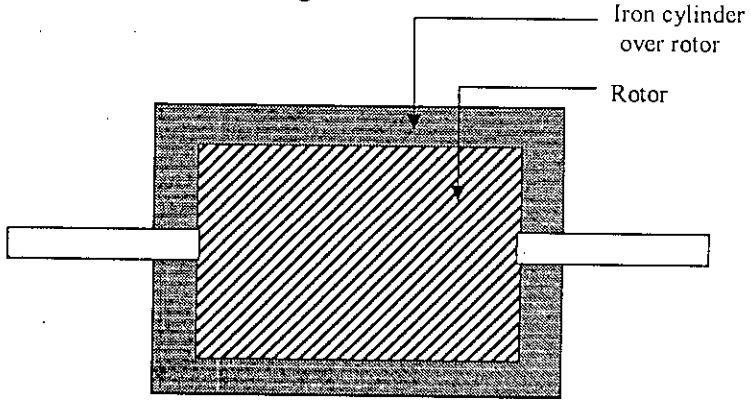

Figure 3.7 : Embedded Iron cylinder over rotor

Another method is to introduce ferromagnetic strip at one of the end rings. Introduction of such strip at the end ring is extremely simple and does not need any sophisticated and complicated casting process as described below.

3.4 Proposed method for ferromagnetic insertion in squirrel cage rotor

In this research work, ferromagnetic insertion at the end ring has been proposed. Firstly the size and number of end rings required for obtaining better starting performance has been determined by software simulation and mathematical calculations. These rings are fixed with the motor shaft before casting of the rotor as shown in fig 3.8

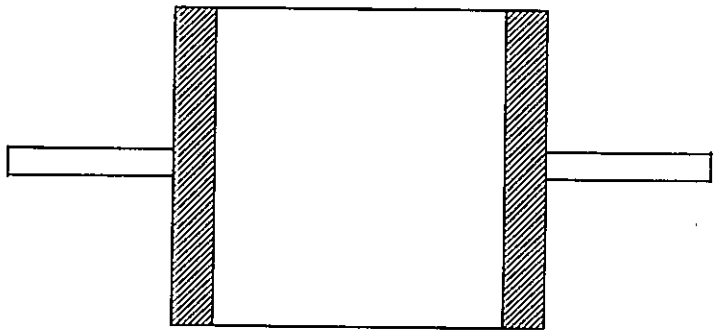

Figure 3.8: Side view of the rotor

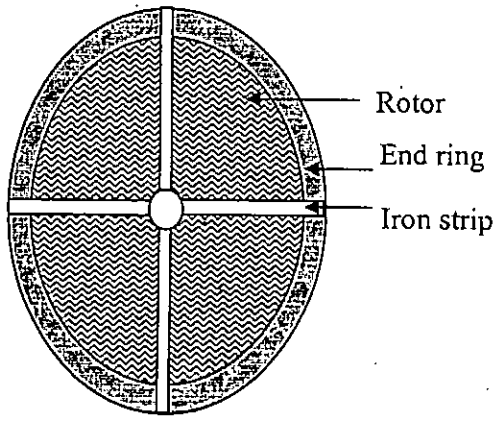

Figure 3.9: Top view of rotor with iron insertion

After fixing the ring with the rotor shaft, liquid Aluminum is poured in the slots and the end ring area. This method of Ferro-magnetic material insertion is simple and free from formation of void space. So, this method of introduction of Ferromagnetic material at the end ring has been proposed in this research work.

3.5 Effect of Ferromagnetic insertion on induction motor performance.

The possible effects of ferromagnetic insertion in the squirrel cage rotor of induction motor are:

(a) Increase of rotor resistance at the time of start due to skin effect

(b) Gradual reduction of rotor resistance as the rotor speeds up

(c) Impact of variation of rotor resistance due to rotor speed on the harmonic generation of the motor

Ferromagnetic materials exhibit significant skin effect at high frequencies. For an induction motor, rotor frequency varies from 50Hz to 2.5Hz from the stand still to the full running condition of the motor.. It is expected that ferromagnetic materials inserted in the rotor should also exhibit better starting performance due to increase in rotor resistance. So there will be enhancement of starting torque and reduction of starting current of the motor. However, at rated speed of the motor, the frequency drops down to almost dc level and subsequently additional rotor resistance generated due to skin effect falls back almost to the value of original rotor resistance. Thus running performance of the motor should remain unaffected even with the introduction of the ferromagnetic material in the rotor.

3.5.1 Improvement of starting performance

Starting performance improvement means enhancement of starting torque and reduction of starting current. Figure 3.10 shows simulated torque speed curve for a 45 kW 3-phase squirrel cage induction motor for three different rotor configurations. Motor parameters are introduced in the simulation software MATLAB to generate Torque-Speed curve of the original motor as shown by the blue curve of figure 3.10. The green curve in the same figure has been generated by the software when a fixed

additional resistance is introduced in the rotor circuit. Finally simulation is done by insertion of ferromagnetic material in the rotor in the form of strip. The dimension of the strip is chosen in such a way so that the starting torque in this case is identical to that of the starting torque with fixed rotor resistance. Red curve shows the Torque Speed relationship for the ferromagnetic rotor. Thus the starting torque for the rotor with fixed resistance and the rotor with ferromagnetic strips are the same and is about 20% higher than the original rotor.

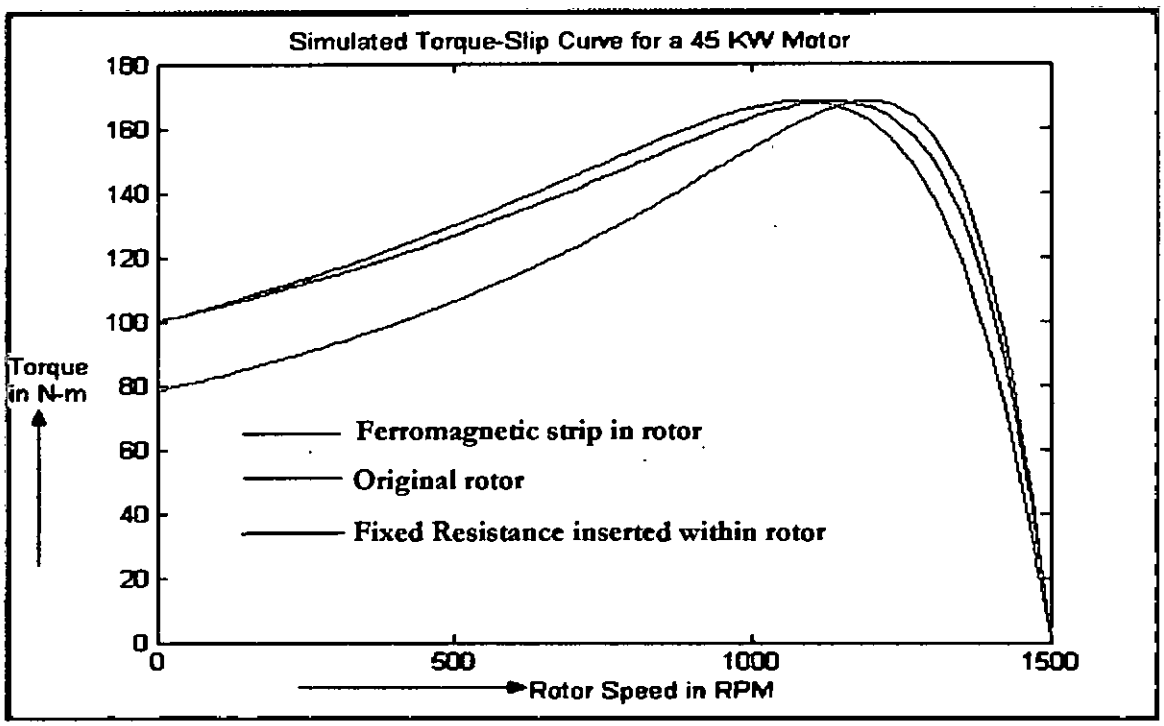

Figure 3.10: Simulated Torque-Speed curve for a modified rotor

This proves the established fact that for an induction motor, higher rotor resistance generates higher starting torque. But the question is: how is running performance affected by insertion of fixed resistance and ferromagnetic material in the rotor respectively? Article 3.5.2 shows how do both starting and running performance can be improved by ferromagnetic insertion in the rotor.

3.5.2 Improvement of running performance

Usually observed fact is: increasing the rotor resistance increases the starting torque. At the same time due to continuous presence of the increased resistance (if extra resistance is inserted in the squirrel cage rotor) the running performance is seriously hampered. Referring to figure 3.10 the green curve (which represents fixed resistance inserted in the rotor) indicates that in the normal operating region of the motor, the curve has drifted to the left compared to of the curve of the original motor (blue). This means that running performance is seriously affected due to insertion of fixed resistance in the rotor. However, red curve (representing ferromagnetic rotor) very nearly coincides with that of the curve of the original motor in the normal running region. This shows that by ferromagnetic insertion, better starting torque has been achieved without affecting the running performance of the motor. Thus the efficiency of the ferromagnetic rotor in the normal running region remains almost identical to that to the original motor.

3.5.3 Effect of harmonics on motor performance

Harmonic distortion is the change in waveform from the ideal sinusoidal waveform. As far as the induction motor is concerned, its major adverse effect is the heating of the induction motor causing accelerated degradation of the motor insulation and loss of life. There are several reasons for harmonic distortion. Saturation of the core, distributed winding and slot positions, employment of solid state switching devices etc are the major factors contributing to the generation of harmonics.

Harmonic distortion is measured by a factor known as THD (Total Harmonic Distortion)

It is the root-sum square value of the harmonic content of the voltages to the root mean square value of the fundamental voltage.

Total harmonic distortion of the voltage waveform is given by:

$$V_{THD} = \frac{\sqrt{V_2^{\,2} + V_3^{\,2} + V_4^{\,2} + V_5^{\,2} + \ldots\ldots\ldots}}{V_1} \text{ X } 100\%$$

Where V_1 is the fundamental component of the voltage waveform and V_2, V_3.... are the harmonic components of the voltage wave.

Current THD:

Total Harmonic Distortion of the current wave form is the ratio of the root-sum-square value of the harmonic content of the current of the root-mean-square value of the fundamental current.

$$I_{THD} = \frac{\sqrt{I_2^2 + I_3^2 + I_4^2 + I_5^2 + ...}}{I_1} X\ 100\%$$

Where I_1 is the fundamental component of the voltage waveform and I_2, I_3.... are the harmonic components of the voltage wave.

A 3-phase winding due to non linearity of the core produces harmonic of the order of $n = 6N \pm 1$ where N is an integer. The movement of the harmonic may be with the rotation or against the rotation of the motor. At standstill, the 3-phase winding will produce a forward rotating 7^{th} harmonic and a backward rotating 5^{th} harmonic for N=1. The 5^{th} and 7^{th} harmonic fluxes generate rotor e.m.f currents whose frequencies are 5 and 7 times the fundamental frequency respectively. Due to high frequency currents generated by harmonics, ferromagnetic rotors will exhibit greater skin effect which further increases the rotor resistance. This will suppress high harmonic currents in the motor. This may be an additional advantage in this thesis work.

3.5.4 Performance of single phase induction motor

Single phase induction motors are not self starting because when the main winding of the single phase motor is energized, two opposite rotating mmfs are produced and hence no torque is generated. They are started normally by split phase or by capacitors placed in series with the auxiliary winding of the motor. Auxiliary coil of the single phase motor minimizes one of the mmfs and the torque generated by interaction of the main and auxiliary windings are similar to that of the three phase motors. So there are two rotating mmfs in both three phase and single phase motors. Due to backward rotating mmf, double frequency current is induced in the rotor that produces high skin effect. So for a single phase motor, rotor resistance is expected to increase due to skin effect and the power factor of the motor is expected to increase throughout the running region of the motor. High resistance will also produce less motor current as well as less locked rotor current. For small single phase induction

motor its resistance R is much higher than its leakage reactance X. Hence with reference to equation 2.20 and 2.21, the running performance of the motor is expected to increase. As fractional horse power motors are widely used, so its performance is also studied with ferromagnetic insertion in the rotor.

3.6 Impact on motor performance for variation of rotor resistance due to variation of speed

Two parameters that are expected to vary with the variation of speed are: i) Rotor resistance and ii) Rotor leakage reactance. Normally conductors of squirrel cage rotors of induction motors are non magnetic materials like aluminum or copper. These materials exhibit very feeble skin effect and change of rotor resistance is extremely small within the frequency variation range of the rotor. However, due to ferromagnetic insertion in the rotor, the change in rotor resistance due to variation of the rotor speed is appreciable and has been very well taken into consideration in this research work.

Major rotor reactance variation [57] takes place in the frequency range 2-15Hz when the rotor is running nearly to the synchronous speed. The rotor leakage reactance almost remains constant in the frequency range 15-50Hz. As far as three phase motor starting performance is concerned, change of rotor leakage reactance is negligible in the low speed region of the motor. So change of rotor reactance will not have any impact on the starting performance of the motor.

Chapter 4

Experimental setup and results

4.1 Experimental Design process

As the main objective of the thesis is to modify the rotor design of a squirrel cage induction motor to enhance its starting performance, iron strips having relative permeability of the order of 5000 have been introduced bisecting the end ring portion between the rotor conductors at the rear end of the rotor. Purpose of introducing iron strip (a ferromagnetic material) is to utilize the skin effect property of the material which is prominent at higher frequency due to its large value of relative permeability (μ_r). Iron cannot be used as a rotor conductor because of its low conductivity. But small percentage of iron introduced within the rotor would greatly improve the performance of the motor.

Design procedure is described as below,

1)Six pieces of 400V, 50Hz, 3-phase, 1/4HP squirrel cage induction motors (Chinese) were purchased for the necessary rotor modifications. The small sized motors were used in view of the laboratory facilities available for the present research work. For all the motors, necessary tests (No load and Blocked rotor) were performed to determine the relevant motor parameters. Test results were found identical for each of the motors. Results were saved for the purpose of comparison.

2) As the rotor modification work (which includes rotor casting and ferromagnetic material insertion) has to be done locally, so the Aluminum in the original rotor was drained out and the slots and the end rings were casted with the locally available pure Aluminum for two sets of rotors. No load and blocked rotor tests were performed for the locally casted rotors and the test results were also found identical for each of the motors and the test results thus obtained were identical to those of original motors.

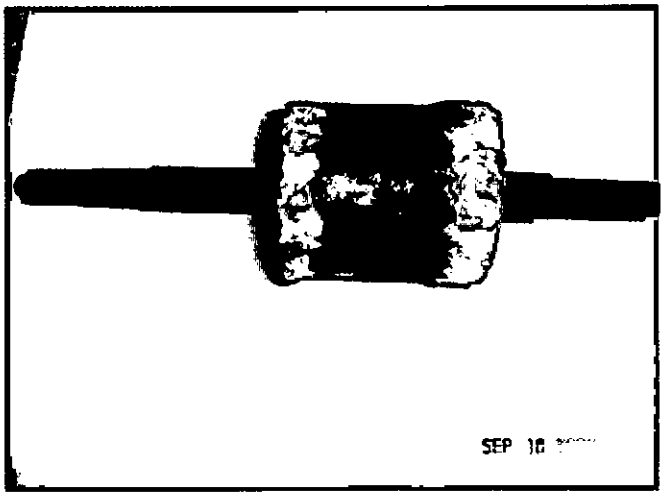

Fig.4.1: Aluminum Rotor (Locally casted)

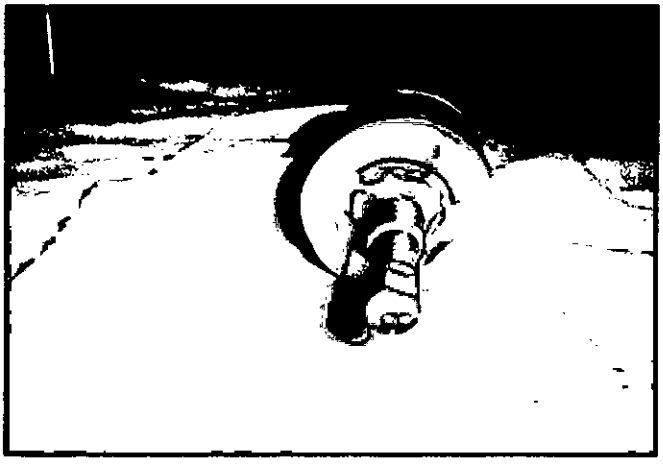

Fig. 4.2: Aluminum Rotor after machining (Front view of Fig.4.1)

3) Motor parameters were determined from the no load and blocked rotor tests for the locally casted aluminum and are shown in Appendix A.
4) Another set of original rotors were taken and the aluminum was drained out from the slots and the end ring. At the rear end of the motor 30 iron strips are fixed in such a way that each strip is positioned between the two slots of the rotor. All the strips are welded to a central ring so that strips are not dislocated while aluminum casting is done. The end ring assembly inserted in the rotor is shown in figure 4.3 and 4.4 respectively.

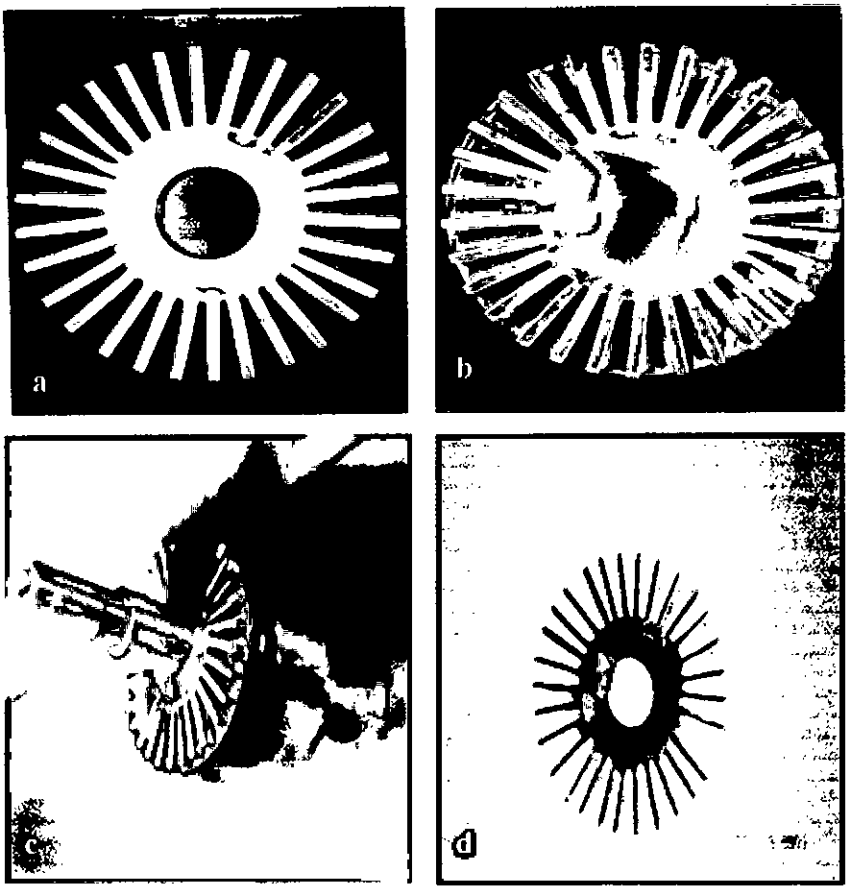

Fig.4.3: Iron strip for insertion in the rotor

The strips are inserted in such a way between the rotor conductors so that current from the each rotor conductor passes through the strip to the adjacent rotor conductor. Thus the rotor current is forced to pass through the ferromagnetic strips inserted at the end ring section of the rotor. After fixing the iron strips at the end ring position, the whole rotor assembly was casted with aluminum.

5) The number of strips are gradually reduced and the motor performance was recorded for each case. The rotor was casted with 15, 10, 5, 3 and 2 strips respectively.

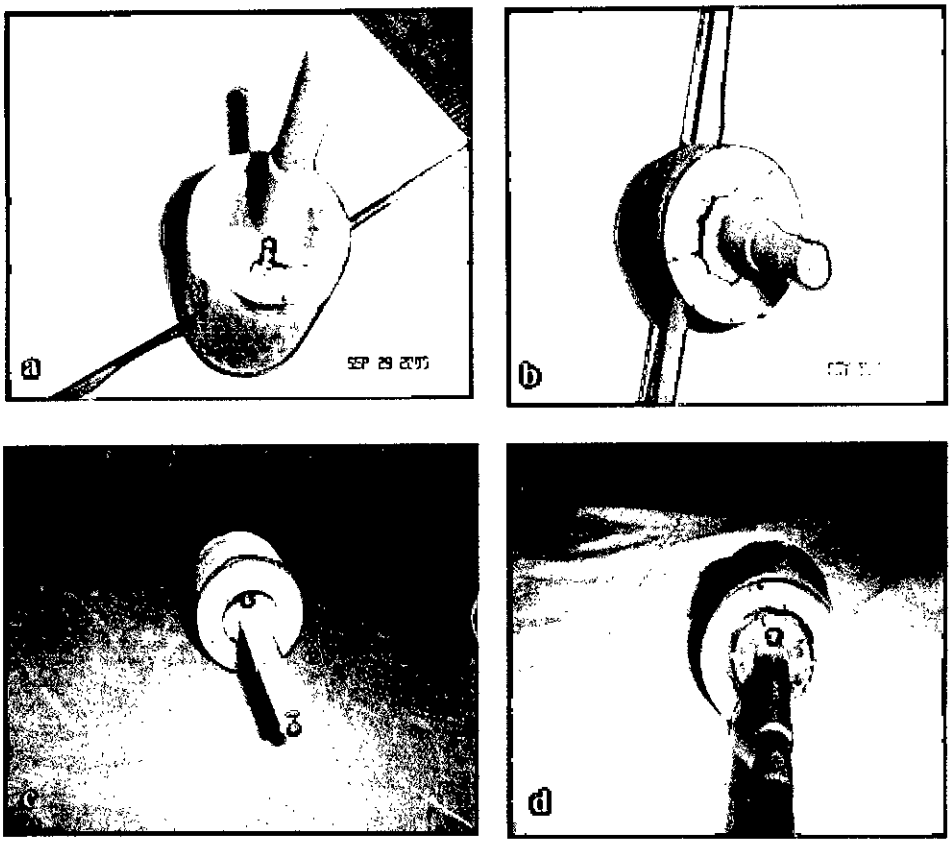

Figure 4.4: Iron strips inserted in the rotor. a) 15 strips b) 10 strips c) 6 strips d) 2 strips

Figure 4.5: Rotor with copper casting

6) The motor parameters were determined experimentally and used in a program developed under MATLAB environment to plot the torque-slip curve of the motor. A subroutine in the program takes into account the effect of ferromagnetic insertion in the rotor and simultaneously calculates the skin depth and the additional resistance that appears in series with the rotor due to skin effect of the ferromagnetic material. The program has the feature of varying the thickness of the inserted iron strip to give a number of torque-slip curves. If the thickness of the strip is increased, the starting torque increases and the starting current (locked rotor current) is reduced. For a certain thickness of the strip, not only enhancement of the starting torque takes place but also the torque-slip curve nearly coincides with the torque-slip curve in the running region of the original motor. This thickness of the strip has been chosen for insertion in the rotor.

   The thickness of the strip thus obtained is sliced into 30 equal parts (for theoretical analysis as there are 30 slots in the rotor) and each slice is inserted between two adjacent rotor conductors as shown in figure 4.3 and 4.4 respectively. The simulation program is given in Appendix B.

7) The necessary mathematical formula for the calculation of the size and number of strips to be inserted for obtaining the required motor performance as described in step (4) is given below;

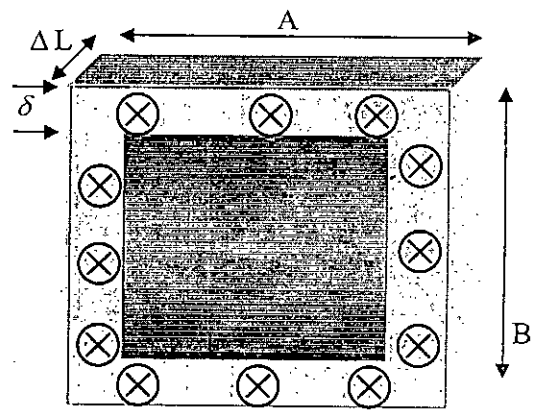

Figure 4.6: Skin effect in an iron strip to be inserted in the rotor
Outer shaded region shows area of current flow due to skin effect

With reference to fig.4.6 the formula for resistance of the rotor after iron insertion in the end ring is;

$$R = \frac{\Delta L}{\sigma * \{(A - 2\delta) + B\} * \delta} \text{ ohms.} \qquad (4.1)$$

Where, A is the length of the strip, B is its width, σ is the conductivity of iron, δ is the skin depth and ΔL is the thickness of the iron strip.

Considering an aluminum conductor in a single slot of the rotor with an iron strip inserted between two slots, let us assume that R_{slot} is the resistance of the aluminum conductor in the single slot and R_{iron} is the resistance of the single strip (figure 4.7) inserted. Let R_{rotor} is the total resistance of the rotor conductors and R_{skin} is the total resistance of the ferromagnetic strips inserted in the rotor at any rotor frequency.

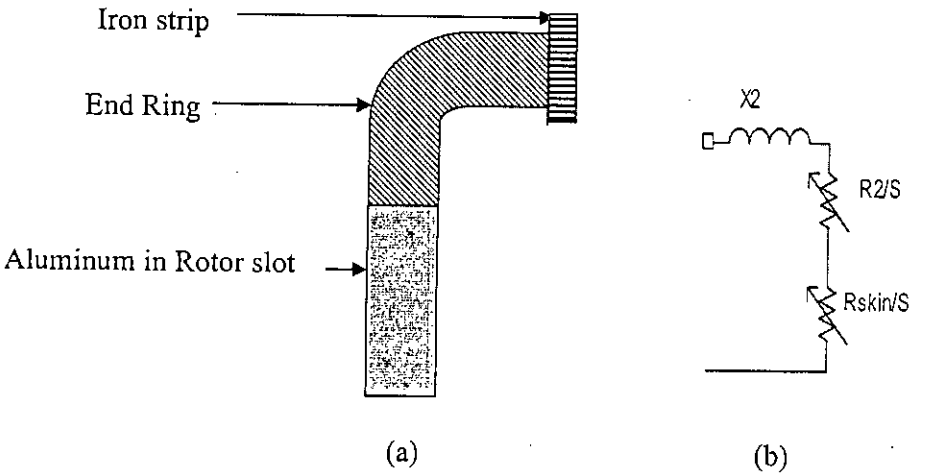

Figure 4.7: (a) Section of rotor slot with end ring and iron strip inserted
(b) Equivalent circuit of the rotor with iron insertion

We can write;

$$\frac{R_{slot}}{R_{iron}} = \frac{R_{rotor}}{R_{Skin}} \qquad (4.2)$$

The formula for R_{skin} can be written as follows with modification of equation 4.1

$$R_{skin} = \frac{K}{\sigma \times \{(A - 2\delta) + B\} \times \delta} \qquad (4.3)$$

Where K is a constant due to skin effect at certain frequency of the rotor.
Let us assume that at 50 Hz, the additional resistance appearing in the rotor due to skin effect is 10 ohms (an indicative value obtained by MATLAB simulation). At 50 Hz, the skin depth δ can be calculated from the formula 3.5 and 3.6. A, B are the dimensions of the strip in contact with the end ring (figure 4.6).

From equation (4.3) the value of K has been found to be 470. The value of R_{rotor} has already been determined as 40 ohms from the blocked rotor test. As the rotor slot dimensions of the motor are known, the resistance value of the rotor conductor in each slot has been calculated and found to be 0.415×10^{-4} ohms. From equation 4.1, the thickness of each strip comes out to be 0.013mm. For 30 slots, 30 such strips are required to be inserted and the total thickness of the strip will be around 0.4mm.
However, such small thickness of 0.013mm cannot be physically realizable for each slot of the rotor. So the thickness of the strip obtained from the simulation results and calculation are concentrated at the two fixed position of the rotor. The fabricated strip of 0.4mm (0.2mm+0.2mm) is shown in figure 4.8. Each strip takes its position between two rotor conductors and each strip is placed in opposite direction to the other so that rotor current distribution is uniform in each half section of the rotor.

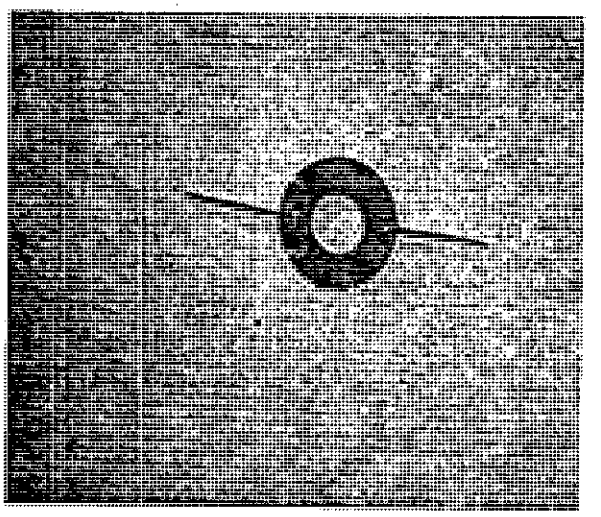

Figure 4.8: Iron strip 0.2+0.2 mm for insertion in the end ring

4.2 Experimental Set up

The motor under test was connected to a dynamometer to measure the torque. The Lab volt Dynamometer (torque meter) has a rotary knob by which the torque setting can be changed. A tacho-generator was coupled to the torque meter assembly to record the speed of the motor. Ammeter, voltmeter and wattmeter were connected with the motor to record the phase current, phase/line voltages and the phase power. Current wave shapes for each type of rotor configurations were recorded for both three phase and single phase motors. For this, voltage drop across ammeter was applied to a storage oscilloscope. The wave shapes on the oscilloscope is collected to a PC through a DSO controller acquisition card and the associated software. First, the original motor with pure aluminum rotor was taken for experimental measurement. No load and blocked rotor tests were performed for the motors. Then motors with different rotor strips (fins) were placed in the testing bench for taking the necessary readings for a) Torque Vs Speed b) Current Vs Speed c) Blocked rotor current d) Motor input power and e) current wave shapes. To record the torque against speed, the torque on the motor was gradually increased and for each step the corresponding speed was noted. This increment of torque was gradually and steadily continued till the motor crosses its breakdown region. The starting torque was recorded by keeping the torque setting on the dynamometer to maximum and quickly increasing the motor supply voltage to its rated value. This method was followed as per Lab volt instructions for the measurement of starting torque. In an alternative method of measuring the starting torque, the load on the motor shaft was gradually increased till the motor runs very near to the lowest possible speed before stalling of the motor. The corresponding torque to this lowest possible speed is noted. Then the torque speed curve is drawn with torque along Y-axis and speed along the X-axis. The torque-speed curve is extrapolated backward till it cuts the torque axis i,e at zero speed of the motor. The torque at this point of intersection with the torque axis (y-axis) is the starting torque of the motor. The starting torque thus obtained is identical to that of the starting torque found earlier as per Lab-Volt instructions. The complete experimental setups are shown in figures 4.9, 4.10 and 4.11 respectively. Motor under test with the LAB VOLT dynamometer is shown in figure 4.9. The motor is

coupled to the dynamometer with the help of rubber belt and the torque on the dynamometer can be set by a rotary knob. Figure also shows a tacho-generator to record the speed of the motor. The power supply unit provides three phase and single phase supply required for the motor and the dynamometer respectively. The measuring units like wattmeter and ammeter are shown in the second row of figure 4.9. Figure 4.10 shows the set up to record the current wave shape in a PC. Voltage proportional to the stator current is fed to the oscilloscope. The oscilloscope has facilities to perform different math functions on the waves being studied. Fast Fourier Transform at different sampling frequency can be performed and the wave shape obtained after FFT have been saved in the PC.

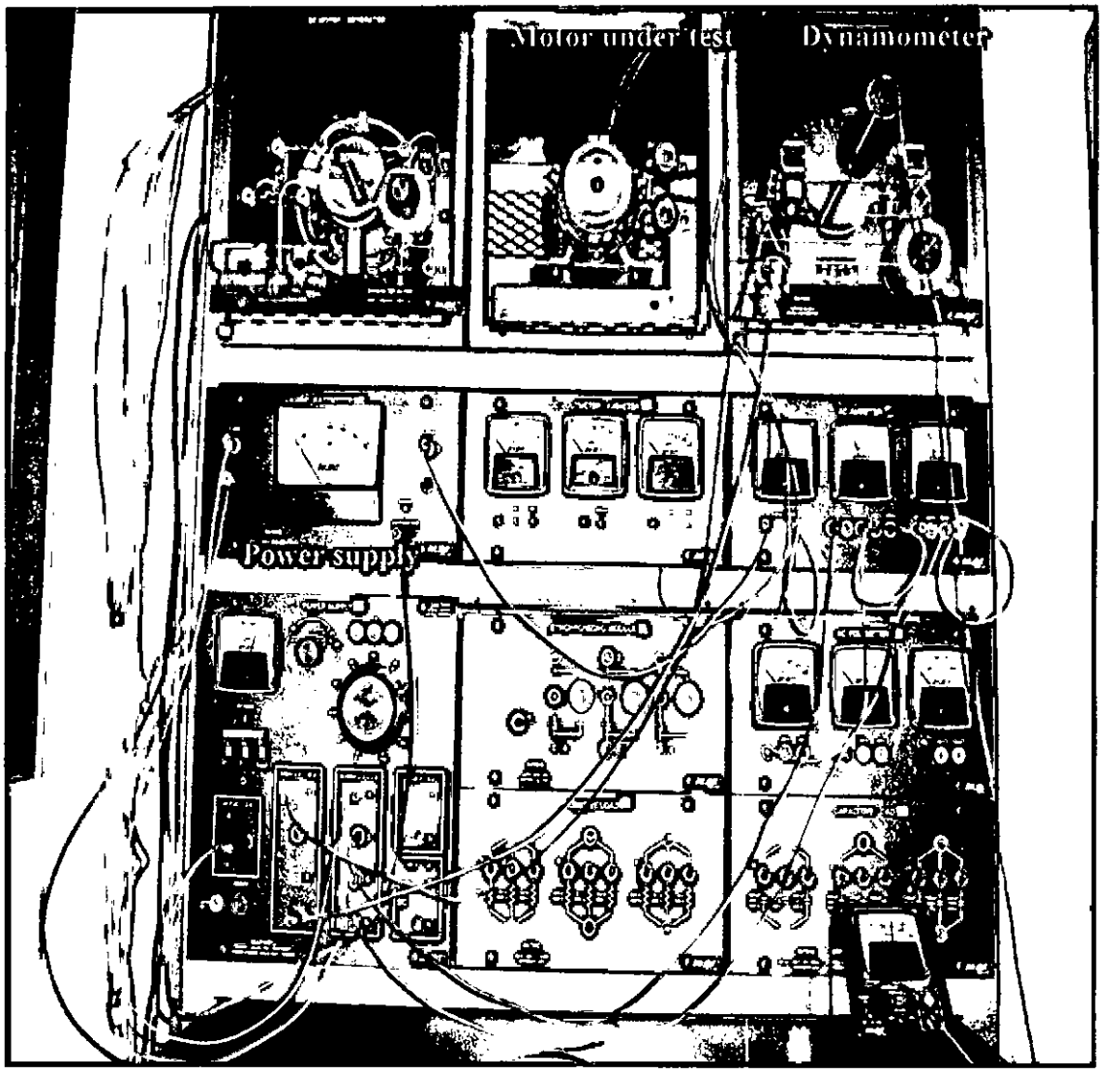

Figure 4.9 Experimental set up

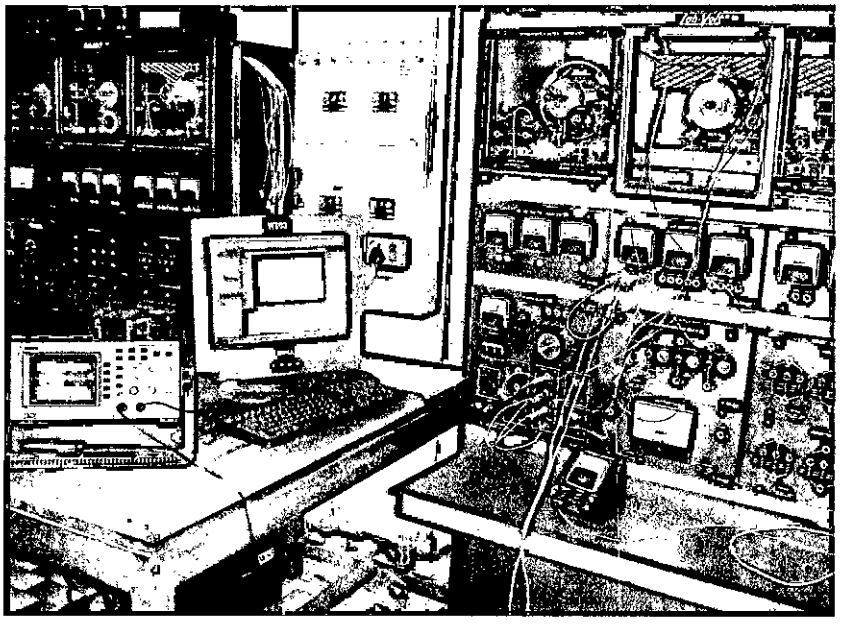

Figure 4.10 Experimental set up

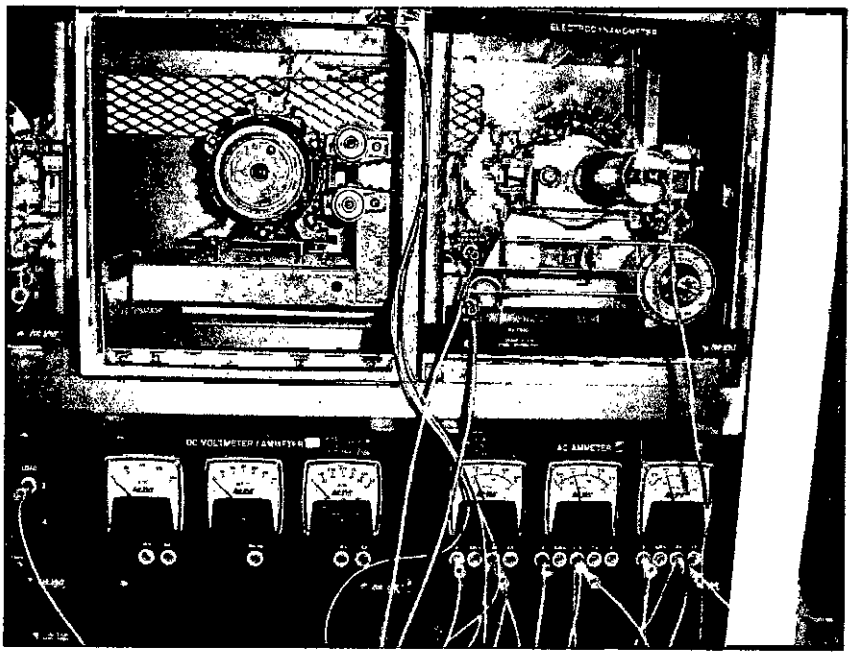

Figure 4.11 Motor coupled to dynamometer

An attempt was made to make higher conductivity rotor by casting the rotor slots with copper (figure 4.5). However, due to high melting point of copper and lack of availability of modern casting facilities, the casting process could not be satisfactorily done and the copper rotor did not produce the expected results.

4.3 Experimental Measurement

Measurement was first made on the standard motor with aluminum rotor. After recording the necessary data, the standard motor was replaced by motor with ten iron strips inserted in the rotor. Similar data to that of standard motor was recorded for this motor. Subsequently, same set of data was recorded for motors with five, three and two rotor strips respectively. Although the copper rotor motor did not produce satisfactory results, for a comparative study, test result for this motor was also recorded and represented through graphical plots. All the readings of motors are presented in Appendix A.

For each type of rotor configuration, the curves presented are; Torque Vs Speed, locked rotor current Vs motor line voltage, efficiency Vs speed and power factor Vs speed. With the increase of number of strips inserted in the rotor, the performance of the motor sharply degraded (as expected) and the corresponding curves (efficiency and power factor) for those motors are not presented. In these motors, with the enhancement of number of strips in the rotor the starting torque enhanced with the reduction of locked rotor current. First, the curves for the motor with ten rotor strips (each strip of 0.2mm thickness) are presented. Then the performance of the motor with insertion of five, three and two strips are presented. The performance of these motors is compared with the performance of the standard motor with aluminum rotor.

Each motor after fixing on the test bench was driven at no load (with the torque setting zero) on the dynamometer. Then the torque on the motor shaft was gradually increased and for each torque setting, the speed, current and power were noted. Power factor and efficiency for each rotor configuration were calculated from the experimental data thus obtained.

4.3.1: Performance of the standard motor (Aluminum rotor motor)

The curves for the pure Aluminum rotor are shown in figure 4.12. Maximum torque occurs at a speed of 600 rpm with corresponding slip of 60% and the rated motor current under locked rotor condition is obtained at the motor line voltage of 170V.

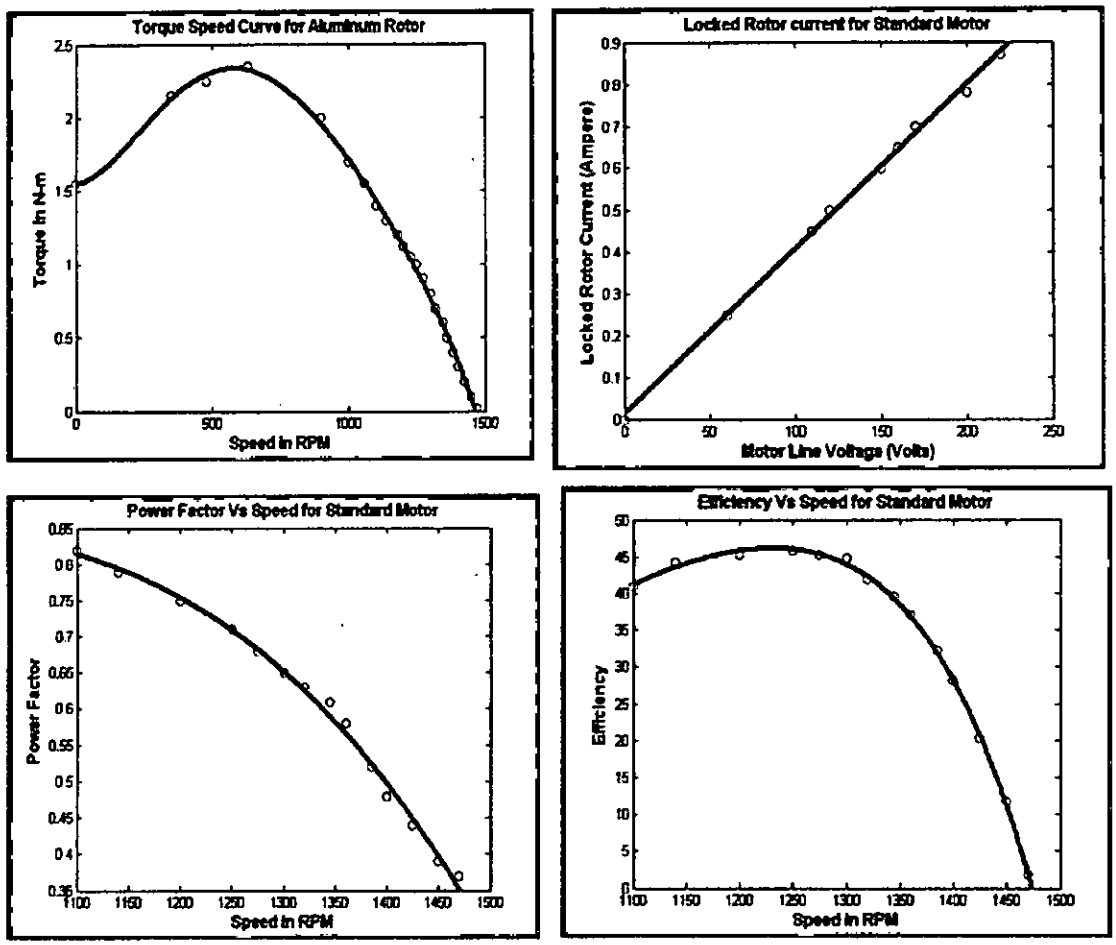

Figure 4.12 Performance of the standard motor

At the rated load (1.1 N-m), the slip is 10% and the power factor is 0.65. The full load efficiency is around 46%. Locked rotor current of 0.90 ampere has been obtained with the motor line voltage of 220V. In the normal running region of the motor torque speed curve shows a linear relationship. Both power factor and efficiency decreases with the increase of speed. The starting torque is about 1.55 N-m.

4.3.2: Performance of the motor with ten strips in the rotor

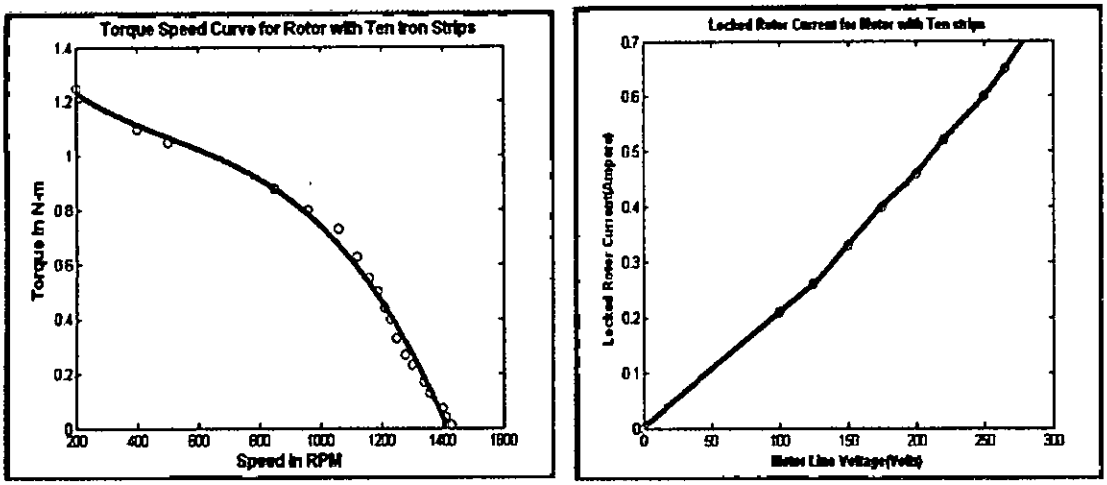

Figure 4.13 Performance curves for motor with ten rotor strips

From figure 4.13, it can be seen that the performance of the motor with ten rotor strips is not satisfactory due to high resistance arising due to insertion of excessive number of strips in the rotor. Although the locked rotor current is significantly low, but the motor becomes sluggish and runs with a very low speed at the rated load and this configuration cannot be used to derive enhanced performance from the motor. The number of strips inserted in the rotor was gradually reduced to improve the motor performance. The next set of figures show the characteristic curves for the motor with five rotor strips (figure 4.14).

4.3.3: Performance of the motor with five strips in the rotor

For five strips in the rotor, the locked rotor current has increased compared to the motor with ten strips. The torque slip curve shows substantial improvement but the slip is high (50%) at the rated load of the motor. For a motor line voltage of 250V the locked rotor current is 0.65A and the motor breakdown torque occurs at a slip of 80%. Thus the motor has sluggish response and in the normal running region of the motor the torque slip curve is nonlinear and the magnitude of torque sharply decreases with the increase of speed. So for further improvement of motor performance, rotor with three iron strips was fabricated and its performance curves are shown in figure 4.15.

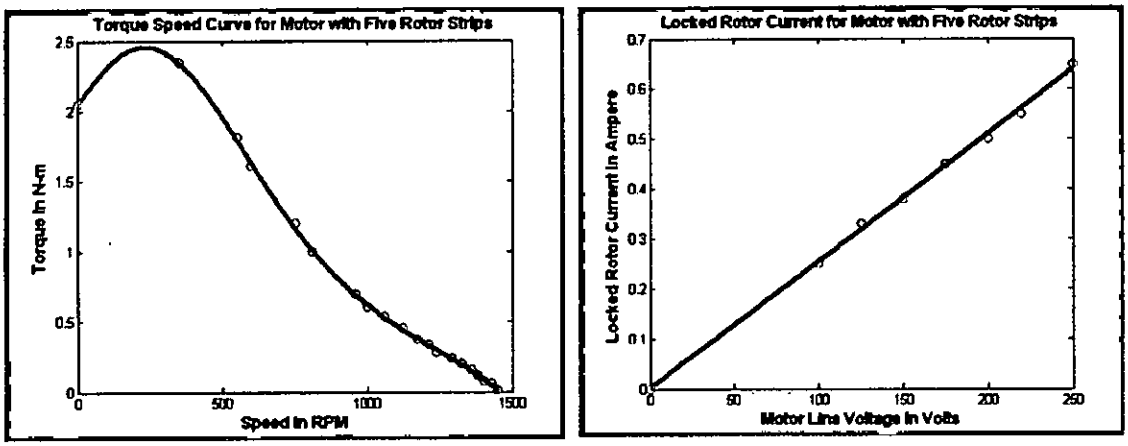

Figure 4.14 Performance curves for motor with five rotor iron strips in the rotor

4.3.4: Performance of the motor with three strips in the rotor

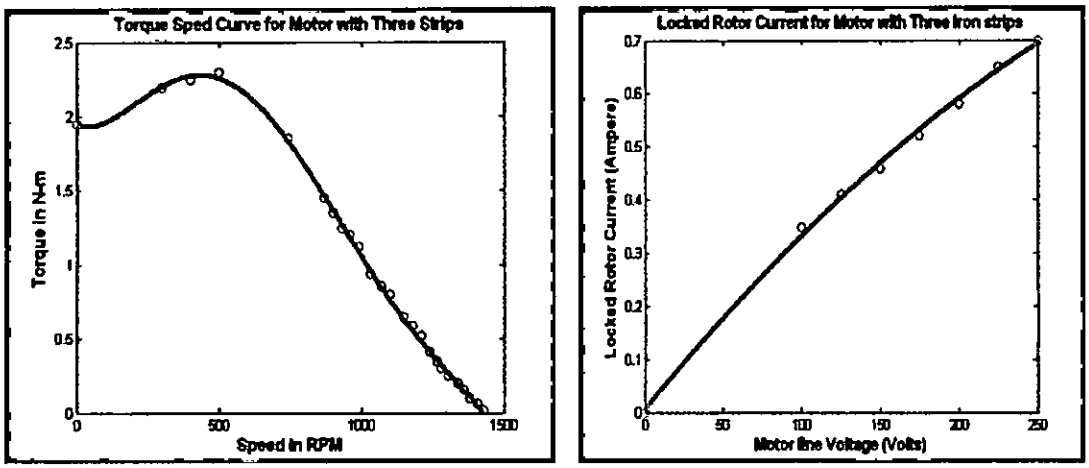

Figure 4.15: Performance curves for motor with three iron strips in the rotor

Although rotor with three iron strips has less starting torque compared to five strip rotor, but the overall performance of the three strips motor is much improved. A comparative study of figures 4.14 and 4.15 shows that at the rated load, the slip for three strip rotor is 20% where as at the same rated load, 50% slip has been obtained for rotor with five iron strips. The maximum torque for three strip rotor occurs at 60% and that of five strip rotor occurred at 80%. A linear torque speed curve has been obtained in the operating region of the motor with three strips also this curve has flattened around the region of maximum torque showing enhancement of the stable region of the motor.

4.3.5 Performance of the motor with two strips in the rotor

As the motor under test is a fractional HP motor having high rotor resistance, so large number of insertion of the iron strips are not possible. Insertion of two strips in the rotor gives the torque-speed curve which almost coincides with the curve of the standard motor. Higher starting torque has been obtained with reduced starting current. Also the efficiency curves are identical when compared to the standard motor. A detailed comparative study on the performance of the motor with different rotor configurations has been shown later in this chapter.

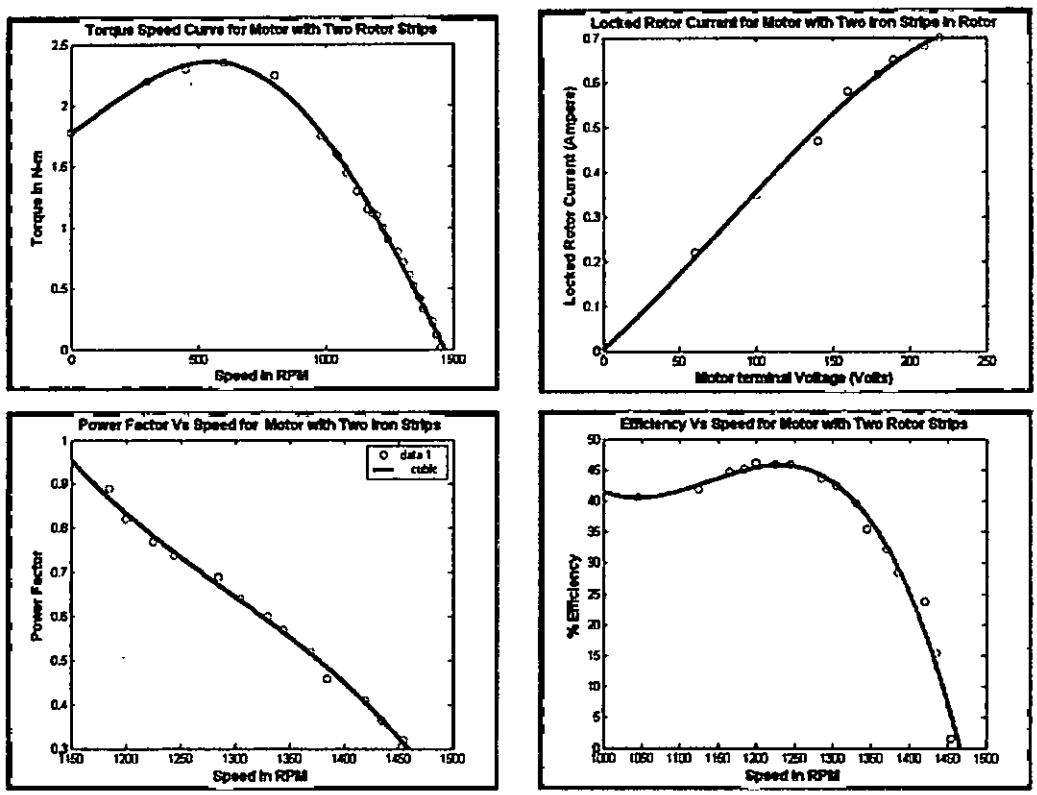

Figure 4.16: Performance curves for motor with two iron strips in the rotor

4.3.6 Copper Rotor Motor

As the casting for the motor could not be accurately done due to high melting point of copper and lack of modern casting facilities for high temperature material like copper, so the test results found were not satisfactory. The copper motor gave low starting

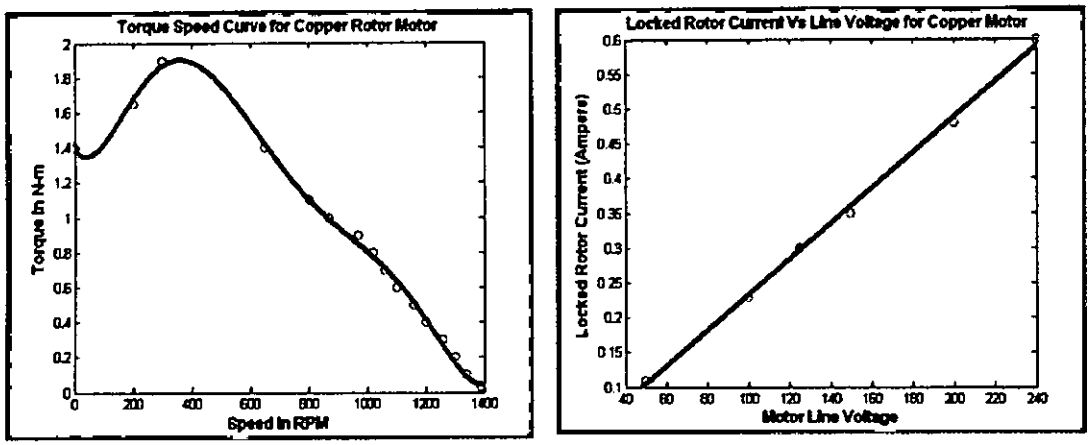

Figure 4.17: Performance of copper motor rotor

torque and the response to the variation of load was sluggish. The rated current under blocked rotor condition was obtained at a motor line voltage of 240 volts. The torque-Speed curve and the locked rotor current curves are presented in figure 4.17.

4.3.7 Comparative study of Three Phase Motor with different Rotor configurations

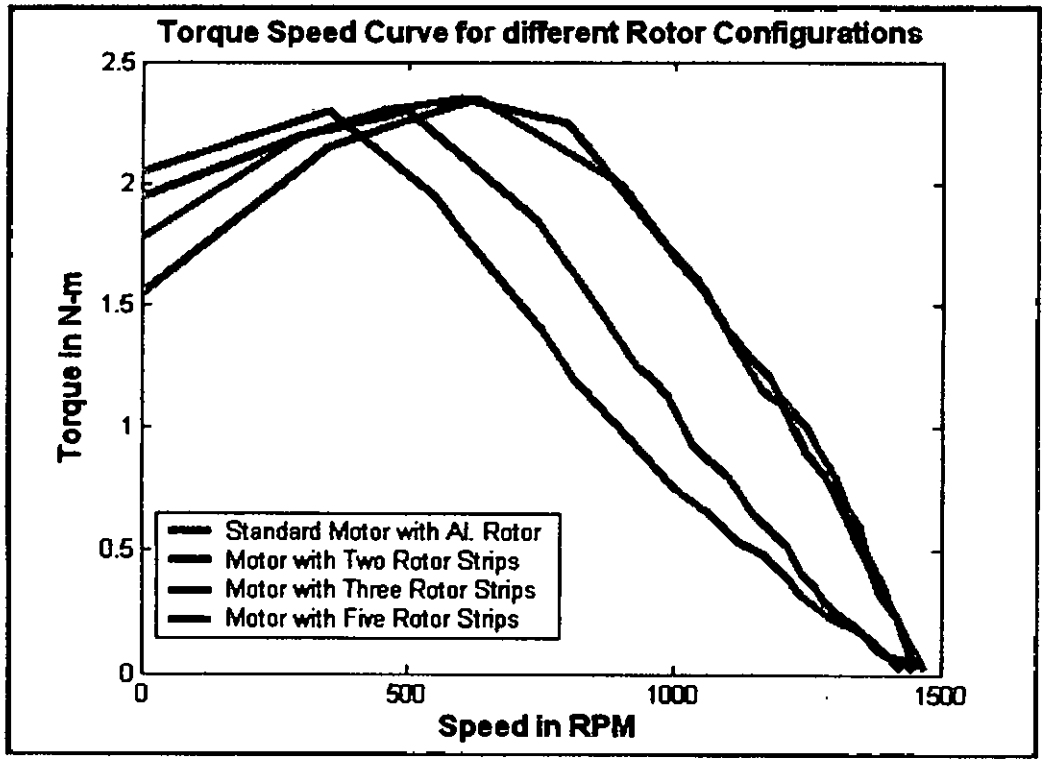

Figure 4.18: Torque-Speed Curve for 3-Phase Motor of different Rotor configurations

From the torque speed (figure 4.18) curve it is seen that the running performance of the motors with Aluminum rotor and rotor with two iron strips are identical. The starting torque of the two iron strip rotor shows an enhancement of about 15%. Thus the motor running performance is unaffected although higher starting torque has been achieved. Although the rotors with three and five iron strips show significant increase in the starting torque, their running performance is affected due to high resistance arising because of increased number of iron strips. So, rotor with two iron strips can be regarded as the ideal case of ferromagnetic insertion for enhancement of starting performance in small and medium size motors. Theoretical study in chapter 3 also validates the experimental results thus obtained. With the introduction of iron strips the torque speed curve tends to get flattened around the breakdown region of the motor showing enhancement of the stable area of operation of the motor.

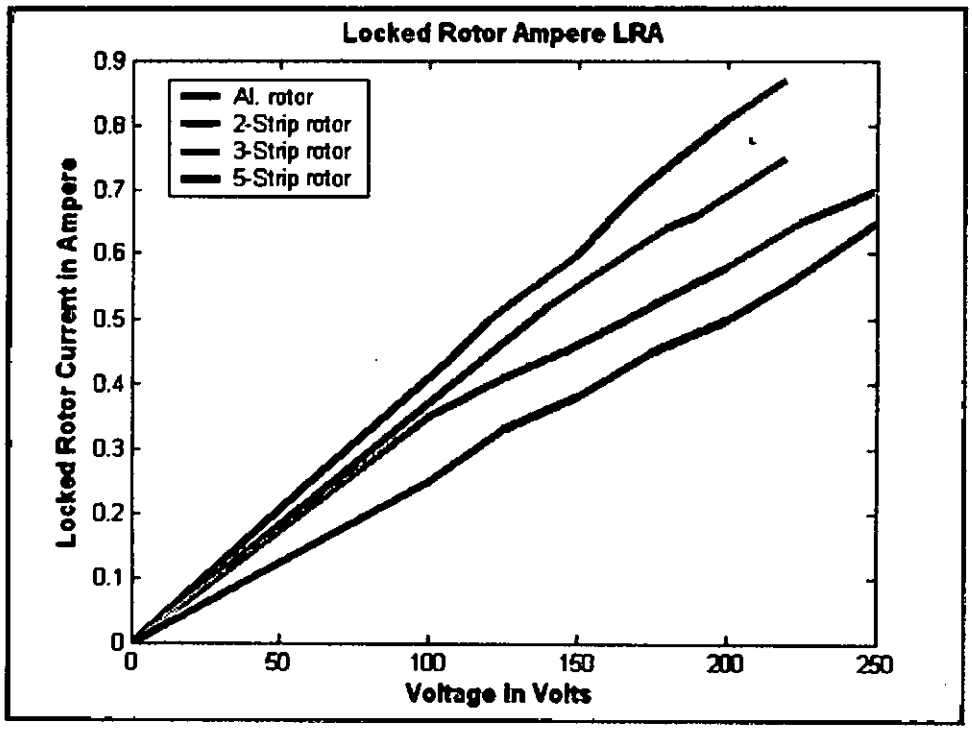

Figure 4.19: Starting Current for 3-phase Motor with different Rotor configurations

Figure 4.19 shows the locked rotor current (Starting current) for different rotor configurations. From the figure it can be seen that the rated locked rotor current (0.65A) has been obtained at different motor voltages for different rotor

configurations. Roughly 18% less line voltage is required for the motor with two iron strips when compared with the motor with the standard Aluminum rotor.

Table 4.1: Table showing starting torque and percentage increase of starting torque with iron insertion

Type of Rotor	T_{Start} N-m	% increase	Calculated Value of T_{ST}	%Slip at Maxm. Torque	Remarks
Aluminum Rotor	1.55		1.57	58	
Rotor with Two iron strips	1.78	14.8	1.78	60	Satisfactory Performance
Rotor with Three iron strips	1.95	25.8	2.05	66.6	Slightly Sluggish response
Rotor with Five iron strips	2.05	32.2	2.1	76.6	Extremely sluggish response

Table 4.2: Table showing starting current for different rotor configurations

Voltage	Al. Rotor	Rotor with 2 strips	Rotor with 3 strips	Rotor with 5 strips
Starting Current at Motor Line Voltage of 220 Volts	.87A	0.70A	0.63A	0.55A
% decrease in current	Reference Value	19.5%	27.5%	36.7%
Starting Current at Motor Line Voltage of 160 Volts	0.65A	0.58A	0.49A	0.40A
% decrease in current	Reference Value	10.7%	24.6%	38.4%

4.3.8 Performance of the single phase motor

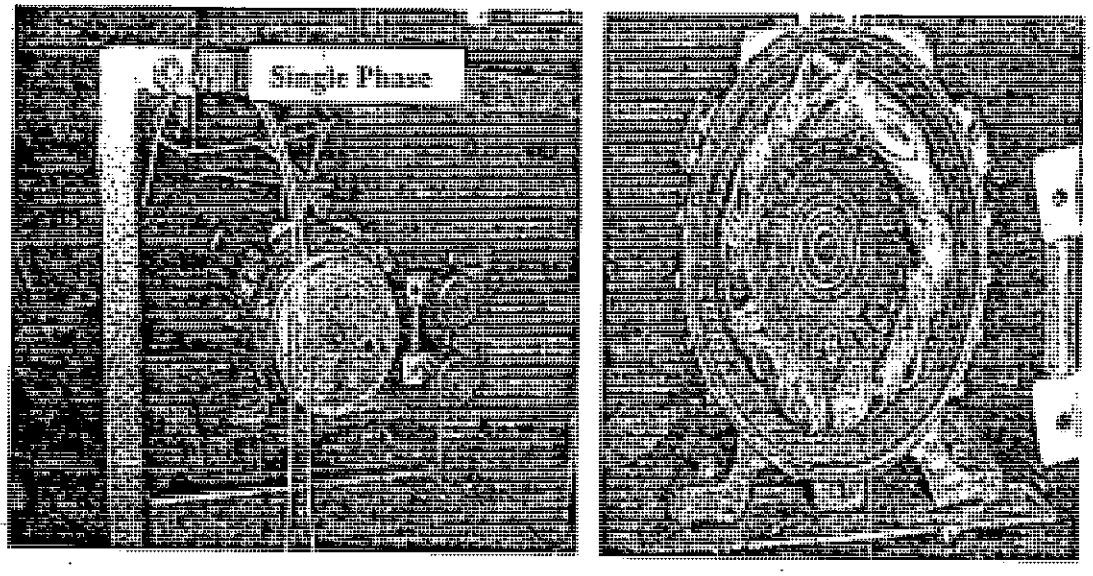

(a) (b)

Figure 4.20: (a) Single Phase Motor (b) Single phase windings placed in stator slots

In order to use the same set of rotors fabricated for the 3-phase fractional HP motor, stator windings of one of the 3-phase motors purchased was taken out and new windings were placed in the stator slots to convert the motor into a single phase motor. This single phase motor had both starting and running windings. However, measurements were taken with the running winding connected to the supply voltage. This is because as the single phase motor does not have starting torque, so study of starting torque has not been considered. The starting winding was disconnected after the motor has attained its rated speed. The load on the motor shaft was gradually increased by coupling the motor with dynamometer. The speed of the motor was recorded for different torque settings. Same sets of reading were taken for rotors of different configurations.

Also for each rotor configuration, the locked rotor current against motor terminal voltage was noted. With the increased number of strips, the motor response was sluggish and like three phase rotor geometry, two strips inserted in the rotor of the single phase motor gave the better performance. The torque-Speed curve and the

locked rotor current (LRA) Vs motor terminal voltage curves are shown in figures 4.21 and 4.22 respectively.

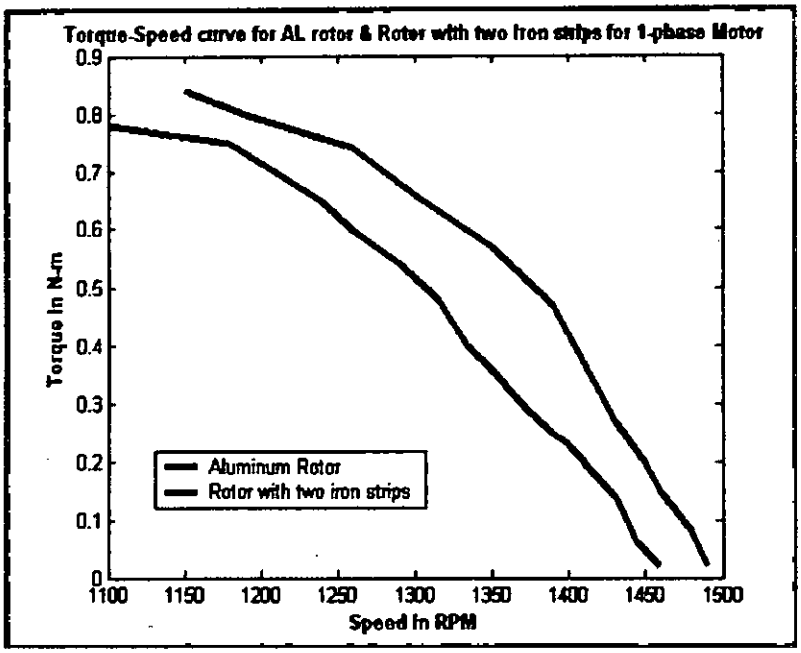

Figure 4.21: Torque Speed curve for Single phase motor.

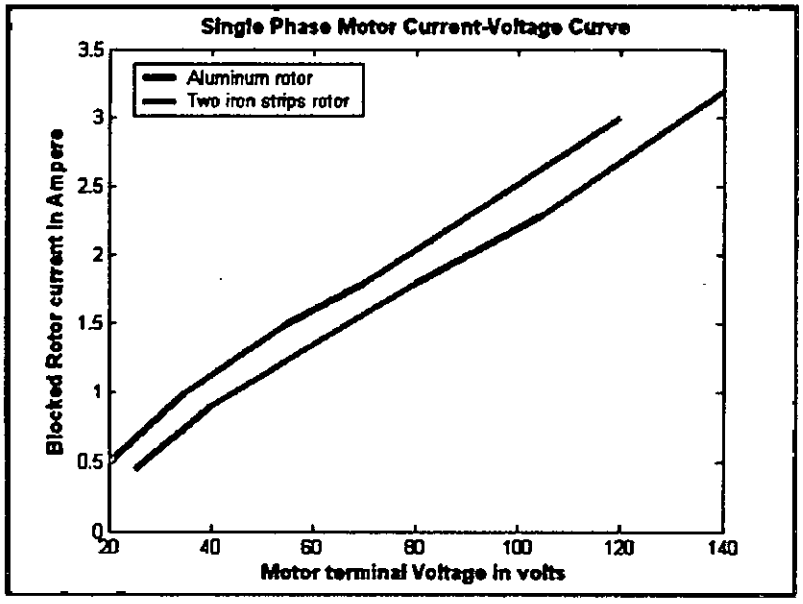

Figure 4.22: Locked Rotor Current-Voltage Curve for Single phase Motor

The result of torque speed curve of the single phase motor is significant. From figure 4.19 it can be seen that higher running torque has been obtained for the motor with two iron strips in the rotor compared to the single phase standard motor. For a small motor, $(R_2'/2s)^2$ is much greater than $(X_2')^2$ and the skin effect is significantly prominent for such type of motors due to backward rotating mmf. Thus compared to 3-phase motor, higher skin effect is experienced by the ferromagnetic material inserted in the rotor which generates higher torque through out the stable region of the motor (equations 2.20, 2.21). For the similar reason, locked rotor current has been reduced for the motor with ferromagnetic insertion.

T05866

4.4 MATLAB simulation results

Experimentally determined motor parameters are introduced in a MATLAB simulation program and the following curves are obtained for the standard Aluminum Three phase motor.

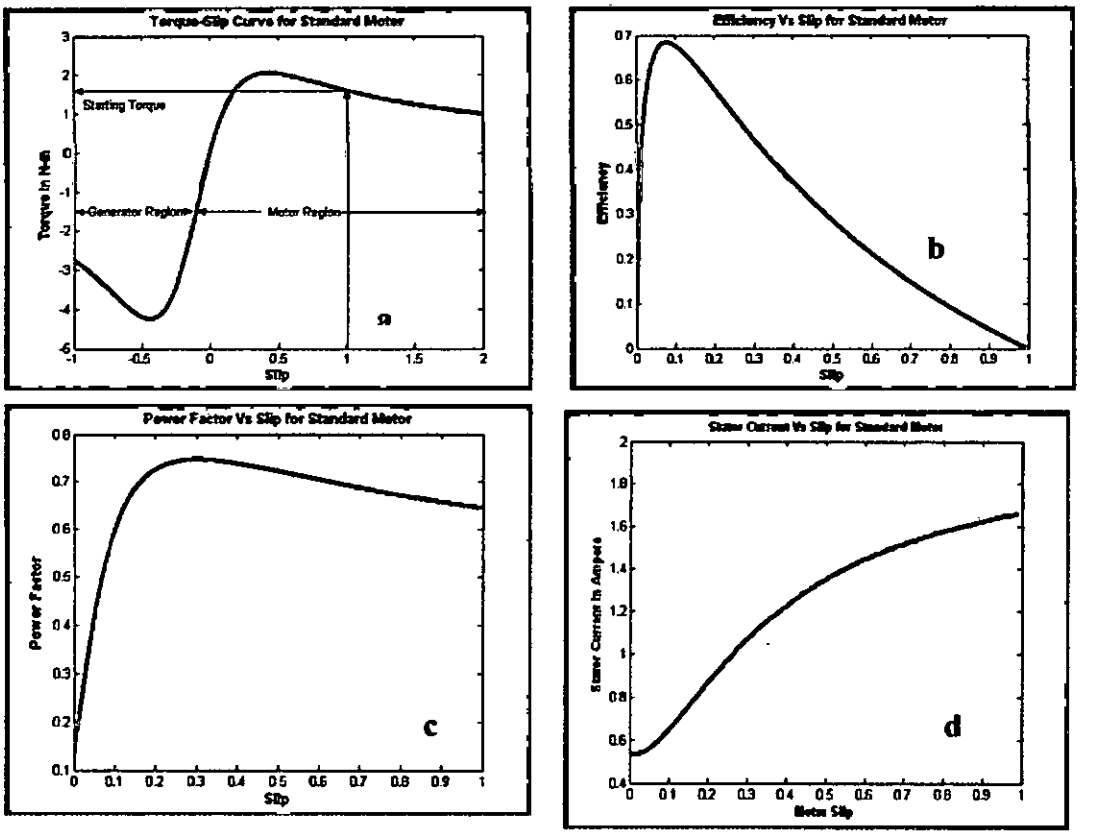

Figure 4.23: simulated curves for the standard 3-phase motor (a) Torque-Slip Curve (b) Power factor-Slip Curve (c) Stator current-slip curve (d) Stator Current-Slip Curve

The starting torque found from experimental data and from simulation results are almost identical. Also experimental values of power factor and efficiency are in agreement with the simulated results. Experimental data for power factor and efficiency could satisfactorily be obtained in the operating region of the motor only because the motor becomes unstable in the low speed region after crossing the breakdown torque. The torque-slip curves for the motor with different sizes of ferromagnetic insertion are shown in figure 4.24.

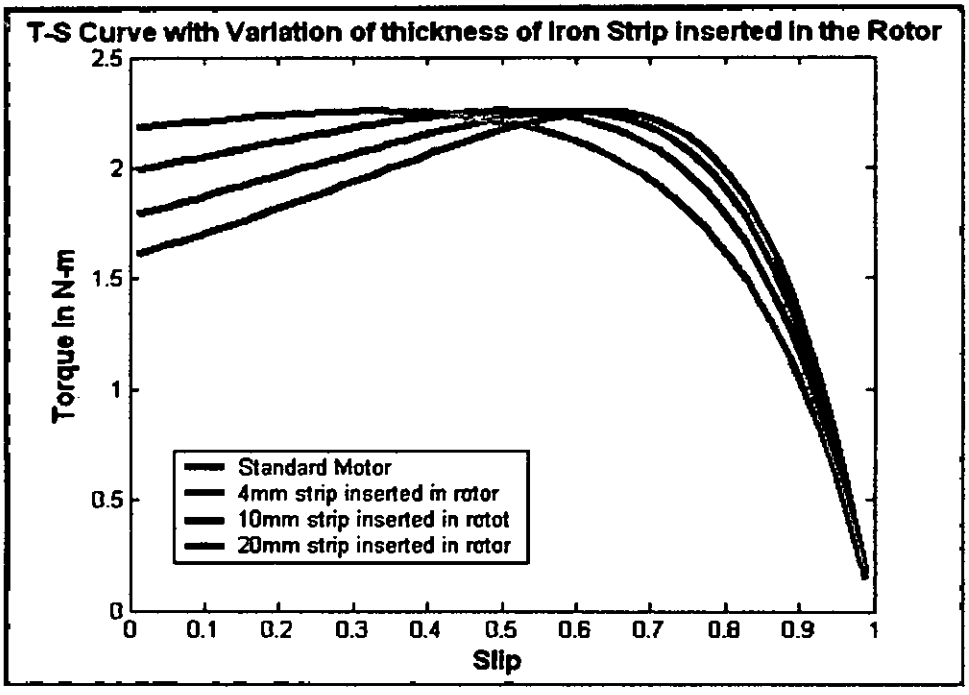

Figure 4.24: Torque-Slip curve for different rotor configuration

The Torque-slip curve for the standard motor is represented by the blue line. The green line shows the torque-slip relationship for the motor with two iron strips. The thickness of each strip is 0.20mm. Red line is the torque slip curve with five iron strips in the rotor, the thickness of each strip is also 0.20mm. The line represented by cyan shows the torque slip relationship with 10 iron strip (each of thickness 0.2 mm) inserted in the rotor. In the normal operating region of the motor, the standard motor (blue) performance and the performance of the motor with two strips almost coincide showing identical performance for both the motors i,e running performance of the motor is not degraded due to insertion of strips in the rotor.

4.5 Current wave shapes for different rotor configuration

The wave shapes for different rotor configurations were studied to calculate total harmonic distortion (THD) for the standard motor and for motors with iron insertion. The stator current of the motor was recorded by an ammeter. Voltage drop across the ammeter was applied to a storage oscilloscope for recording the wave shapes. The wave shape on the oscilloscope was collected to a PC through a DSO controller acquisition card and its associated software. The oscilloscope has a built in math function by which Fast Fourier Transform (FFT) can be performed on the wave shape appearing on the screen of the oscilloscope. Original current wave and wave shape obtained after FFT operation were saved in a PC.

Figure 4.25(a) shows the stator current (motor rated current 0.65A) wave shape and figure 4.25(b) shows the corresponding FFT. Similar set of wave and its FFT are shown in figure 4.25(c) and (d) respectively for the motor having two iron strips in the rotor. Figure 4.26 shows current wave shapes and the corresponding FFT for motor having five and ten iron strips inserted in the rotor respectively. Total harmonic distortion shows significant improvement with increased number of iron strips inserted in the rotor with the exception of figure 4.26(f) where THD is slightly higher compared to motor with two iron strips. This may be due to excessive noise generated for this particular case.

For single phase motor also (figure 4.27) insertion of iron strip in the rotor gives a better value of THD.

4.5.1: Current wave shape & Fast Fourier Transform for 3-phase motor

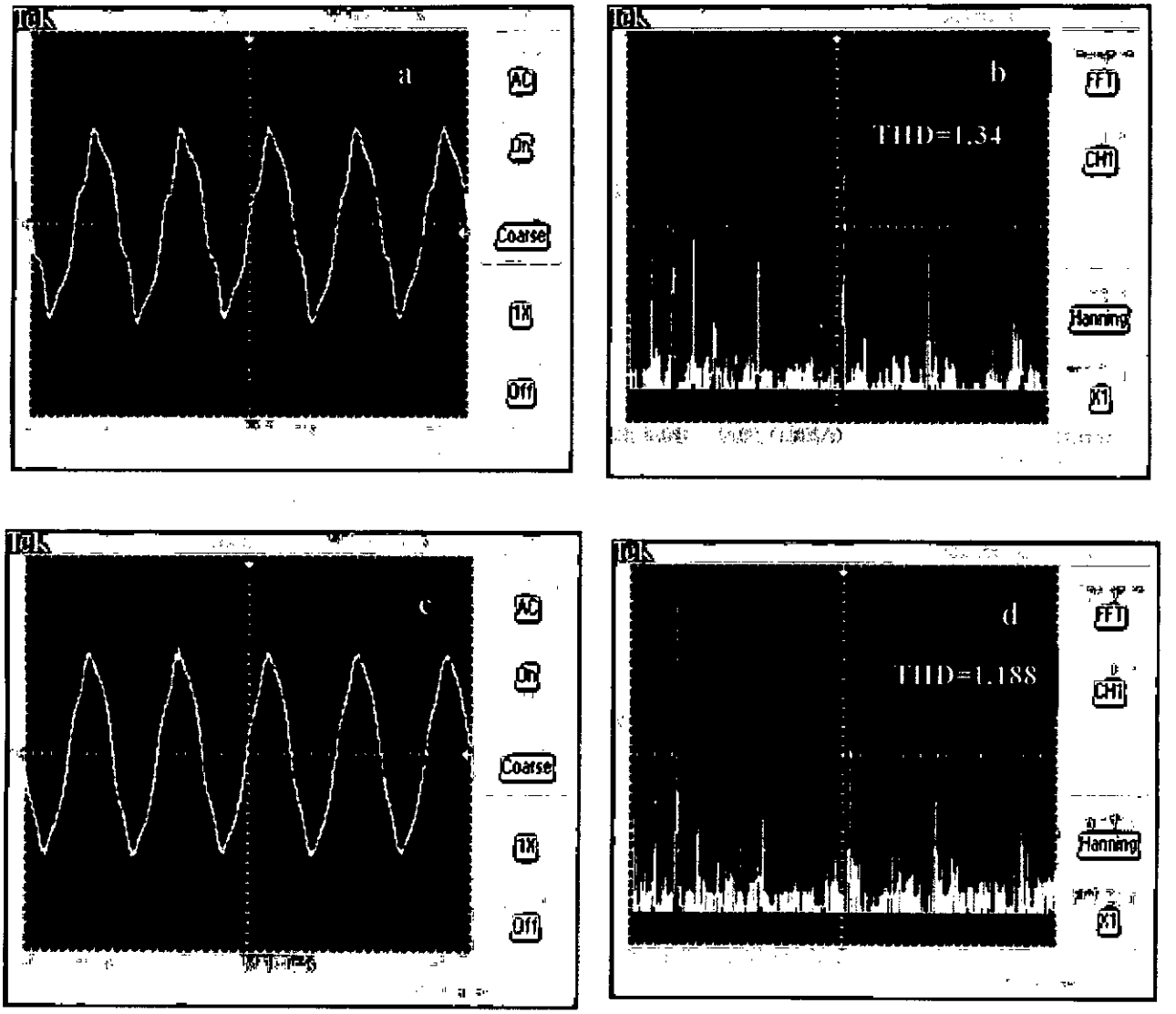

Figure 4.25: Stator Current wave shapes and corresponding Fast Fourier transform for different rotor configurations. a) Standard motor b) FFT for current of standard motor c) motor with two iron strips d) FFT for current of motor with two iron strips

Current wave shape & Fast Fourier Transform for 3-phase motor (Contd.)

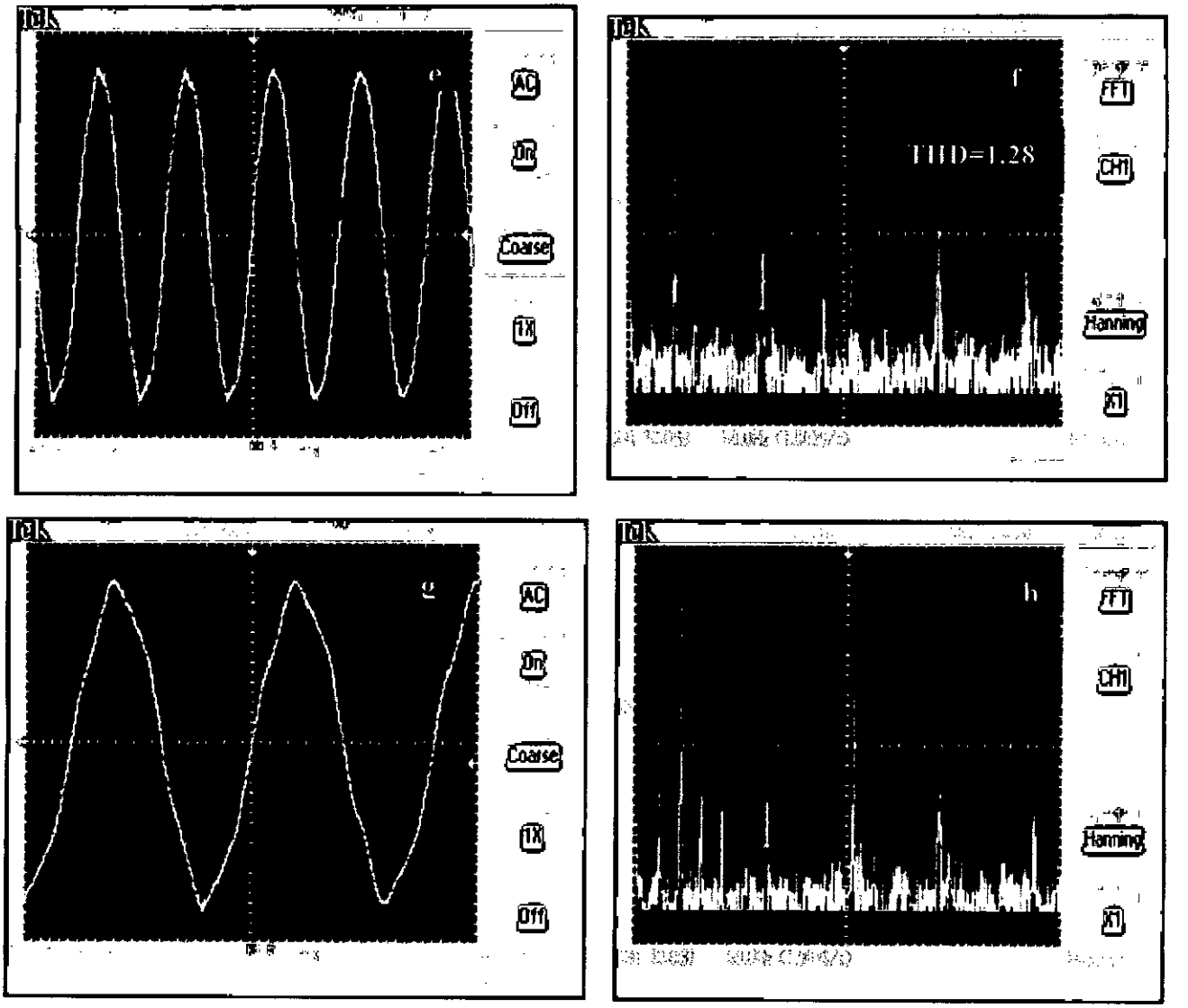

Figure 4.26: Stator Current wave shapes and corresponding Fast Fourier transform for different rotor configurations. e) Current wave shape for motor with five rotor strips f)FFT for current of motor with five rotor strips g) Current wave shape for motor with ten rotor strips h) FFT for current of the motor with ten rotor strips

4.5.2: Current wave shape & Fast Fourier Transform for 1-phase motor

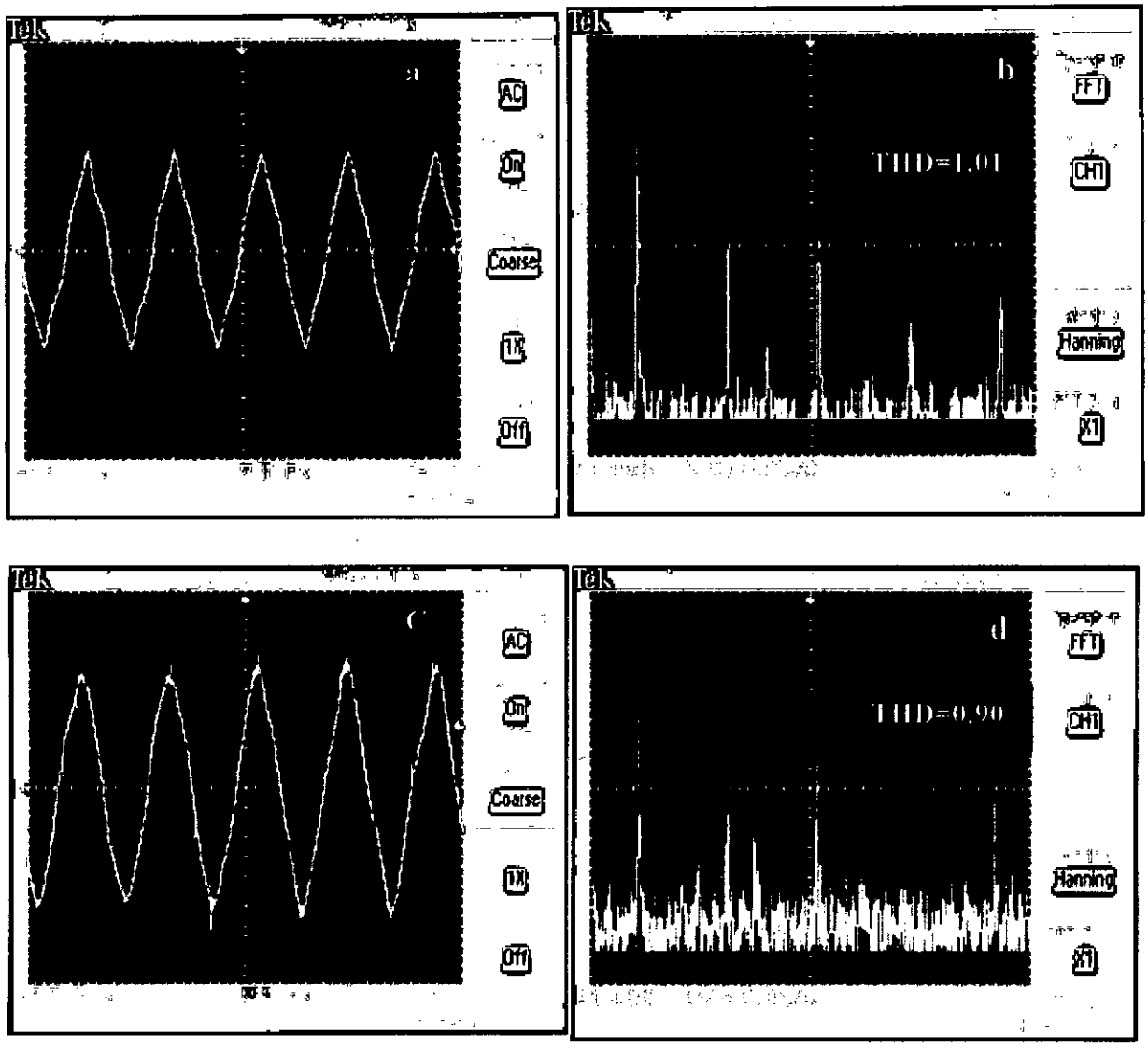

Figure 4.27: Stator Current wave shapes and corresponding Fast Fourier transform for different rotor configurations. a)Single phase standard motor b) FFT for current of standard motor c) Single phase motor with two iron strips d) FFT for current of single phase motor with two iron strips

4.6 Discussion on the results

Experimental results show marked improvement in the starting performance of the three phase induction motor. Due to ferromagnetic insertion, starting torque increases and starting current (locked rotor current) decreases without having any significant effect on the running performance of the motor.

As the motor under test was a fractional horse power three phase squirrel cage induction motor having high rotor and stator resistances, so insertion of iron strip of extremely small thickness (0.4mm) was enough to show marked improvement in the starting performance of the motor. Also it can be seen from the figure 4.21, the torque-Speed curve for the original motor and the motor with two iron strips in the rotor almost coincided in the normal operating region of the motor. This reveals that running performance of both the motors is identical at low slip values. However, at high values of slip (at low speed of the motor), the torque-speed curve for the two strip rotor motor runs above the torque speed curve of the standard motor signifying generation of higher starting torque for the ferromagnetic rotor. With the increase of the number of strips in the rotor, the curve tends to be flattened in the region of the maximum torque of the motor. This result is significant and proves that insertion of iron strip enhances the region of stability of the motor i,e motor does not stall abruptly unlike the original standard motor.

Also there has been significant improvement in the starting current of the motor with the introduction of iron strips in the rotor. In a power system, most of the loads are either single phase or three phase squirrel cage induction motors. So, starting KVA requirement for any power system can be significantly reduced with the introduction of ferromagnetic material in the rotor. Other important results obtained are i) improvement of power factor in the normal operating region of the motor with the insertion of ferromagnetic material and ii) similar efficiency in the operating region for the standard motor and the motor with iron insertion.

4.6.1 Comments on Power Factor and Efficiency

Iron strips were introduced at the end ring to enhance the rotor resistance by 15Ω at the starting point of the motor by utilizing the skin effect. This increased rotor resistance diminishes significantly as the motor attains its rated speed. It can be seen from the efficiency-speed curve, the efficiency in the stable region of the motor almost remains the same for motor with Aluminum rotor and the motor having rotor with iron strip. This is significant in the sense that overall running performance of the motor remains unaffected due to introduction of the iron strip as the skin effect diminishes at the rated speed of the motor.

For a certain speed range (1250-1350 rpm) the change in power factor for the two types of rotor (Fig. 3.24) is not appreciable, but as the load increases on the motor, the pf shows a rising tendency for the rotor with iron strip. This is expected as shifting towards the starting position of the motor introduces more resistance in the rotor due to rise in rotor frequency, which ultimately increases the power factor.

4.6.2 Comments on the current wave shapes & harmonics:

A glance at figures 4.25 to 4.27 reveals that harmonics are appreciably suppressed by insertion of ferromagnetic material in the rotor. Figure 4.25(a) shows the current wave shape (at the rated current) of the standard motor and (b) represents its corresponding Fast Fourier Transform (FFT). From figure 4.25(b) it can be seen that sub harmonics above and below the fundamental frequency are present in the motor. Also odd harmonics (third, fifth and seventh) are dominant. The total harmonic distortion (THD) is 1.349.

Figure 4.25(c) shows the current wave shape of the motor with two iron strips inserted in the rotor. Figure 4.25(d) shows its FFT. In this case also similar sub harmonics below and above the fundamental are present like that of the standard motor, however the sub harmonic above the fundamental is 50% less. Compared to the standard motor, the 3^{rd} harmonic is less by 30% and the 5^{th} and 7^{th} harmonics are around 20% less. The THD for the motor with iron insertion in the rotor gives the value of THD 1.188 which is 88% of the THD of the standard motor.

Figure 4.26(g) represents current wave shape with 10 iron strips inserted in the rotor. In this case also, odd harmonics are less compared to the standard motor and that of

the motor with two iron strips inserted in the rotor. THD for this motor has been found to be 1.063.

For the single phase standard motor, the current wave shape has been shown in figure 4.27(a) and its FFT is shown in figure (b). For the motor with two iron strips in the rotor, the current wave shape and the corresponding FFT are shown in figures 4.27 (c) and 4.27(d) respectively. Although sub harmonics for both the waves are identical, but higher harmonics for the motor with iron insertion in the rotor are suppressed showing less THD value for this modified rotor geometry. In this case, THD for the standard motor has been found to be 1.01 and that of the motor with two iron strips is 0.90.

Chapter 5

Validation of Proposed Scheme

5.1 THEORETICAL CALCULATION

Equation 2.4 is written below for the calculation of starting torque.

$$T = \frac{3 \times I_2^2 \times \frac{R_2'}{s}}{\omega_s}$$

$$= \left(\frac{3}{W_s}\right) \frac{\left(V_{TH}^2 \times \frac{R_2'}{s}\right)}{\left(R_{TH} + \frac{R_2'}{s}\right)^2 + \left(X_{TH} + X_2'\right)^2}$$

Applying Thevenin's Theorem to the motor equivalent circuit (p 20-21, Chapter-2) and using the formula for torque (Eqn.2.4) the motor performance can be evaluated. The data from the no load and Blocked Rotor tests are first used to determine the equivalent circuit parameters of the motor. The parameters are:

1) Determination of Machine parameters (All referred to the stator), Y connected Motor

No load test:

Phase Voltage = 207V [360V (L-L)]

Phase Power = 37W

Line current = 0.47A

Volt-Ampere input $S_{NL} = V_{NL}I_{NL} = 207*0.47 = 97.29VA$

Reactive input $Q_{NL} = [S_{NL}^2 - P_{NL}^2]^{1/2} = 90$ VAR

Total Reactance $X_{NL} = Q_{NL}/I_{NL}^2 = 407.4ohms = X_1+X_M$

All the above values are referred to the stator side of the motor.

Blocked Rotor test:

Line Voltage = 160V

Phase Power = 41W

Line current = 0.65A

$Z_{BR} = V_{BR}/I_{BR} = 92.31/0.65 = 142\Omega$

$R_T = P_{BR}/I_{BR}^2 = 41/(.65)^2 = 97\Omega$

$X_{BR} = [Z_{BR}^2 - R_{BR}^2]^{1/2} = 103.7\Omega$

$X_1 = X_2 = X_{BR}/2 = j51.8\Omega$

$X_M = X_{NL} - X_1 = j355.6\Omega$

$R_1 + R_2' = 97\Omega$

Measured stator resistance/phase $R_1 = 57\Omega$

Rotor resistance (referred to stator) $R_2' = 40\Omega$

V_{TH}= Thevenin's Voltage at the terminals AB (Fig. 2.3) = 175 Volts.

Z_{TH}= Thevenin's Equivalent Impedance looking into AB: (figure 2.3 reproduced below)

$R_{TH} + X_{TH} = 42.6 + j51.1$

Also $R_2' = 47$, $X_2' = 51.8$

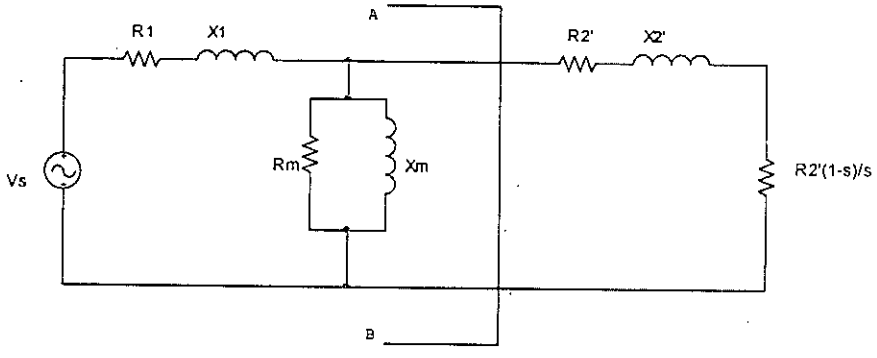

Value of R_m is three times higher than X_m and is neglected. The Thevenin's equivalent circuit reduces to:

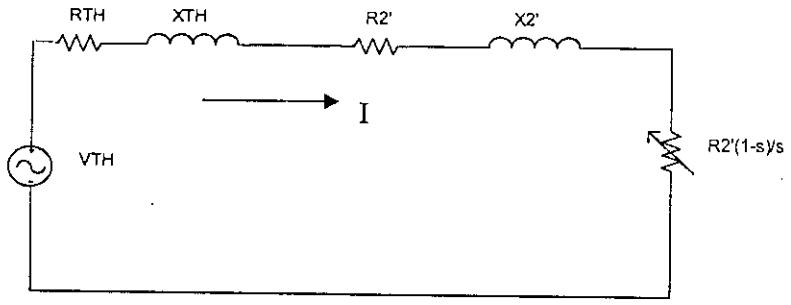

Figure 2.4 has been reproduced above for the calculation of current and power factor.

The current equation for the motor is given by equation 2.3

$$I^2 = \frac{V_{TH}^2}{\left\{\left(R_{TH} + \frac{R_2'}{s}\right)^2 + \left(X_{TH} + X_2'\right)^2\right\}}$$

Calculated Results for different rotor configurations

Standard Motor	**Motor with two Iron Strips**
Rotor Current= I= 1.33A Pf= 0.64 Starting Torque= 1.60N-m Maximum Torque= 2.25 N-m	Rotor Current= 1.23A Pf = 0.70 Starting Torque= 1.78 N-m Maximum Torque= 2.25N-m
Motor with Three Iron strips	**Motor with Five Iron strips**
Rotor Current= 1.22 A Pf = 0.75 Starting Torque = 2.05N-m. Maximum Torque = 2.25 N-m	Rotor Current = 1.20 A Pf = 0.77 Starting Torque= 2.1 N-m Maximum Torque = 2.25 N-m.

5.2Torque and current characteristic of induction motor by SLIM

The SLIM software developed by AREVA T&D Limited [48] is an useful software to evaluate motor performance. SLIM software is based on finite element method (FEM analysis). SLIM uses window based environment in which the software modules may be used concurrently and thus allow the user to move freely between tasks. Four basic steps involved in slim are i) Mesh generation ii) Solver data preparation iii) Field solution and iv) Post processing. Analysis is done on a 2-D cartesian model formed from a section of the machine under study with a single pole being modeled. The remainder of the machine is implied with periodic boundaries. First rotor dimensions (in metric) are introduced in a template. In another template rotor bar profiles are inserted. Then mesh for the rotor is built after introducing the dimension through a command "Build mesh". A separate form is selected to introduce the stator dimensions and stator slot dimensions. Like rotor mesh generation, stator mesh is also generated in the similar manner. Later both stator and rotor meshes are joined together. The material properties of stator and rotor are inserted in a form called "data preparation tool". Material properties like permeability, stacking factor, winding type, conductivity etc are introduced from the slim library. For the rotor bar 1 and rotor bar 10 of the 90 KW motor the relative permeability has been chosen as 5000 (permeability of iron) and for the rest of the rotor bars relative permeability of 1 (Aluminum) is chosen to simulate the condition of introduction of ferromagnetic material in the rotor. For the winding, the input current and the turns per phase are assigned. The machine parameters like voltage, phase, frequency, phase resistance, pitch factor (.97) and distribution factor (.95) of the stator winding are introduced. Then Dirichlet boundary condition on the outer surface of the stator is introduced. In this case, the potential is (0-0). Then the post processing phase is initiated to generate the torque-speed and the current-slip curves. Iron insertion in the rotor shows significant increase of starting torque with decrease of starting current.

5.2.1 Mesh generation for the 1/4 HP 3-Phase Motor.

The parameters (in mm) introduced in the rotor template are:

Rotor Radius:	28.8375
Rotor air-gap:	0.155
Shaft radius:	6.905
Number of rotor bars in machine:	30
Number of rotor bars in mesh:	10

Rotor bar Topology (Figure 5.1)

d_0 : distance to rotor surface:	1
d_1 : rotor bar depth:	10.1
d_2 : rotor neck depth:	0.4
w1: rotor bar side width:	3
w2: side width at lower end:	1

Rotor bar Topology:

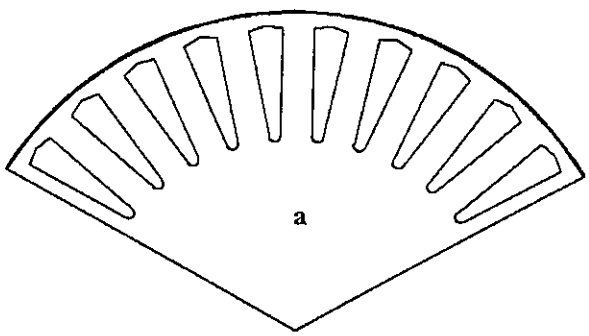

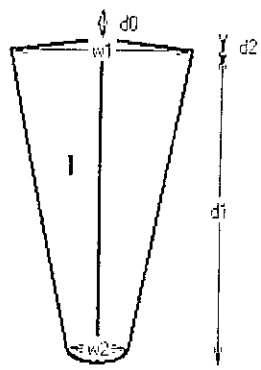

Fig 5.1(a) Outline of Rotor in a 90^0 section. (b) Dimension of each rotor slot for ¼ HP motor

The next step is to construct the stator portion mesh. The parameters introduced for the stator are: (in mm):

Slot depth d_1:	12	Stator bore radius: 29.305
Bridge depth d_2:	0.01	Stator depth: 51
Wedge inner depth d_3:	0.01	Stator air gap: 0.155
Winding depth d_4:	0.01	Number of Stator slots: 24
Slot width bottom w_1:	6	Slot width top w_2 : 4
Slot width (bore) w_3:	4	

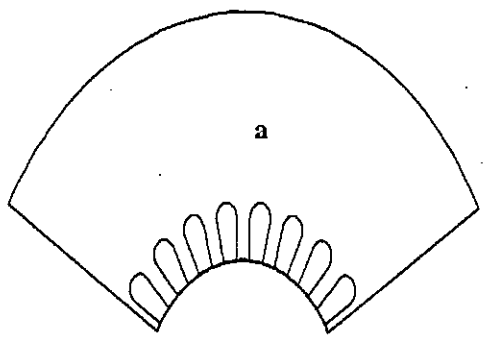

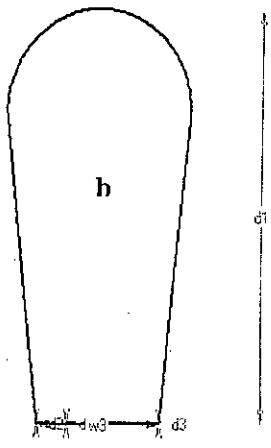

Figure 5.2: (a) 90^0 Section of Stator (b) Dimension of stator slot

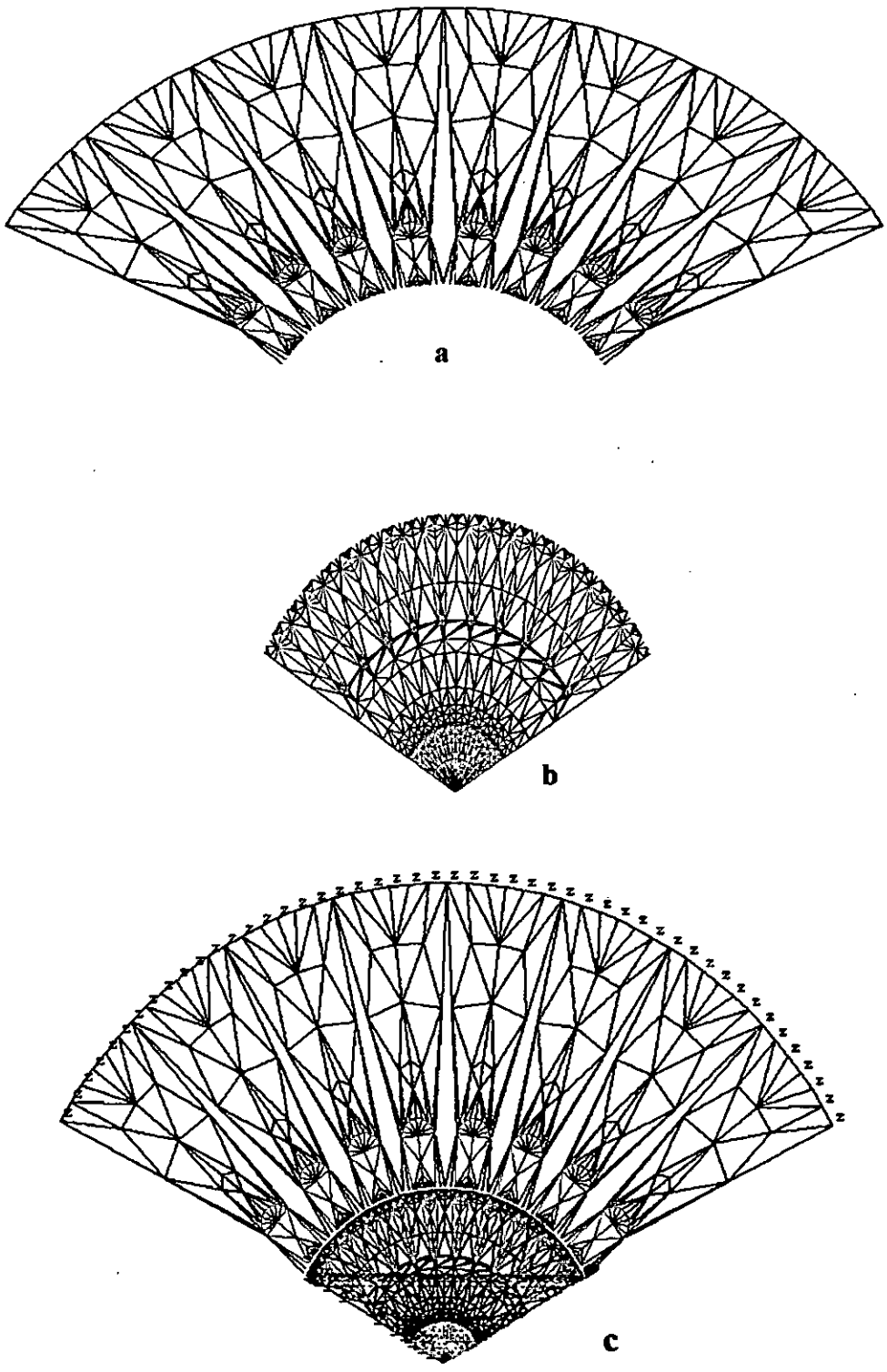

Fig.5.3 Mesh for ¼ HP 3-Phase motor (a) Stator mesh (90^0 section) (b) Rotor mesh (c) Combined Stator and Rotor mesh Total nodes 1355, total element 2496 for ¼ hp motor

5.2.2 Mesh Generation & Performance Curves for 90KW 415V 3-Phase Motor:

Although stator and rotor mesh can be generated for the fractional horse power motor under test by SLIM software, however the software does not support the post processing phases for the small motor for the generation of torque-Slip and Current slip curves. In order to validate the performance enhancement obtained from the practical results a 90 KW motor is taken as reference and necessary motor data are inserted in the template wizard. The rotor slot dimensions and necessary rotor dimensions are introduced first. Then the rotor mesh is generated as shown in figure 5.6(b).

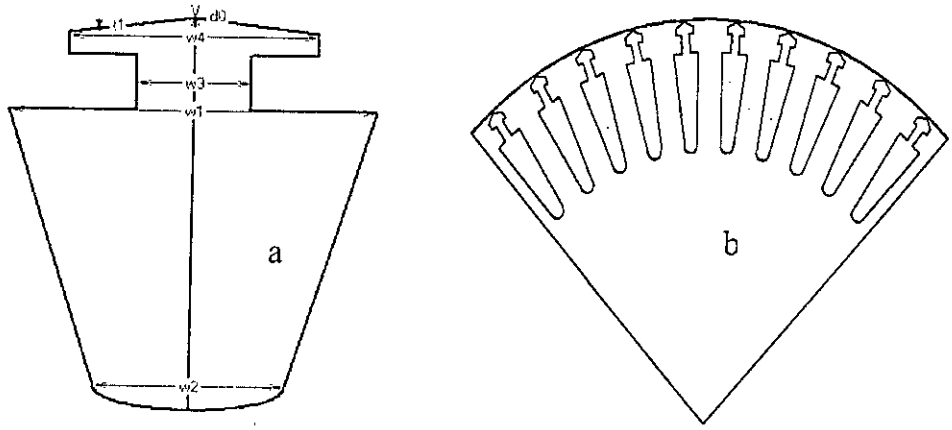

Rotor radius: 128.875, Rotor air gap: 0.3 Shaft radius: 52, Number of bars in Machine: 40 Number of bars in mesh:10, d_0=0.6, d_1=32, d_2=6, d_3=4, w_1=9.6, w_2=5, w_3=3,w_4=6.5, t_1=1.5 (dimensions are in mm).

Figure5.4: a) Rotor slot dimension and b) Rotor 90^0 section

Then stator dimensions are introduced in the stator template wizard to generate the stator mesh. The corresponding meshes are shown in figure 5.6

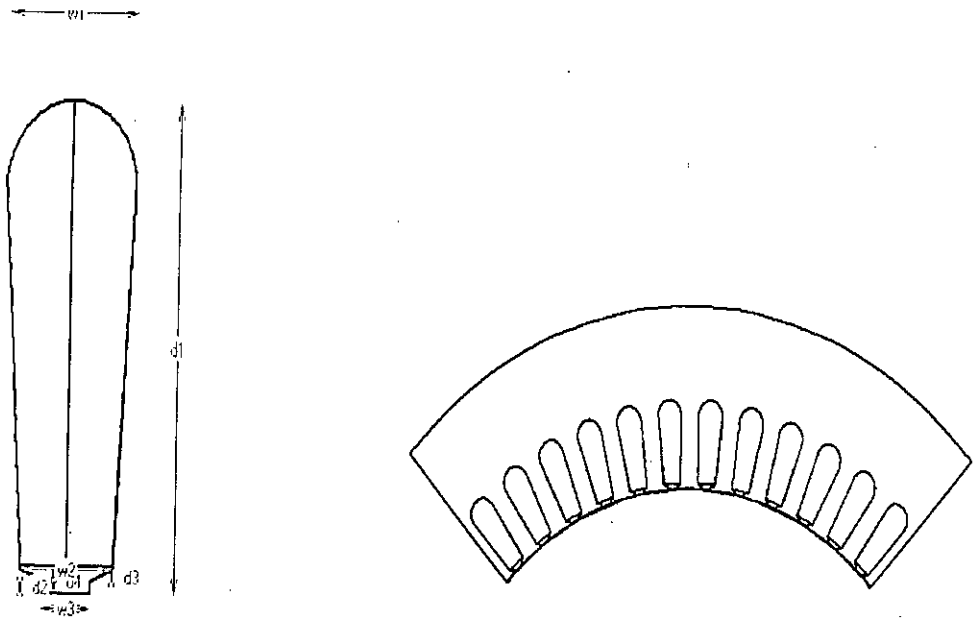

a b

Figure 5.5: (a) Stator Slot dimension (b) 90^0 Section of the Stator Slot.

Stator bore radius: 129.725
Stator depth=70.3

Number of stator slots=48
d_1=34, d_2=1, d_3=0.72, d_4=2,
w_1=12, w_2=8.5,w_3=4.5
Stator air gap width=0.3,

The above dimensions in (mm) are inserted in the stator template wizard. Optimum mesh generation is made by varying the mesh generation concentration option tool.

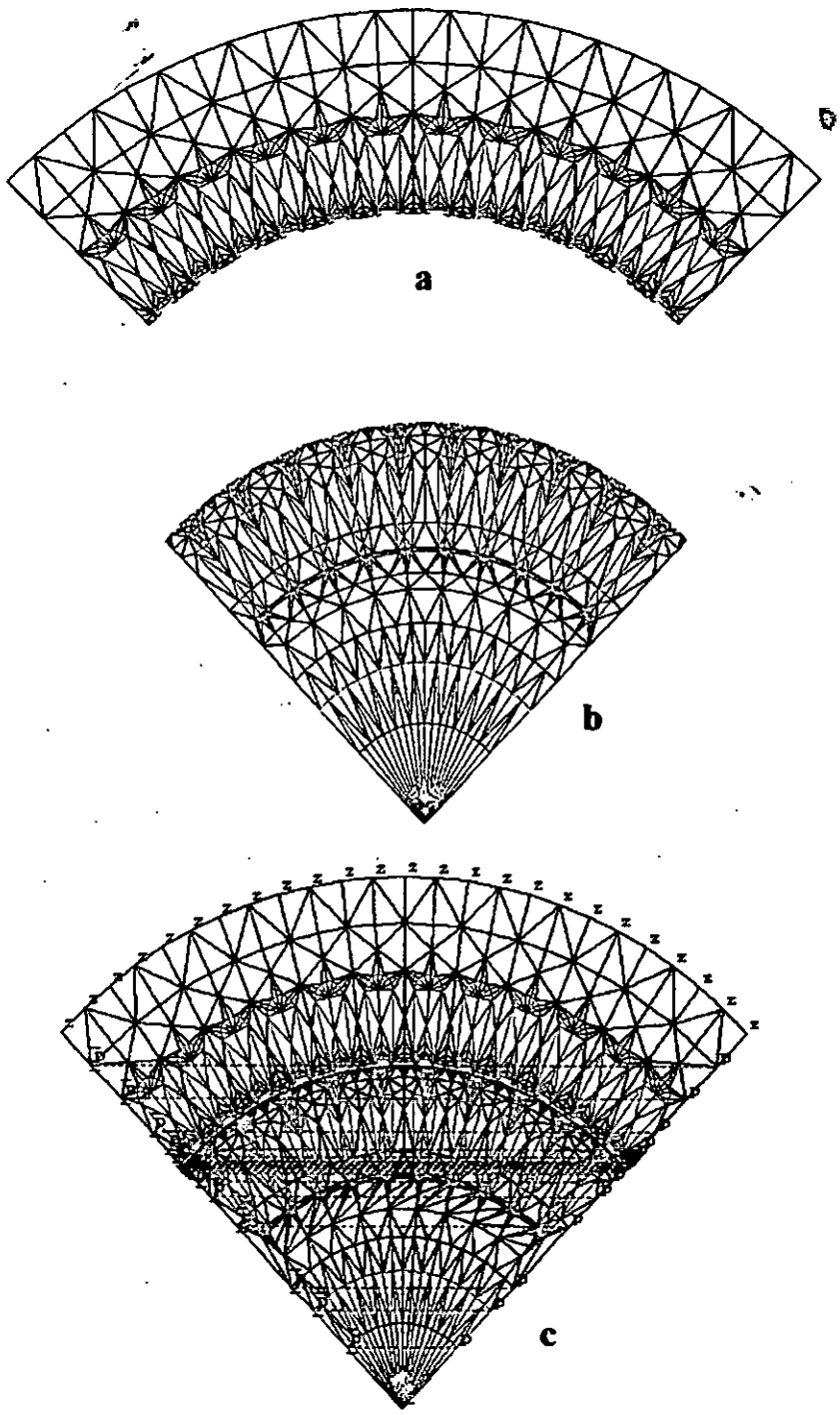

Figure 5.6: Mesh for 90 KW motor. (a) Stator mesh (b) Rotor mesh (c) Combined Stator & Rotor mesh

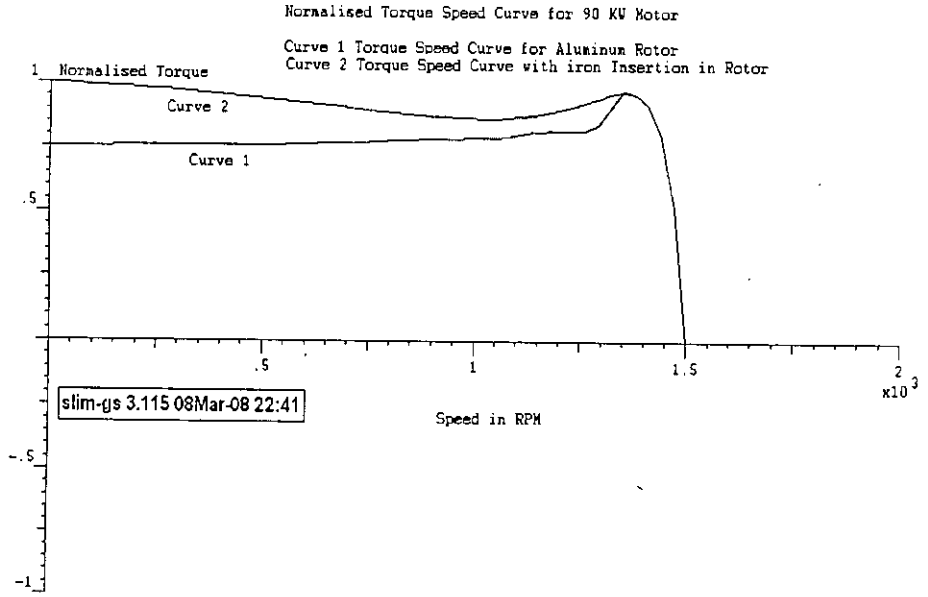

Figure 5.7: Torque Speed Curve of 90 KW motor (by SLIM simulation software)
1 pu =1200 N-m

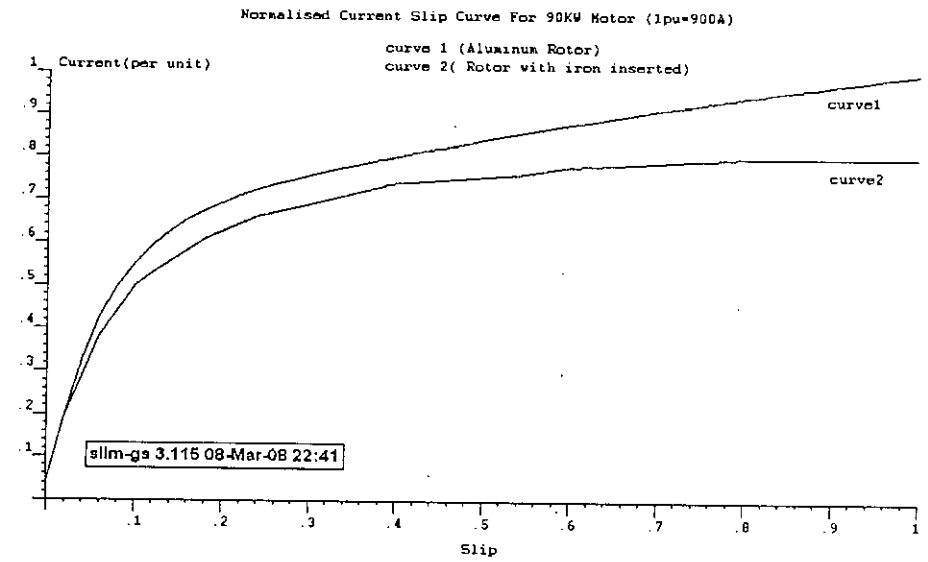

Figure 5.8: Current Slip Curve of 90 KW motor (by SLIM simulation software)

5.2.3 Discussion on the simulation results

From the torque speed and current slip curves of the simulated results, it can be seen that the starting torque increases by more than 24% while the starting current decreases by 25% (figures 5.7 and 5.8 respectively). As mentioned earlier, ferromagnetic materials have been introduced in two rotor slots to simulate a rotor with iron insertion. In this case, iron has been inserted in rotor slot number 1 and slot number 10 respectively in the 90^0 section of the rotor. The curves are generated in the post processing phase as mentioned before. The simulation software slim also validates the practical results of the proposed scheme of enhancement of starting performance by introduction of ferromagnetic material in the rotor. Figure 5.7 also validates that by ferromagnetic insertion, the running performance of the motor has not at all degraded. Rather, the curve representing the original motor without any insertion in the rotor and the curve representing the ferromagnetic rotor have coincided in the normal operating region of the motor which proves that running performance due to insertion of magnetic material in the rotor has not been affected. In comparison to the original rotor, current for the rotor with ferromagnetic insertion showed gradual decrease with the increase of slip. Maximum decrease of current has been obtained at the standstill condition of the motor as expected.

Chapter 6

Conclusions

6.1 Conclusion

Squirrel cage motors are the most commonly used motors and their applications as residential, commercial and industrial uses are immensely large. During starting, these motors produce large voltage dips due to high starting current requiring higher size transformers and generators.

In this research work, insertion of Ferro-magnetic material at the end connections of the motor has proved to be an effective method of reducing the starting current and increasing the starting torque. During the research work, special attention was given in the design work so that rotor modifications required are kept at a minimum level. This has been done to minimize the manufacturing cost of the machine and to make the rotor casting process simple. Casting of aluminum in rotor slots and at the end ring positions after placement of iron strips is very simple with no extra casting technique or special tools required for such casting.

The main focus of the research work has been to utilize the skin effect property of ferromagnetic material by inserting this material within the rotor end ring. Mixing of iron granules with aluminum or copper as suggested in literature review for improvement of performance of squirrel cage motors have limitations. Mixture of iron and aluminum is highly viscous and there is possibility of void space formation during the casting process. In this research work, the iron insertion is external to the rotor conductors that make the manufacturing process simpler and cheap. Another proposal put forward in the literature review is to employ HTS (High temperature superconducting tape) over the rotor conductors and end rings. This makes the fabrication of the rotor quite complicated and needs special tools for manufacture of

such modified rotors. Smooth mixing of iron with aluminum is not possible due to large density variations of these materials and there are possibilities that iron particles if the sizes are too small will float on the surface of liquid aluminum during casting process. There are possibilities of formation of void space as well. Considering all these points, insertion of iron at the end ring may be considered as a better choice of improving the starting performance of the motor.

Simulated results and the experimental results highlight the following points;

With reference to figure 4.18, starting torque with two iron strips in the rotor shows an enhancement of around 15% compared to the starting torque of the standard motor. The same figure indicates an increase of starting torque to nearly 26% for the motor with three iron strips in the rotor. This motor with three iron strips shows slightly sluggish response. Further enhancement of starting toque has been attained with higher number of strips inserted in the rotor. But the running performance of the motor is seriously affected under such circumstances. Figure 4.19 shows locked rotor current for different rotor configurations. At the motor line to line voltage of 220V under locked rotor condition, starting current decrease by 20% with two strips in the rotor when compared to the blocked rotor current of the standard motor. Motor with three strips gave 27% decrease of starting current when compared to the starting current of the standard motor. The simulated Torque slip curve (figure 4.24) shows that the curve becomes more flattened in the region of the maximum torque of the motor with the introduction of iron strips in the rotor. This indicates broader stable region and higher pick up of the motor that will reduce the accelerating time of the motor.

Table A.3 shows performance data for the standard motor. The rated load for the motor is 1.18 N-m and at full load efficiency is about 46%. For the same rated load, the two strip iron rotor motor gave an efficiency of 45% (Table A.4). Two strip motor has slightly less efficiency, but this does not show any serious shortcomings due to introduction of iron strips in the rotor. The efficiency for both the rotor configurations may be assumed to be identical.

A comparative study of power factor vs speed from figures 4.12 (curves for standard motor) and 4.16 (curves for two strip rotor) respectively shows that at the rated load,

two strip rotor has higher power factor (0.75) compared to that of the standard motor (0.71). The starting current has been appreciably reduced by insertion of iron at the end rings. The motors taken for the research work is a small ¼ hp motor. Due to physical dimensions and due to high motor parameter values of the equivalent circuit (especially high stator and rotor resistances), there were some limitations for having large variation of starting torque of the motor. Simulation through SLIM also shows 24% increase in starting torque and 25% decrease in starting current.

Salient outcome of ferromagnetic insertion as achieved in this research work has been summarized below:

- Ferromagnetic insertion has been proposed at the end ring connection. Such insertion is simple due to advantageous location of the end ring. No complicated casting method (like high pressure die casting) is necessary and there is no risk of void space formation during casting.
- Better running performance has been achieved for single phase fractional horse power motor due to iron insertion in the rotor.
- For 3-phase motor, the torque speed curve flattens at the peak due to iron insertion. This indicates enhancement of the region of stability of the motor.
- Overall power factor of the motor improves with iron insertion.
- The overall efficiency in the normal operating region of the motor remains almost unchanged (compared to the original motor) due to iron insertion.

6.2 Limitations of the work

Due to small range of equipments available in the lab, the motor selected for the research work is a small fractional hp motor. Due to its high stator and rotor resistances, the starting torque could be varied within a small range by variation of rotor resistance through ferromagnetic insertion in the rotor. Although increasing the number of strips in the rotor reduces the starting current of the motor but at the same time the running performance of the motor degrades due to high parameter values of the standard motor. Even with introduction of five thin strips (each 0.2 mm thick) the motor response was sluggish.

Also due to the small thickness of the iron strip found by theoretical calculation, iron strip could not be uniformly distributed between each slot of the rotor at the end ring position. Rather these strips were lumped in certain rotor slot positions. This might have led to uneven distribution of rotor current. For a large size motor such problem of non uniform distribution of iron strip may be avoided due to low equivalent circuit parameter values. However, due to small size of the motor, no abnormal performance was noted as far as unbalance rotor current is concerned. But for a large motor if strips are lumped in certain region of the rotor, then some unbalance or knocking may occur.

6.3 Suggestions for further research

1) As skin effect is dependent relative permeability of the material to be inserted, magnetic material with high permeability and good conductivity may be used to have better starting performance of the motor. One such conductor may be Finemet (Fe-Si-Fe) having permeability in the range 10,000 to 15000.

2) The acceleration of a motor load system is caused by the difference between the developed torque (motor) and the absorbed torque (load). The larger the difference the faster the acceleration and less time is required to attain the full speed of the motor. As starting torque has increased with the introduction of iron strips, so the accelerating time of the motor at rated load is expected to reduce. Further study can be made about the effect on accelerating time with insertion of ferromagnetic material in the rotor.

3) As the research work shows that major harmonics can be suppressed with the introduction of iron strips in the rotor, further study can be made to analyze the harmonic contents in the system with different rotor configurations. Periodic variation of magnetic circuit reluctance caused by rotor and stator slots results in a non sinosoidal space distribution on the rotating flux. Analysis of this rotating flux pattern shows that it consists of a number of rotating field called space harmonics. The 5^{th} space harmonic normally rotates backward at $1/5^{th}$ speed of fundamental while the 7^{th} space harmonic rotates forward at $1/7^{th}$ speed of the fundamental and so forth. The component of torque produced by 5^{th} and 7^{th} harmonics are called parasitic torques and may cause undesirable bumps and dips in the motor torque

characteristics during acceleration of the motor. Effect on such sub harmonic torques on the motor performance may be studied with ferromagnetic insertion in the rotor. In this research work, harmonic suppression has been achieved with iron insertion in the rotor. Based on this finding, parasitic torques may decrease with iron insertion in the rotor.

4) As single phase fractional horse power motors are widely and commonly used motors, the performance of such type of motors may be studied by insertion of high conductivity and high permeability materials in the rotor.

5) Also it is necessary to study critically whether there is generation of noise and vibration in 3-phase and single phase motors due to non uniform distribution of iron strips in the rotor in cases when uniform distribution of ferromagnetic strips inserted between rotor slots is not possible.

6) In this research work better running performance has been found for single phase fractional horse power motor with only running winding of the motor energized. Further study can be made on the performance of such motors with both starting and running windings in the circuit with ferromagnetic insertion in the rotor.

7) Optimum casting process with ferromagnetic insertion in the rotor of squirrel cage induction motors may be studied for adoption in industries.

References

[1] ,[5] D.P. Kothari and I.J.Nagarath. *Electric Machines.* The McGraw-Hill Companies 3rd Ed.2005, p.8, p9.

[2] A.F.Puchstein and T.C.Lloyd *Alternating Current Machines.* John Wiley & Sons, 3rd Ed., 1996, p.254.

[3] P.L.Cochran. *Polyphase Induction Motors: Analysis, Design and Applications* . Mercel Dekker Inc. NY., p.254-258.

[4],[6],[7],[8] M.H.Rashid. *Power Electronics.* 2nd. Ed., 1994, Prantice Hall Pvt. Ltd. p.550,p560,p568,p572.

[5] D.P. Kothari and I.J.Nagarath. *Electric Machines.* The McGraw-Hill Companies, 3rd Ed., 2005, p.9.

[9] Kometani,H. et al. 3-D Electromagnetic analyses of a cage induction with rotor skew. *IEEE transactions on Energy conversions.* 11(2): 331-337, June 1996

[10] Smith, A.C. Influence of End ring shape on induction motor performance . *Eighth International conference on Electrical Machines and Drives.* Publ.No.444:143-147.1-3Sept., 1997.

[11] Dorell,D.G. Calculation and effects of end ring impedance in cage induction motor. *IEEE transactions on Magnetics,* 41(3):1176-1183. March 2005.

[12] Williamson Stephen and Danielle R. Gerch. Finite element calculation of double cage rotor equivalent circuit parameters. *IEEE transactions on Energy Conversions.* 11(3): 41-48. March 1996.

[13] J.R.Bumby, E. Spooner and M.Jagiela. Equivalent circuit analysis of solid rotor induction machines with reference to turbo charger accelerator applications. *IEE Proceedings on Electric Power Applications.* 153(1): 1024-1031. Jan. 2006.

[14] C.C.Chen, Leytong Yen et al. Analysis of electromagnetic and thermal fields for induction motor during starting. *IEEE transactions on Energy Conversion.* 9(1):53-57, March 1994.

[15] M.Rezwan Khan, I.Hussein and M.F.Momen. Paramagnetic rotor bars three phase squirrel cage induction motor. *IEEE Transactions on Industry Applications,* .40(6):1536-1540. December 2004.

[16] W.Levy, C.F.Landy and M.D.McCulloch. Improved models for the simulation of deep bar induction motors. *IEEE Transactions on Energy Conversion.* 5(2):393-400. June 1990.

[17] Katasumi Yamazaki. Induction motor analysis considering both harmonics and end effects using combination of 2D and 3D finite element method. *IEEE Transactions on Energy Conversion.* 14(3):698-703, September 1999.

[18] A.Boglietti, A.Cavagnino et al. Induction motor efficiency improvement with low additional cost. *Conference on Power Electronic Machine and Drive.*(PEMD 2004, Conference Publication no. 498), April 2004.

[19] F.Parasiliti, M.Villanie et al. Three phase induction motor efficiency improvements with die cast copper rotor cage and premium steel.*SPEEDAM Conference, 2004,* Italy.p.338-343, June 16-18, 2005.

[20] C.Stark, J.G.Cowie et al. Copper in the rotor for lighter, longer, lasting motors. *Fleet Maintenance Symposium 205, ASNE,* San Diego Section, 30 Aug.-1 Sept. 2005.

[21] John Cowie and Edwin Brush. Electrical energy efficiency results of die cast copper rotors. *icowie@cda.copper.org.*

[22] G.H.Choe and M.H.Park. A new injection method for ac harmonic elimination by active power filter. *IEEE Transactions on Industrial Electronics.* 35(1):141-147. February 1988.

[23] M.Poloujadoff , J.C.Nipo and M.Nurdin. Some economical comparison between Aluminum and copper squirrel cages. *IEEE Transactions on Energy Conversion.* 10(3): 415-418,Sept.1995.

[24] R.De Weerdt, K.Hameyer and R.Belmans. End ring inductance of a Squirrel cage induction motor using finite element method. *Industry Application Conference (Thirtieth IAS Annual Meet.)* Orlando, USA 1: 515-522, 8-12 Oct. 1995.

[25] A.R.Munoz and T.A.Lipo, Complex vector model of the squirrel cage induction machine instantaneous rotor bar currents. *IEEE Transactio on Industry Applications.* 35(6):1332-1340, Nov.1999.

[26] S.Williamson, M.A.Muellor. Calculation of the impedance of rotor cage end rings. *IEE Proceedings on Power Applications.* 140(1):51-60.Jun 1993.

[27] Circuit and method for power efficiency improvement of induction motors. *http://www.freepatentsonline.com/4954764*.

[28] A.A.Hasan Improving power efficiency of a rotor flux oriented induction motor drive. *Electric Power Components and Systems* 30(5): 431-442. May2005.

[29] SIM Jungwook et. al Development of a HTS squirrel cage induction motor with HTS rotor bars. *IEEE 8th International Conference on Magnet Technology.* No.18,Morioka city.p.914-916. Oct.20-24,2003

[30] R.W.Fei and J.D.Lloyed.An experimental study of single phase induction motor starting performance and its dependency on winding harmonics. *30th IEEE Industry Applications Conference*, (1):571-578. 8-12 Oct. 1995.

[31] Improvement of torque characteristics for a new prototype six phase pole change induction motor for EVs. *Paper on technical meeting on rotating machinery, IEE Japan* RM01(129):83-88, 2001.

[32] www.ilib.cn/A. A new strategy to improve electromagnetic starting torque for thyrister controlled induction motors. *Proceedings of the society for Electrical Engineering,* China.

[33] E.Chiricozi, F.Parasiliti and M.Villiani. New materials and innovative technologies to improve the efficiency of 3-phase induction motor. A case study, *Dept. of EE, University of L'Aquila, Italy.*

[34] Copper Motor Project. *www.copper-motor-rotor.org/process0116shtml*

[35] Isanu Ohyama et al Efficiency of model Induction motor using various non-oriented electrical steels. *www.ilib.cn*, 2002.

[36] James L.Kirtley Jr. Designing squirrel cage rotor slots with high conductivity. *MIT, USA.*

[37] Stephen Paul McDonald, Geoffery David Baines et. al http://www.patentstorm .*us/patents/5969497.html*

[38] Steven L.Stephan and Tran N. Nguyen.High starting torque induction motor. *United States patent 5751082*, http:// www.patentstorm../5751082.html.

[39] Zu Li Application of fuzzy control in constant current soft starting of induction motor. *Journal of Shenyong Univ. of Technology*, China.

[40] Louis Lefevre. Design of line start permanent magnet synchronous motor using analytical and finite element analysis. *Thesis of Royal institute of Technology(KTH),* traita-eme-0003, June, 2000.

[41] B.J.Chalmers, L.G.Atkinson et. al Design of 400Hz saturister motor with improved starting performance. *IEE proceedings, Part-B Electric Power Applications,* 127(6):341-348.Nov.1980.

[42] Lyann Lundquist. Reduced starting current mechanism for three phase squirrel cage motors. *US Patent 5068560,* Nov.1991.

[43] Steven L. Stephan High starting torque induction motors. *US Patent 5751082.* May12, 1998.

[44] Nikolai P.Popov et. al. Rotor for Asynchronous motor with multiple layered screen. *US Patent 5001380,* March.1991.

[45] Mark W.Bailey. High torque, reduced starting current electric motor *US Patent 6246141,* June 12, 2001.

[46] Higashi. High efficiency motor. *US Patent. 4885494.*

[47] Neumann. *Standard Handbook for Mechanical Engineers.* p. 55-63 7th ed. 1967.

[48] M.Cistelecan and E.Dcmeter. Induction motors with low copper windings improved performance. *IEEE Electrotechnical conference,* 3:.1183-1186, May 1996.

[49] Edelson. Jonathan. Polyphase induction electrical rotating machine. *US Patent No. 6054837.* April 2000.

[50] Induction motor with shot circuitcd armature and a pipe cage. *http://www.wipo.int/pctdb/en/wo.jsp.* Feb.1981.

[51] Satake,ToshihikoandOnogi,Yukio. Brushless induction synchronousMotor withtwostators. *SatakeCorporation,Japan. http://patents.ic.gc.ca/Cipo/cpd/en/patent/2075791.* Jan.1997.

[52] Munoz-Garica Alfredo and Lipo Thomas A. A new induction motor V/f control method capable of high performance regulation at low speed. *IEEE Transactions on Industry Applications,* 34(4): 813-820. Jul/Aug.1998.

[53] T Nakamura et al. Novel rotating characteristics of a squirrel cage type HTS induction/synchronous motor. IOP electronic journals: Super Conductor Science & Technology, May 2007.

[54] Whitney.Eugene C. Starting motors for large inertia loads. http:// www. freepatentsonline.com/4048528.html. Sept.1977.

[55] Davis et al. Torque/Speed curve of a solid rotor machine. Proceedings of *Institution of Electrical & Electronic Engineers*..124(12): 1187-1196. May 1977.

[56] P.Di.Barba, E.R. Magnaschi et al. *The international journal for computation And mathematics in Electrical & electronic Engineering.* 24(3): 796-804. July 2005.

[57] Colin Grantham, Douglas Mckinon Rapid parameter determination for induction motor analysis and control *IEEE Transactions on industry applications* 39(4):1014-1020, July/August 2003

APPENDIX A

A.1 Important Formulae

1. Skin Depth $\delta = \frac{1}{(\pi f \mu \sigma)^{1/2}}$ where μ is the permeability of the material and σ is the conductivity of the material. For commercial Iron, μ_r is 5000 and the conductivity σ is $10^7\ \Omega$-m.

2. Effective Resistance $R_e = \frac{1}{\pi r_0^2 \sigma}\left[1 + \frac{1}{48}\left(\frac{r_0}{\delta}\right)^2\right]$ per unit length.

Where r_0 is the conductor outer radius

3. The effective resistance for a slab of length L and width w is given by:

$$R = \frac{L}{w\sigma\delta} \text{ ohms}$$ where L is the length and w is the thickness in m.

1) Determination of Machine parameters (All referred to the stator), Y connected Motor.

No load test:

Phase Voltage = 207V [360V(L-L)]

Phase Power = 37W

Line current = 0.47A

Volt-Ampere input $S_{NL} = V_{NL}I_{NL} = 207*0.47 = 97.29VA$

Reactive input $Q_{NL} = [S_{NL}^2 - P_{NL}^2]^{1/2} = 90$ VAR

Total Reactance $X_{NL} = Q_{NL}/I_{NL}^2 = 407.4\text{ohms} = X_1 + X_M$

Blocked Rotor test:

Line Voltage = 160V

Phase Power = 41W

Line current = 0.65A

$Z_{BR} = V_{BR}/I_{BR} = 92.31/0.65 = 142\Omega$

$R_T = P_{BR}/I_{BR}^2 = 41/(.65)^2 = 97\Omega$

$X_{BR} = [Z_{BR}^2 - R_{BR}^2]^{1/2} = 103.7\Omega$

$X_1 = X_2 = X_{BR}/2 = j51.8\Omega$

$X_M = X_{NL} - X_1 = j355.6\Omega$

$R_1 + R_2 = 97\Omega$

Measured stator resistance/phase $R_1 = 57\Omega$

Rotor resistance (referred to stator) $R_2 = 40\Omega$

A.2 Calculation of Resistance of the iron strip inserted at the end ring.

Using eqn. 3.3 the skin depth for the iron has been found to be 0.318mm.

$$R = \frac{\Delta L}{\sigma * \{(A + B - 2\delta)\} * 2\delta} \quad \text{ohms.}$$

The stator has 12 sets of coils each coil consisting of 250 turns. The stator has 24 slots. So, each phase contains 4 sets of coils. The number of turns per phase is 1000. All the rotor conductors are shorted by end rings. The number of turns per phase in the rotor stands at 1. The turns ratio 'a' is 1000/1.

For optimum starting torque, the value of rotor resistance was found to be 10 ohms (referred to the stator). The value of the rotor resistance referred to the rotor side is: $15/a^2 =$ ohms.

Putting the values of A, B, σ and δ.

$$\text{Or, } 0.000010 = \frac{\Delta L}{0.5 \times 10^7 [(.011) + (.005 - .000636)] \times .000318}$$

Or, $\Delta L = 0.46$mm. Two strips each of .2mm fabricated as shown in fig.4.8

At the normal speed of the motor (1470 rpm; 2% slip) the rotor frequency drops down to 1 Hz.

At this frequency of 1Hz, the skin depth becomes 2.25mm. The value of the resistance of the iron strip becomes 2.5×10^{-6} ohms referred to the rotor i,e 2.5 ohms referred to the stator. Thus the value of the rotor resistance at the normal speed becomes 25% of that of resistance at the starting of the motor (resistance decreased

by 75%). Due to fall in the resistance of the rotor at the rated speed, the normal performance of the motor at the rated load remains unaffected.

A.3 Motor Name Plate Data

3-phase Squirrel Cage Induction Motor

380V, 0.65A, 1400 rpm, Y

0.18KW, 0.25HP, 50Hz

IP 44, Insul. B, Ambient Temp. = 40^0C

Manufacturer: Jinlong Heavy Industry Co. China.

Detailed Machine Rating:

1. Full load Output: 0.25 HP
2. Line Voltage: 380V
3. Frequency: 50 HZ
4. Phase: 3
5. Efficiency: N/A
6. P.f: 0.8
7. No. of Poles: 4
8. Synchronous Speed: 1500 rpm
9. KVA input: 0.427
10. Full load Line Current: 0.65A

STATOR DETAILS

1. Connection: Wye
2. Phase Voltage: 220V
3. Flux per pole: 3.95 mwb
4. Turns per phase: 1000
5. No. of Slots: 24
6. Slots/pole: 6
7. Slots/Pole/Phase: 2
8. Coil Span: 4 Slots
9. Conductors per Slot: 250

10. Conductor: bare diameter:= 0.316mm
    Insulated diameter: = 0.367mm Area: 0.078mm^2
11. Phase resistance: 57 ohms
12. Depth of Stator Core: 51mm

MAIN DIMENSION :

1. Stator Bore: (radius): 29.305mm
2. Gross Iron Length: L 51mm

ROTOR:

1. Length of air-gap: 0.155mm
2. Diameter of Rotor: 57.66mm
3. Type of winding: Squirrel Cage
4. Number of Slots: 30
5. Slots/Pole/Phase: 2.5
6. Conductors/slot: 1
7. Rotor Bar Cross-section: 38.67mm^2
8. End Ring cross-section: 57.2mm^2

Experimental Results

Table A.1: Table of experimental data for torque-speed curve of different rotor geometry. Torque was measured as per instruction sheet of Lab-Volt Manual

Aluminum Rotor		Rotor with 2 iron strip each 0.2mm		Rotor with 3 iron strip each 0.2mm		Rotor with 5 iron strip each 0.2mm		Rotor with 10 iron strip each 0.2mm	
Torque in N-M	Speed r.p.m	Torque in N-M	Speed r.p.m	Torque in N-M	Speed r.p.m	Torque in N-M	Speed r.p.m	Torque in N-M	Speed r.p.m
0.015	1470	0.015	1455	0.02	1430	0.01	1450	0.01	1430
0.1	1450	0.12	1435	0.06	1410	0.06	1430	0.04	1410
0.2	1425	0.23	1420	0.1	1380	0.08	1400	0.07	1400
0.3	1400	0.33	1385	0.16	1360	0.12	1380	0.13	1360
0.4	1385	0.42	1370	0.20	1340	0.16	1360	0.17	1340
0.5	1360	0.52	1345	0.25	1305	0.20	1325	0.23	1300
0.6	1345	0.61	1330	0.30	1280	0.24	1290	0.27	1280
0.7	1320	0.71	1305	0.35	1265	0.28	1240	0.33	1250
0.8	1300	0.80	1285	0.41	1240	0.34	1210	0.40	1230
0.9	1275	0.90	1245	0.52	1210	0.38	1175	0.44	1210
1	1250	1	1225	0.59	1180	0.46	1120	0.50	1190
1.05	1230	1.1	1200	0.65	1150	0.54	1060	0.55	1160
1.12	1200	1.12	1185	0.73	1100	0.60	1000	0.63	1120
1.20	1180	1.15	1165	0.86	1070	0.70	960	0.73	1060
1.30	1140	1.30	1125	0.92	1030	1	810	0.80	960
1.40	1100	1.45	1085	1.12	990	1.20	750	0.88	850
1.55	1060	1.60	1045	1.2	960	1.61	600	1.05	500
1.70	1000	1.75	985	1.25	930	1.82	550	1.1	400
2.00	900	2.25	800	1.35	900	2.35	350	1.25	200
2.38	630	2.35	600	1.45	870	2.05	0		
2.35	480	2.30	450	1.85	740				
2.25	350	2.2	300	2.3	500				
1.55	0	1.78	0	2.25	400				
				2.2	300				
				1.95	0				

Table A.2: Blocked Rotor current with different rotor configurations

Aluminum Rotor		Rotor with Two Iron Strips		Rotor with Three Iron Strips		Rotor with Five Iron Strips		Rotor with Ten Iron Strips	
V1 (L-L)	I1 (Amp)	V2 L-L	I2 (Amp)	V3 L-L	I3 Amp	V4 L-L	I4 (Amp)	V6 L-L	I6 (Amp)
0	0	0	0	0	0	0	0	0	0
60	0.25	60	0.23	100	0.35	100	0.25	100	0.20
110	0.45	100	0.35	125	0.41	125	0.33	125	0.28
120	0.50	140	0.47	150	0.46	150	0.38	150	0.33
150	0.60	160	0.58	175	0.52	175	0.45	175	0.40
160	0.65	180	0.62	200	0.58	200	0.50	200	0.46
170	0.70	190	0.65	225	0.65	220	0.55	220	0.50
200	0.78	210	0.68	250	0.70	250	0.65	250	0.60
220	0.87	220	0.70					265	0.65

Table A.3: Table of Efficiency & power factor for Aluminum rotor (for stable Region of motor)

Torque N-m	Speed rpm	Stator Current Ampere	Input Power Per phase	Efficiency	Power Factor
.015	1470	.53	40	1.5	.32
.10	1450	.54	43	15.4	.364
.20	1425	.54	49	23.7	.44
.30	1400	.55	52	28.4	.458
.40	1385	.555	60	32.3	.547
.50	1360	.56	64	35.5	.57
.60	1345	.56	71	39.7	.60
.70	1320	.58	77	42.5	.64
.80	1300	.60	81	43.7	.69
.90	1275	.62	88	45.9	.74
1.0	1250	.64	95	45.8	.77
1.1	1200	.66	103	46.1	.82
1.2	1180	.68	109	45.1	
1.3	1140	.72	118	44.7	
1.4	1100	.75	129	41.9	
1.55	1060	.76	135	40.5	

Table A.4: Table of Efficiency & power factor for rotor with two iron strips
For stable region of motor

Torque N-m	Speed rpm	Stator Current Ampere	Input Power Per phase	Efficiency	Power Factor
.015	1455	.48	32	1.5	.32
.12	1435	.53	39	15.4	.364
.23	1420	.535	48	23.7	.44
.30	1385	.55	51	28.4	.458
.42	1370	.56	62	32.3	.547
.50	1345	.57	66	35.5	.57
.60	1330	.575	70	39.7	.60
.71	1305	.58	76	42.5	.64
.80	1285	.58	82	43.7	.69
.90	1245	.59	89	45.9	.74
1.0	1225	.60	94	45.8	.77
1.1	1200	.605	101	46.1	.82
1.12	1185	.605	110	45.1	
1.15	1165	.61	120	44.7	
1.3	1125	.61	131	41.9	
1.45	1085	.62	144	40.5	

Table A.5 Torque-Speed data for Single phase motor

T1 N-m	N1 RPM	T2 N-m	N2 RPM
0.02	1460	0.02	1490
0.06	1445	0.08	1480
0.09	1440	0.15	1460
0.14	1430	0.20	1450
0.20	1410	0.27	1430
0.23	1400	0.37	1410
0.25	1390	0.47	1390
0.30	1370	0.56	1350
0.36	1350	0.66	1300
0.40	1335	0.74	1260
0.48	1315	0.80	1190
0.54	1290	0.84	1150
0.60	1260		
0.65	1240		
0.70	1210		
0.75	1180		
0.78	1100		

T1, N1: Torque & Speed for the Standard Aluminum Rotor
T2, N2: Torque & Speed for Rotor with Two Iron Strips